20. Combustion Diagnostics

Combustion processes consist of a complex multi-dimensional interaction between fluid mechanics and chemical kinetics. A comprehensive experimental analysis needs therefore measurements of flow and scalar fields. These measurements need to be performed in-situ with high temporal and spatial resolution as well as high accuracy and precision. In addition, any disturbances during the measurement should be avoided. These requirements are fulfilled best by laser-optical techniques. Whereas flow fields are commonly measured by methods like laser Doppler or particle imaging velocimetry discussed elsewhere, the focus of this chapter is on scalar measurements based on spectroscopy. Scalars of interest are temperatures, chemical species concentrations, or rate of mixing between fuel and oxidant. Following an introduction, Sect. 20.3 presents the interconnection between experimental analysis and numerical simulation of combustion processes. In Sect. 20.4, various spectroscopic techniques are described exemplary in their application to different fields of combustion research. The chapter concludes with aspects on future developments in combustion diagnostics.

Abbreviations and Acronyms

AM	amplitude modulation
AS	absorption spectroscopy
CA	crank angle
CARS	coherent anti-Stokes Raman scattering
CCD	charge-coupled device
CFD	computational fluid dynamics
CL	chemiluminescence
CLD	chemiluminescence detector
CMD	count median diameter
CRDLAS	cavity-ring-down laser-absorption spectroscopy
DFB-DL	distributed feedback diode lasers
DFG	difference-frequency generation
DFWM	degenerate four-wave mixing
DNS	direct numerical simulation
EGR	exhaust gas recirculation
ELIF	excimer-laser-induced fragmentation fluorescence
FARLIF	fuel/air ratio LIF
FWHM	full width at half maximum
FIR	far IR
FMS	frequency-modulation spectroscopy
FTIR	Fourier transform infrared
HCCI	homogeneous charge compression ignition
IC	internal combustion
ICCD	intensified CCD
ICLAS	intra-cavity laser-absorption spectroscopy
IR	infra red
LAS	laser-absorption spectroscopy
LES	large-eddy simulation
LDV	laser Doppler velocimetry
LIF	laser-induced fluorescence
LII	laser-induced incandescence

MS	mass spectrometry
MIR	mid IR
NDIR	nondispersive infrared photometer
NIR	near IR
NIR-DL	near-IR diode laser
OD	optical density
OPO	optical parametric oscillator
PAH	polycyclic aromatic hydrocarbons
PDA	phase Doppler anemometry
PDF	probability density function
PIV	particle image velocimetry
PS	polarization spectroscopy
QCL	quantum cascade laser
RANS	Reynolds-averaged Navier–Stokes equations
REMPI	Resonance-enhanced multiphoton ionization
RMS	root mean square
SFG	sum frequency generation
SHG	second harmonic generation
TEM	transmission electron microscopy
TDC	top dead center
TDL	tunable diode laser
TDLAS	tunable diode laser absorption spectroscopy
THz	terahertz
TiRe-LII	time-resolved LII
UV	ultraviolet
VCSEL	vertical cavity surface emitting laser
WMS	wavelength-modulation spectroscopy

20.1 Basics

Combustion is the oldest and one of the most successful technologies of mankind. An early important spectroscopic observation in a combustion process was made in 1859 by Robert Wilhelm *Bunsen* and Gustav Robert *Kirchhoff* [20.1], who recognized the origin of some of the famous dark lines in the solar spectrum first seen by Wollaston and indexed in 1814 by Josef Fraunhofer. Bunsen and Kirchhoff realized that it could not happen by chance that 60 of the Fraunhofer lines coincided with 60 iron emission lines measured in the hot nonluminous flame gases of the Bunsen burner. Their experimental success, however, was based on Isaac Newton, who introduced the word spectrum into physics. After Bunsen and Kirchhoff, spectroscopy in flames became a rapidly growing field. However, the meaning of all the observed lines was not known until 1913 when Niels Bohr formulated his model of the atom. A few years later, Albert *Einstein* [20.2] published his famous paper *Zur Quantentheorie der Strahlung* in which he derived Planck's law and Bohr's rule by discussing the possible elementary process of energy and momentum exchange through radiation. Despite Einstein's clear description of the stimulated emission, the practical application of this principle was achieved only many years later in 1955, first in the microwave region with the maser (an acronym for microwave amplification by stimulated emission of radiation) [20.3] and in 1960, in the visible spectral region with the laser (an acronym for light amplification by stimulated emission of radiation laser) [20.4]. The principle of stimulated emission has now been realized in all states of the matter: solids, liquids, gases and free electrons. This allows the generation of coherent radiation from the far-infrared to the X-ray region. Compared to flame spectroscopy with conventional light sources [20.5] the introduction of tunable lasers and the development of nonlinear optical techniques [20.6] greatly expanded the possibilities of combustion spectroscopy. Now the spectroscopic states of atoms and molecules in combustion process can be observed non-intrusively with high temporal, spectral and spatial resolution. An excellent overview can be found in the book by *Eckbreth* [20.7] and *Kohse-Höinghaus* and *Jeffries* [20.8].

Combustion processes consist of a complex multidimensional and time-dependent interaction of a large number of elementary chemical reactions with different transport processes for mass, momentum and energy. To increase the rate of chemical conversion in practical applications, turbulent flow conditions are mostly applied. Similar to the laminar case, turbulent reactive flows can be described by solving the conservation equations for total species mass, momentum (Navier–Stokes equations) and enthalpy [20.9]. However, solving the conservation equations by direct numerical simulation (DNS) is, even in the days of modern parallel computing, a very demanding task. For a realistic system of liquid hydrocarbon oxidation in an internal combustion engine one would need more than 10^{21} computing steps. Therefore, at present and for the near future direct numerical simulation of three-dimensional turbulent reactive flows in technical combustion systems will not be possible. Instead, turbulence has to be modeled either by the use of Reynolds-averaged Navier–Stokes (RANS) or spatially filtered conservation equations (large-eddy

simulation, LES). Reaction rates can be evaluated with the help of probability density functions (PDF). These models can then be validated by multidimensional non-intrusive laser measurements. Quantities of interest are multifarious and include temperature, chemical species concentration, flow velocities, or their turbulent fluctuations. In addition, such laser techniques can be applied directly in practical combustion systems to study details of the complex interaction of chemical kinetics and transport processes and act as sensors in active control loops to improve fuel efficiency and reduce the environmental effects of combustion.

20.2 Laser-Based Combustion Diagnostics

Laser-based combustion diagnostics as well as other optical diagnostic methods extensively exploit the direct interaction of light and matter, providing an important tool to observe the spectroscopic states of molecules and atoms with high spectral and spatial resolution in time regimes from hours to the femtosecond (10^{-15} s) scale, using optical power densities from picowatts (10^{-12} W) to multi-terawatts (10^{12} W) per square centimeter. A main feature of optical techniques is the non-intrusive in-situ investigation of the sample without significant interference between the sample and the measuring device itself. This is especially important for reactive and aggressive environments such as combustion processes where probe sampling techniques are of questionable value. In all cases light with a certain intensity and temporal and spectral distribution is sent onto or through a sample. The energy re-emitted (in most cases in the form of light) from the interaction region of the irradiated sample is observed and used to characterize the composition and/or structure of the sample. This is done by a detailed analysis of the intensity, spectral composition or angular and temporal distribution of the re-emitted light. Only absorption techniques determine the losses of the incoming light along the line of sight.

Excellent reviews about the advancement of laser-based combustion diagnostics are presented in [20.10] and [20.8]. In general, laser combustion diagnostics can be classified into flow field measurements, scalar field measurements and combined flow–scalar diagnostics. Flow field measurements rely either on Doppler shift (laser Doppler velocimetry, LDV), Doppler broadening (filtered Rayleigh scattering), tracking of particles (particle imaging velocimetry, PIV) or spatial structures of molecular tracers (molecular tagging velocimetry and gaseous image velocimetry). As these flow field diagnostics are discussed in detail in Chap. 5 here the focus is on measurement of scalars such as temperature and chemical species concentrations. However, it needs to be pointed out that high-temperature environments in flames demand for an adaptation of these afore mentioned flow diagnostics. For example, oil droplets commonly used as seed material tracking the turbulent flow in cold PIV or LDV applications are not feasible in flames due to their evaporation. Instead, solid metal-oxide particles with high melting points are used. These materials are more difficult to seed into the turbulent flow. It must be checked that the presence of the seed particles does not impart on the thermokinetic state of the flame. Otherwise, chemical kinetics might be affected by the seed material and the technique is not anymore non-intrusive. For this reason, seeding densities must be fairly low. In consequence, spatial resolution such as in PIV applications or data rates in LDV especially in hot parts of the flame are often lower than in cold flow applications.

Laser-induced fluorescence (LIF) with excitation in the ultraviolet (UV) is frequently used for the detection of minor combustion-related species such as NO, OH, CH, C_2, HCHO. Fluorescing organic molecules have found interest as fluorescent tracers that allow the quantitative observation of fluid mixing processes as well as fuel concentration in combustion devices [20.11, 12]. Further techniques using laser radiation include: optical absorption [20.13, 14] and cavity ring-down [20.15] of CH_3, and two-photon LIF of atoms [20.16]. Raman scattering is frequently used to simultaneously measure the concentration of major combustion species and temperature [20.17]. Nonlinear techniques such as coherent anti-Stokes Raman scattering (CARS) [20.18], degenerate four-wave mixing (DFWM) [20.19] and polarization spectroscopy (PS) [20.20] have been applied for combustion diagnostics. Elastic scattering off droplets is frequently used for observing the droplet distribution in spray systems and Rayleigh scattering from the gas phase is used to measure gas density, and hence, temperature [20.21]. Particle sizes and concentrations are observed by laser-heating the particles and detection of the subsequent incandescence in a process called laser-induced incandescence (LII) [20.22]. The variety of species and techniques that can be probed with laser-based techniques offers the option for simultaneous measurements of several species with similar experi-

mental apparatus, but this in turn can cause reduced selectivity due to interfering signal contributions.

The advantage of laser-based techniques is that they do not intrude into the observed object and that in most cases, information is gained from a well-defined volume element. Whereas absorption techniques typically accumulate information over the line of sight, several techniques generate a signal from a well-defined point in space. Furthermore, the use of pulsed lasers and fast detectors allows time-specific data acquisition.

Several techniques can be expanded to measure combustion-relevant quantities not only in single points in space and time but also to investigate concentrations along the laser beam (one-dimensional spatial resolution), across planes that are defined by laser beams that are expanded to a so-called *light sheet* (two-dimensional spatial resolution). In few cases these techniques are also applied to three-dimensional measurements by combining several two-dimensional images into information that covers a restricted three-dimensional volume element.

Time-dependent measurements are often carried out for point and line-of-sight measurements. With the advent of high-repetition-rate solid-state lasers and fast multi-frame cameras techniques with one- and two-dimensional spatial resolution can also be carried out in a time-resolved way as high-repetition-rate imaging.

Another way to increase the dimensionality of the technique is the simultaneous application of multiple techniques (i. e., multiple species concentrations) or the determination of multiple characteristics of one quantity (i. e., determination of concentration, temperature and/or pressure from the analysis of line-shapes, integral and time-resolved measurements). This was done by wavelength multiplexing or fast wavelength tuning of absorption measurements. Raman scattering per se has the potential to observe multiple species and temperature at the same time. Other experiments require the combination of multiple lasers and/or multiple detectors to gain simultaneous information about multiple species and properties.

In the following sections examples of these various diagnostics approaches for combustion will be presented. The chapter will be structured according to the types of combustion systems rather than the different techniques. Clearly, many techniques can be applied to different combustion systems. This will be mentioned in the corresponding subsections and backed by giving appropriate references.

20.3 Experimental Data Devoted to Validation of Numerical Simulations and Modeling

20.3.1 General Remarks

Combustion technology reached a level of development where further improvements rely on complementary methods. The classical trial-and-error approach based on experimental experience was enhanced by numerical simulation of turbulent combustion processes. A comprehensive model that describes all relevant aspects of turbulent combustion taking place in applications such as internal combustion (IC) engines, furnaces, aero- or stationary gas turbines consists of various submodels that are based on conservation equations, elementary chemical reactions and closures such as physical models for transport processes and the equations of state. Due to the complexity of the underlying chemical and physical processes as well as their mutual interaction, simplifying assumptions are necessary. Because it is not granted a priori that these underlying assumptions are valid for a specific problem, experimental validation is imperative.

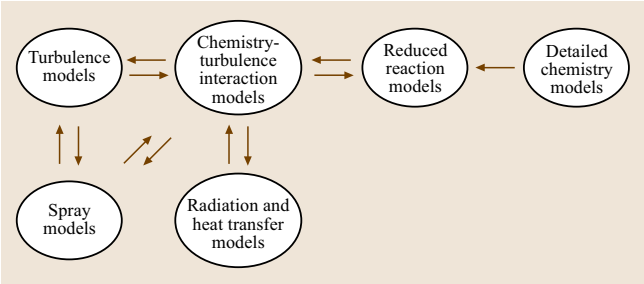

Fig. 20.1 Various submodels that build up a comprehensive model suitable for the numerical simulation of turbulent combustion processes

A thorough experimental validation should consist of each submodel as well all mutual interdependencies between the various physical and chemical processes [20.23]. This is an enormous task and can in practice only be fulfilled piecewise. Figure 20.1 sketches the basic architecture of a mathematical model suitable for numerical simulations. The different submodels call for individual

test rigs and specific diagnostic methods as outlined below.

Laser-based optical diagnostics have emerged in the past two decades as superior methods for studying combustion processes due to their low intrusiveness compared to probe techniques, their high temporal and relatively high spatial resolution. However, their application requires optical access that is not always easy to realize. Especially environments that mimic industrial processes such as internal combustion (IC) engines, gas turbines or furnaces, high pressure, dusty conditions, thermal radiation, and rapid contamination of optical accesses pose a challenge to these methods. Therefore, experiments devoted to the validation of numerical simulations are usually performed under somehow idealized conditions and are briefly discussed in the subsequent paragraphs. Furthermore, inlet and boundary conditions that have a significant impact on any process downstream of a mixing device (nozzle, intake port, etc.) in a burning chamber can be more easily controlled or measured with sufficient precision in test rigs that have been especially designed for validation purposes.

20.3.2 Submodels and Their Specific Demands for Validation

Figure 20.1 shows the modules (submodels) that comprise a comprehensive model describing turbulent combustion processes. Herein, the model for detailed chemistry describes combustion on the basis of elementary reactions. For the combustion of hydrocarbons, detailed chemical reaction mechanisms encompass hundreds of elementary reactions and species [20.9] and are therefore far too large to be used directly in computational fluid dynamics (CFD). Consequently, reduced reaction models are derived from detailed reaction mechanisms that contain a few reactive scalars only [20.24–26]. For the development and validation of chemistry models, a large and reliable experimental database is required. To circumvent problems linked to turbulence, chemical kinetics experiments are carried out for well-characterized boundary conditions such as laminar low-pressure flames [20.27, 28], flow reactors, shock-tube experiments [20.29] or rapid compression machines [20.30]. A survey of experimental methods to measure the chemical rate coefficients of single elementary reactions necessary for a detailed chemical reaction mechanism can be found in [20.31].

Turbulence models describe the properties of the flow field. The state of the art is to use the Reynolds-averaged Navier–Stokes equations (RANS) is used in most CFD models [20.32]. Within this approach, averaged conservation equations are solved for the statistical moments, assuming isotropic conditions. Unclosed terms are modeled on the basis of one- or two-equation models [20.33]. As a result, the CFD model predicts mean values and fluctuations in a pointwise manner. No spatially -correlated information is obtained. For this reason, experimental validation of RANS-based models can be restricted to quantitative, single-pulse, and pointwise measurements of species concentrations, temperature, and velocities. Of special importance are the experimental determination of well-characterized inlet conditions and the dissipation rate of turbulent kinetic energy based on two-point correlations.

Large-eddy simulation (LES) is an approach that has recently been extended to describe turbulent combustion. The conservation equations are spatially filtered before they are numerically solved on a spatial grid. Phenomena occurring on a scale smaller than the filter width are accounted for by subgrid-scale models [20.34]. The implicit LES combustion approach has various advantages. With increasing computational power, an increasing fraction of turbulent structures will be resolved, and the importance of an elaborated subgrid model will decrease. Unsteady effects can be described owing to the temporal resolution of the LES approach, and spatially correlated information is available. As a consequence, the requirements for the experimental validation increase. In addition to quantitative pointwise measurements, spatially correlated information is needed for validation purposes, such as turbulent length scales in different spatial directions [20.35] or gradients of scalar quantities such as temperature [20.36] or mixture fraction [20.37, 38]. It is worth noting, however, that direct numerical simulation (DNS) of the conservation equations is of growing importance for submodel development and validation [20.39]. Within this approach the grid resolution resolves all turbulent structures but – at least for three-dimensional (3-D) applications – it still relies on reduced chemical reaction models. DNS is a tool that ideally supplements experimental approaches.

In turbulent flames, a strong mutual influence of chemical reactions and the turbulent flow [20.40] is evident. Various chemistry–turbulence interaction models [20.41–43] exist. The state of the art is the commonly used flamelet and presumed probability density function (PDF) approach. However, a more comprehensive approach is to derive a PDF transport equation that may be solved by Monte Carlo methods or by unsteady flamelet modeling [20.44]. This approach shows great potential to describe, for example, flame extinction but is compu-

tationally expensive. To develop and validate submodels for the chemistry–turbulence interaction, quantitative experimental information for various simultaneously measured quantities is necessary, such as the main species, temperature, velocity, and reactive (radical) species. This requires sophisticated optical techniques, especially the combination of reliable velocity measurements simultaneous to main species concentration measurements. Although the combination of Raman, Rayleigh, and laser-induced fluorescence (LIF) [20.45] has already been developed to a high degree, the additional simultaneous measurement of gas velocities is at an early stage. Early approaches are discussed, for example, in [20.46–49] and show great potential.

In the case of liquid fuels, a submodel is required that describes breakup and the formation of a dense thin spray, as well as the evaporation and turbulence modulation [20.50]. The numerical and experimental investigation of this complex phenomenon is an ongoing task. Laser-based techniques such as spontaneous Raman scattering suffer on the one hand from optical density (multiple scattering in dense sprays, strong extinction, liquid core) as well as large local variations in number density at the interface between the liquid and gas phases, which necessitate a large dynamic range of the detector. However, for the development and validation of spray submodels, quantitative information regarding the liquid and gas phase is required. For the liquid phase, droplet diameters, droplet velocities and droplet size distribution need to be measured. For the gas phase, the local fuel–air ratio, temperature distribution, and gas velocities must be recorded. While for stationary conditions pointwise measurements such as phase Doppler anemometry (PDA) [20.51] are appropriate to characterize the liquid phase, the level of complexity rises if the spray characteristics for unsteady conditions (e.g., pressure oscillations that give rise to time-dependent spatial droplet distributions) are investigated. For this purpose, at least two-dimensional techniques, such as the interferometric particle imaging technique [20.52], are required. In addition, laser-induced fluorescence (LIF) schemes have been used in combination with Mie scattering to determine Sauter mean diameters [20.53, 54].

In many practical applications, it is necessary to account for radiation effects, particularly to predict thermal stress in walls correctly. The state of the art is to treat radiation either by integral methods [20.55–57] or by differential techniques. To account for the spectral characteristics of radiation, gray gas models [20.58] or spectral line models [20.59] are used. In open flames thermal radiation can be measured directly by pyrometers. Convective heat transfer to walls in the case of enclosed combustion can be measured spectroscopically as well, using a combination of thermographic phosphors and filtered Rayleigh scattering [20.60] or LIF [20.61].

20.3.3 Example: Generic Turbulent Flame

To ensure that a comprehensive model is valid for a certain range of operational conditions and capable of predicting trends correctly, a series of flames must be investigated where general parameters such as Reynolds number and fuel composition are varied. The burner configuration should exhibit some important aspects that

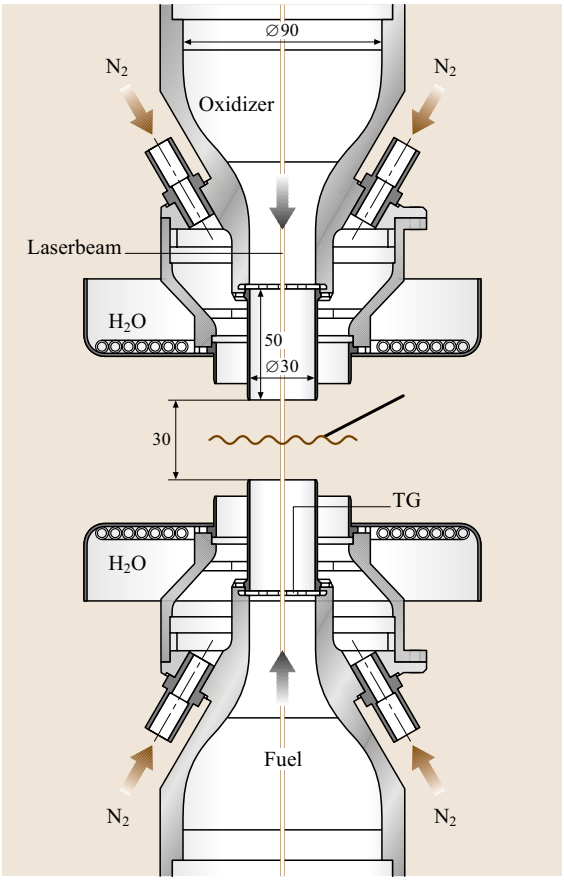

Fig. 20.2 Sketch of a turbulent opposed-jet burner. TG: perforated plates. The laser beam exciting Raman/Rayleigh scattering was directed along the symmetry axis of the burner. Laser radiation for LDV, PIV and LIF diagnostics entered the region of interest from the side

may arise in a similar manner within a practical realization. To demonstrate some of these special needs of experiments devoted to validation of numerical simulations, some recent measurements on a turbulent opposed jet burner are briefly outlined.

Opposing jets are a generic configuration in many industrial applications where fuel and oxidizing air impinge on each other, mix on a molecular level, and finally burn. The progress of chemical reactions in this turbulent mixing layer, however, depends on the mixing time, which can be quantified by the scalar dissipation rate [20.44]. If the residence time compared to typical finite-rate chemical time scales is too short, chemical reactions may even be extinguished. Flame extinction is indeed a problem in various practical combustion processes such as lean, low-NO_x gas turbines or direct-injection IC engines. The advantage of a generic setup such as the turbulent opposed jet burner is that the flow conditions leading to extinction can be well controlled. The location where extinction most probably starts is limited to a rather small volume. Therefore, data recording can be concentrated to the most important region, cutting down experimental effort enormously.

Figure 20.2 shows the cross section of a burner that allows to study these effects by detailed laser diagnostics. Details can be found in [20.37, 62]. Air emanating from the upper nozzle impinges on a rich methane/air mixture outside the flammability limits from the lower nozzle. The momentum of both streams is equal. Turbulence is enhanced by perforated plates located downstream of the contraction of each nozzle. A stagnation plane is formed which is located at the half nozzle distance (15 mm). The nozzles (30 mm diameter) are surrounded by a 60 mm-wide nitrogen co-flow to prevent mixing with ambient air. Optical access is possible along the burner center line through the central holes of the perforated plates and from the side perpendicular to the burner axis. The Reynolds number of the flows can be varied from stable towards extinguishing conditions and the equivalence ratio of the fuel can be varied.

To characterize the inflow conditions, the flow field between the two nozzles and the scalar field, the following diagnostics have been applied:

- Hot wire anemometry: nozzle exit velocity profiles and turbulent time scales [20.62].
- Two-dimensional laser Doppler velocimetry (LDV): radial and axial profiles of mean velocity, turbulent kinetic energy and Reynolds stress components [20.63].
- Planar LIF and particle imaging velocimetry (PIV), in part simultaneously: OH radical distribution during stable and extinguishing conditions, flame orientation, flow field conditioned on flame front [20.64, 65].
- Picosecond time-resolved LIF: absolute mean OH profiles, OH time series to characterize OH statistics [20.66].
- One-dimensional Raman/Rayleigh scattering: mean and fluctuations of major chemical species concentrations, temperature and mixture fraction, scalar dissipation rate [20.37, 63].

This database allows detailed comparisons with results from numerical simulations. Control and knowledge of the inlet boundary conditions as well as flow and scalar field are essential. Of special interest in this configuration are finite-rate chemistry effects due to the turbulence–chemistry interaction and turbulent mixing. The data have been used for comparison with Monte Carlo PDF models in combination with a RANS approach [20.63] and combustion LES [20.67]. Some of the results are discussed in Sect. 20.4.3 and in [20.37, 63].

20.4 Application of Laser-Based Techniques

20.4.1 Detection Sensitivity, Selectivity and Resolution

The detection sensitivity attainable in combustion environments is an essential parameter for the application of the various laser-based techniques. These limits cannot be stated generally since they depend on the line strength of the species to be detected, system parameters such as absorption length, response time or optical output power [20.68], while especially for in-situ measurements temperature and pressure in the probe region and disturbing effects of the in-situ beam path (dust, background emission) are most important factors for system-specific detection limits. A figure of merit for absorption spectrometers is the minimum detectable absorption change (MDA $= \Delta I/I_0$). In a precisely controlled absorption cell 10^{-3} is achievable with non-coherent light sources on a routine basis, while the

Method	Species	Transition	Energy of transition (cm^{-1})	p (total) (bar)	T (K)	Environment	Detection limit (abs.) (cm^{-3})	Detection limit (ppm)	Ref.
LAS	HO_2	$2\nu_1$-band	6625.8	6.7 (−3)	295	photolysis cell	3 (13)[b]	16.8	[20.69]
	NO	(3, 0)-band	5524	1	1040	H_2/air flame	2.7 (15)	100	[20.70]
	CH_4	$2\nu_3$-band	6048	1	300	absorption cell	1.8 (14)	7	[20.71]
	NH	$A^3\Pi - X^3\Sigma(0, 0)$, $R_2(8)$	29762	1	2100	$NH_3/N_2/O_2$ flat flame, $\phi = 1.28$	3.0 (13)	7.9	[20.72]
CRDLAS	OH	$A^2\Sigma - X^2\Pi(0, 0)$	32500	0.04	1800	CH_4/air flame	2.0 (10)	0.12	[20.73]
	CH_3	$^rR(6, 6)$	3224.42	0.05	1400	CH_4/air flame	1.5 (13)	57.6	[20.74]
ICLAS	HCO	$A - X(09^00) - (00^10)$	16260	0.047	1800	$CH_4/O_2/N_2$-flame	1.4 (11)	0.57	[20.75]
LIF	OH	$A^2\Sigma - X^2\Pi(0, 0)$	32500	1	2000		25.6 (11)	0.07	[20.76]
		$A^2\Sigma - X^2\Pi(0, 0)$	32500	9.2	1700	$C_2H_6/O_2/N_2$-flame	1 (14)	2.5	[20.77]
	NO	$A^2\Sigma - X^2\Pi(0, 0)$	44247.8	1	2000		8 (11)	0.22	[20.7]
DFWM	OH	$A^2\Sigma - X^2\Pi(0, 0)$	32500	1	1700	premixed CH_4/air flame	2.0 (13)	4.66	[20.78]
	OH	$A^2\Sigma - X^2\Pi(0, 0)$	32500	1	2200	premixed CH_4/air flame	7.0 (13)	21.1	[20.79]
	NH	$A^3\Pi - X^3\Sigma(0, 0)$	29762	1	2100	$NH_3/O_2/N_2 = 2.1/1.5/1.0$			[20.80]
	CH_4	ν_3, Q(5)(1, 0)	3017.5	1 (−6)	300	CH_4/N_2	1.5 (11)	6174	[20.81]
	HF	ν_1, R(5)(1, 0)	4000	1 (−3)	300	HF/He	1.0 (10)	0.41	[20.82]
	CH_3	$3s^2A_1' - 2p^2A_2''$	46185	1	1600	$CH_4/N_2/O_2$ flame, $\Phi = 1.25$	3.0 (14)	65	[20.83]
	C_2	$d^3\Pi_g - a^3\Pi_u$	19354	1	3000	C_2H_2/O_2 flame (welding torch)	5 (11)	0.19	[20.84]
CARS	C_2	Q(10)(1, 0)	1611.7	1	2500	C_2H_2/O_2 flame (welding torch)	1.0 (10)	0.003	[20.85]
	OH	O_1(7.5)(1, 0)	3065.3	1	≈ 1800	H_2/air flame (premixed)	1.0 (13)	2.5	[20.86]
	CO	Q(10)(1, 0)	2143	1	2000	flame	4.8 (16)	13000	[20.87]
	CO	Q(10)(1, 0)	2143	1	2000	flame	7.3 (16)	20000	[20.88]
	OH	Q_1(7.5)(1, 0)	3560	0.0106	300	HNO_3/He	1.4 (15)	5400	[20.89]
	NH_2	ν_1, $/2\nu_4$, (1, 0)	3210	0.0005	300	NH_3	1.2 (12)	99	[20.90]
REMPI	1, 1 − DCE	$p^{-3}d(1 + 1)$	33863.9	–	5	molecular beam	6 ppbv[a]		[20.91]
	C_6H_6	$S_0 - S_1(1 + 1)$	38610	–	5	molecular beam	0.09 ppbv[a]		[20.91]
	C_2H_4	3 + 1	68181	–	5	molecular beam	10 ppbv[a]		[20.92]
PS	C_2	$d^3\Pi_g - a^3\Pi_u(0, 0)$	19357	1	1800	C_2H_2/O_2-flame	1.0 (12)	0.19	[20.93]
	OH	$A^2\Sigma - X^2\Pi(0, 0)$	32500	1	2100	propane/air flame	1.0 (13)	2.9	[20.94]

[a] Mass-spectrometric inlet system with molecular-beam sampling; the detection limits are referred to the concentration levels in the original sample mixture
[b] $1(11) = 1 \times 10^{11}$
[c] Mostly estimated temperatures

Table 20.1 Detection limits for minor, combustion-relevant species of various linear and nonlinear laser-spectroscopic techniques discussed in this review. The spectroscopic transitions probed for each species, their transition frequency (in cm^{-1}), total pressure p, an estimate of the temperature T, and the sample environment are given. The detection limits are approximate values, either determined directly or extrapolated from the respective experimental data ◀

best laser-based spectrometers provide MDAs in the 10^{-8} range, resulting in a dynamic range of 10^2–10^7. Table 20.1 is a (far from complete) collection of experimental work in the literature that stated the detection limits of combustion-relevant minor species for the various techniques introduced here at different pressures and environments to give a general impression of their practical applicability.

Species selectivity is another feature that has improved greatly through the introduction of lasers, since high radiance and small source linewidth are available simultaneously. For the case of continuous-wave (CW) lasers (diode and dye lasers) the laser line width can be of the order of 10 MHz, compared to molecular linewidths in the gas phase of several 100 MHz under low-pressure conditions and several GHz at atmospheric pressure. Ultimate selectivity can be ensured, if a spectral region or so-called *spectral window*, can be found where the species under investigation is the only (or at least the dominant) absorber.

Spatial and temporal resolution is another attribute that was improved significantly by the advent of lasers in diagnostics. Using the extremely short pulses of Q-switched or mode-locked lasers, the shortest turbulent time scales such as Kolmogorov time scales (in the µs regime) can be resolved even for very high turbulence levels. In contrast, the spatial resolution of laser diagnostics is in general insufficient to resolve the smallest fluid flow structures (Kolmogorov scales) or the smallest scalar structures (Batchelor scales) in turbulent flames. The latter is even worse for high-Schmidt-number flows. The spatial resolution is limited by the extension of the laser beam profile in the probe volume. Laser operation in the TEM_{00} transversal mode using short focal lengths and large beam diameters through the last convex lens are typical measures taken to reduce the probe volume size. Constraints resulting from the high flame temperatures, flame enclosure, optical damage of windows used for optical access or gas breakdown, pulsed laser operation etc. typically limit the attainable spatial resolution to 100 µm at best in each direction of space. For high Reynolds numbers this is much larger than the smallest flow and scalar scales. Therefore under-resolving probe volumes act as spatial filters. Depending on the quantity, this under-resolution can cause a bias [20.95].

20.4.2 Laminar Flames

Low-Pressure Flames

Laminar premixed flames at low pressures on a flat-flame burner constitute an ideal experimental arrangement to study the interaction of elementary chemical combustion reactions. Experimental data on temperature as well as on concentration profiles for stable and unstable species are used to validate and further develop mathematical models that predict these profiles by numerical solution of the underlying conservation equations, including convection and molecular transport processes.

Figure 20.3a shows such an arrangement used for a low-pressure $CH_4/O_2/NO$ flame. Absolute concentration profiles of methyl and hydroxyl radicals as well as nitric oxide are measured by laser absorption spectroscopy. CH radicals are detected by LIF. In this example (Fig. 20.3b) the shape and absolute values of the concentration profiles for OH and CH_3 radicals as well as the initial reduction of nitric oxide are predicted well by the models. Further improvements in sensitive absorption spectroscopy in flames can be obtained by using long-path absorption techniques such as cavity-ring-down laser-absorption spectroscopy CRDLAS [20.96] and intracavity absorption.

Resonance-enhanced multiphoton ionization (REMPI) – combined with molecular-beam sampling mass spectrometry – is a highly selective and sensitive technique for combustion diagnostics and environmental chemical analysis [20.91]. Detection sensitivities in the lower ppb to ppt (per volume) range for chloroethylenes, toluene and p-chlorphenol have been obtained in a helium carrier gas, whereas – due to cross sensitivities and nonresonant multiple-species ionization – this limit increases into the percent range in sample mixtures drawn directly from real-world industrial devices. To increase selectivity with an appropriate choice of excitation wavelengths various electronic transitions in large molecules can be accessed in one- or multiphoton transitions from which ionization is accomplished in a second step at the same or different laser frequency. Portable instruments have been designed that offer sufficient flexibility in switching between different laser wavelengths for the excitation of numerous unsaturated hydrocarbons, radicals and polycyclic aromatic hydrocarbons (PAH) for monitoring in real time. An example

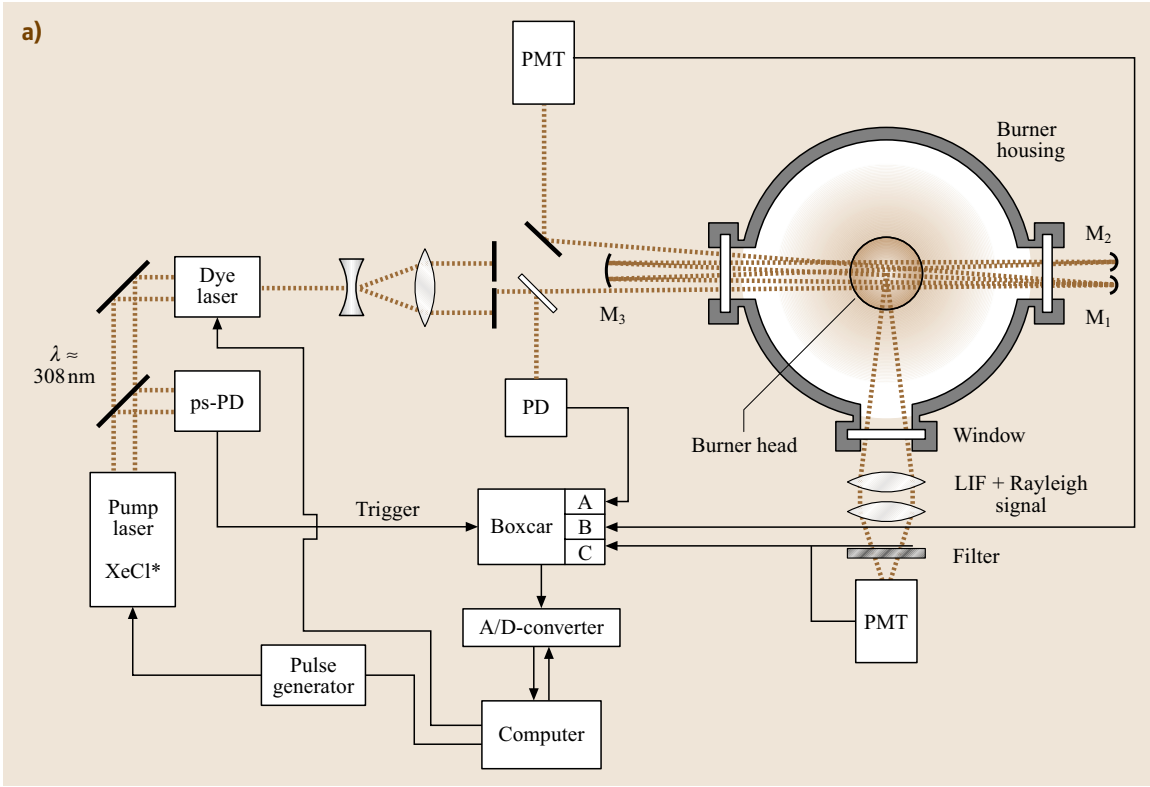

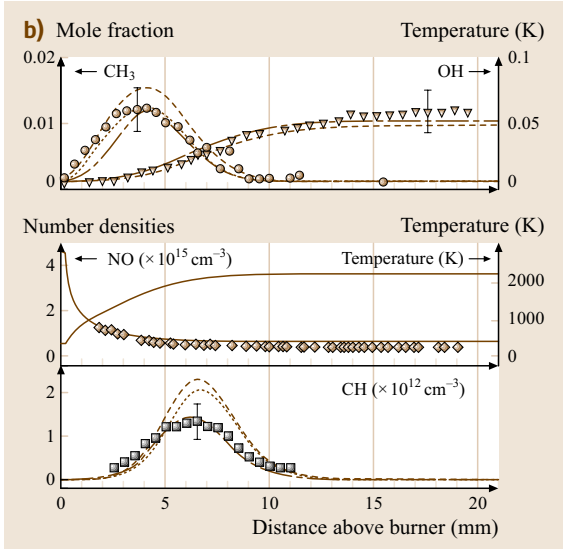

Fig. 20.3 **(a)** Experimental setup for laser absorption and LIF spectroscopy in low-pressure flames using tunable dye lasers and a long-path White-mirror arrangement. PD: photodiode, (ps-PD: picosecond resolution) **(b)** Comparison of measured and calculated concentration profiles in a laminar $CH_4/O_2/NO$ premixed flame at 1.33×10^3 Pa. Models: GRI 2.11 (*dashed*), Warnatz (*dash-dotted*) and Lindstedt (*dotted*) [20.97]

is the extraction and sensitive online REMPI detection of automotive exhaust gas pollutants at different engine loads and speeds [20.92].

Laser-ionization mass-spectrometric (MS) detection has also been successfully employed for spatially-resolved species analysis in low-pressure sooting flames to study the chemical kinetic mechanisms responsible for soot precursors and particle growth. Most soot precursors possess absorption maxima at 200–300 nm with ionization thresholds of 6–9.5 eV. Special scavenging techniques allow the sampling and subsequent REMPI/MS analysis of possible radical precursors that could act as important building blocks for the growth history of soot particles and carbon cages such as C_{60}, C_{70} in flame gases. *Homann* et al. [20.98] determined correlations between the number of hydrogen and carbon atoms contained in highly-condensed isomers of

polycyclic aromatic hydrocarbons (PAHs) as precursors of C_{60} and their formation and destruction in low-pressure sooting flames. These authors claim the C_{60} cage is the final product in the chain of hydrogen abstraction, folding, condensation and isomerization of smaller fragments of five- and six-membered aromatic-ring condensates [20.99]. The detailed study of the fragmentation behavior, ionization efficiencies and absolute calibration of a variety of PAHs is essential for quantitative comparisons with numerical modeling of soot in flames [20.100].

Higher Pressure Flames

In laminar flames spatially-resolved temperature measurements using coherent anti-Stokes Raman scattering (CARS) are possible with high precision. Figure 20.4 shows a comparison of the temperature readings deduced from the pure rotational spontaneous Raman spectrum (squares) and the Q-branch vibrational CARS spectrum of molecular nitrogen (triangles) acquired at the same location and under the same operating conditions of a stable high-pressure premixed methane/air flame. Both data sets agree within the 3% limit of precision estimated from the spontaneous Raman data [20.101]. The pure rotational spontaneous Raman spectra exhibit well-resolved lines even at the highest pressures investigated. The spectrally dense CARS Q-branch of N_2 suffers from partial collisional collapse of its rotational structure at the band origin, which usually degrades the temperature measurement accuracy at low temperatures (300–700 K) and even higher pressures [20.102]. Temperature measurements using pure rotational CARS have also been carried out in laminar flames and are often an alternative if higher precision is required in the low-temperature (300–870 K) higher-pressure (1–15 bar) regime [20.103].

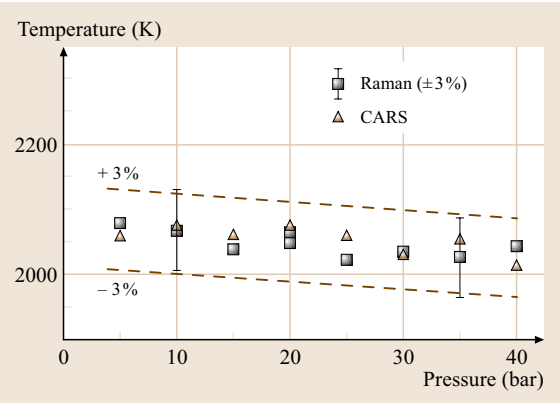

Fig. 20.4 Comparison of measured temperatures (deduced from fitting spectral shapes) in a methane/air flame at various pressures. Spectra were obtained from either spontaneous pure rotational Raman scattering (*squares*) or Q-branch vibrational CARS (*triangles*) measurements of molecular nitrogen at the same location in the post flame gases [20.101]. Shown as *dashed lines* are the ±3% temperature measurement accuracies inherent in fitting results from the spontaneous Raman data

For the detection of minor species fully resonant nonlinear techniques, such as DFWM, polarization spectroscopy (PS) and resonance-enhanced CARS are necessary to achieve sufficient detection sensitivity. DFWM spectra of electronic transitions have been recorded and gas temperatures determined in flames from OH, NH [20.80], NO [20.104], CN [20.105], CH [20.106], and in cell experiments from NO_2 [20.107], HCO [20.108]. Using polarization spectroscopy, important radicals in flames such as OH and NO were analyzed by *Nyholm* et al. [20.109] and *Löfstedt* et al. [20.110], respectively. The potential of polarization spectroscopy for two-dimensional imaging of these species and for single-shot temperature measurements was also shown [20.94, 109]. Because the total angular momentum of the photon–molecule system is conserved during the interaction process, a proper choice of beam polarizations can be exploited to excite P-, Q- or R-branch transitions selectively. Careful modeling of the PS spectral structure for OH and NH is essential for in-situ temperature measurements in atmospheric-pressure flames [20.20]. The intensity and collision frequency dependence of PS signal intensities has been modeled using the rigorous approach of direct numerical integration (DNI) of the Liouville equation for the density operator [20.111], which promises to address these effects more closely in practical measurement situations. To increase the Raman resonant susceptibility in a CARS interaction process, Stokes, pump and the generated anti-Stokes signal frequency should be tuned close to single-photon-allowed electronic transitions in the studied molecule. This makes the experimental approach rather complicated, since up to three narrow-band tunable laser systems must be employed. Nevertheless, spatially-resolved measurements of C_2 and OH distributions in pressurized flames have been performed by *Attal* et al. with high detection sensitivities [20.85, 86].

20.4.3 Turbulent Combustion

Fundamental studies of flames are based on various experimental setups tailored to select certain aspects of

combustion. Practical combustion processes traditionally rely on non-premixed, turbulent combustion for reasons of efficiency and safety. However, demands for low NO_x emissions require the use of lean premixed combustion such as in stationary gas turbines. Detailed information about chemistry–turbulence interaction and complex recirculating flows is necessary to invent models suitable for simulating practically relevant flames. The understanding of the underlying processes is best verified through direct comparison of numerical simulation results with experimental measurements of properties such as temperature and species concentrations. Furthermore, detailed knowledge of the underlying flow field patterns is essential.

Laser-based techniques are ideal for studying turbulent processes since they do not disturb the flow and, using pulsed lasers, they are fast enough to resolve the smallest relevant timescales. Statistical investigations of correlations between temperature and the concentrations of different reactive species have been investigated using point measurements based on Rayleigh and Raman scattering and LIF diagnostics. Quantitative comparisons of the thermokinetic states in turbulent flames with idealized representations, such as steady strained laminar flames, perfectly stirred reactors, or adiabatic equilibrium are thus possible. Comparisons with direct numerical simulation (DNS) calculations on the other hand give insight into the validity of some of the basic assumptions upon which turbulent combustion models are built and allow the evaluation of the predictive accuracy, strengths and limitations of a wide variety of combustion models.

Revealing the structure of turbulent flames has attracted increasing interest and has been addressed using laser imaging for temperature, mixture fraction and reactive species such as OH and CH [20.113]. Simultaneous measurements of multi-scalars, yielding scalar dissipation rates, are critical for the validation of turbulent combustion models describing molecular mixing and extinction processes [20.37]. Simultaneous measurements of Rayleigh scattering and fuel Raman imaging provide information about temperature distribution and mixing. Both can be used to further quantify OH-LIF data by correcting for temperature and collisional quenching effects. These measurements (see Fig. 20.5) showed the correlation between the reaction zone width and jet Reynolds numbers and addressed the influence of local dissipation rate on flame extinction [20.112]. A review article that covers this topic in detail is given by *Masri* et al. [20.114].

With careful spectral filtering Raman measurements are possible even in dense media involving strong Mie scattering from small droplets. By forming a thin light sheet from the output beam of a XeF excimer laser at 351 nm *Decker* et al. [20.115] were able to image the Raman-scattered light from a dense cryogenic jet of liquid nitrogen onto a charge-coupled device (CCD) camera to study the evaporation and breakup of the fluid nitrogen exiting through a small (1.9 mm diameter) nozzle as employed in rocket engines, and performed temperature and density measurements from the Stokes/anti-Stokes intensity ratio and the Rayleigh intensity, respectively.

There are numerous applications of CARS as a temperature measurement technique in turbulent combustion processes. From the Q-branch spectrum of nitrogen, temperature measurement accuracies of 2% or better within a single laser pulse have been obtained [20.116], and applications have spread into diverse fields of technical combustion systems such as liquid-fuel combustors and swirl burners, IC engine combustion [20.117], gas turbines and jet propulsion devices [20.118–120] etc. High-resolution line-shape measurements of combustion-relevant species such as N_2 [20.121], O_2 [20.122], H_2 [20.123], CO [20.124], CO_2 [20.125], and NO [20.126] have improved modeling of CARS spectra – an important prerequisite for

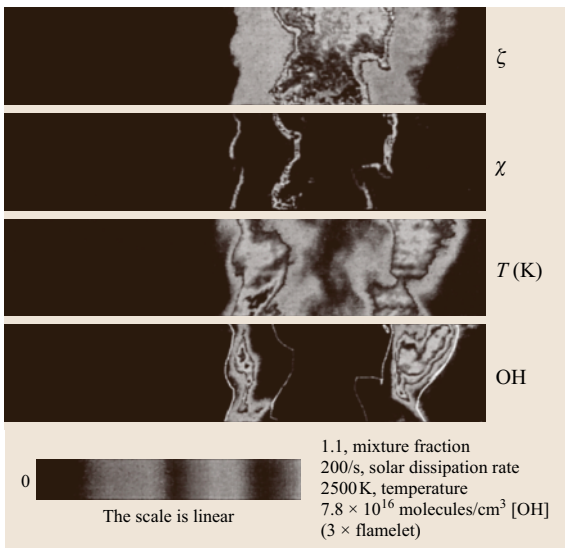

Fig. 20.5 Images of mixture fractions (ξ), scalar dissipation rates (χ), temperatures (T) and OH concentrations in turbulent CH_4/air diffusion flames obtained by 2-D Raman, Rayleigh and LIF spectroscopy [20.112]

precise temperature measurements through spectral simulation. Figure 20.6 shows temperature profiles from single-shot broadband N_2-CARS thermometry across the shear layer region of a supersonic air-fed combustor fueled with hydrogen [20.119]. The left-hand side of the graph depicts the mean temperature across the shear layer that is formed after injection of the fuel hydrogen into the supersonic air flow; it slowly decreases as the measurement point moves upstream. The necessity to do single-pulse measurements is clearly demonstrated. In the temperature histograms on the right-hand side of the picture the fluctuation in this parameter is illustrated as a function of position, which gives a more-detailed picture of the mixing properties and burning behavior of the combustor.

Multidimensional Diagnostics

While two-dimensional images yield a wealth of structural information [20.127, 128] and provide insight into the combustion process (Fig. 20.7), in many cases more information is desirable.

Multispecies measurements are of major interest to fully describe the thermochemical state of the observed volume element and to understand correlations between different species concentrations and potentially their local variations. In some cases linear combinations of different scalars correlate well with quantities such as heat-release rate that are otherwise difficult to measure [20.128]. For multispecies point measurements Raman scattering has been applied especially for the investigation of turbulent flames [20.17]. These techniques have been expanded for line measurements [20.37, 95, 129, 130] and allow – under special conditions – spatial multidimensional detection with limited resolution [20.131]. For two-dimensional imaging with high resolution, however, laser-induced fluorescence has been used to observe either different species at the same time in the same volume element [20.128, 132, 133], or to use the photophysical properties of fluorescent molecules to obtain information about more than one quantity (i. e., the concentration and the ambient conditions) [20.134, 135]. This will be shown in the following sections for organic tracers that allow not only concentration measurements but also the observation of temperature and local oxygen concentrations.

Turbulence is a three-dimensional process and therefore, three-dimensional measurements are desirable. Furthermore, the temporal behavior of concentrations and temperatures is of interest to understand turbulent phenomena, ignition, combustion instabilities, and transient phenomena. Imaging with high repetition rates

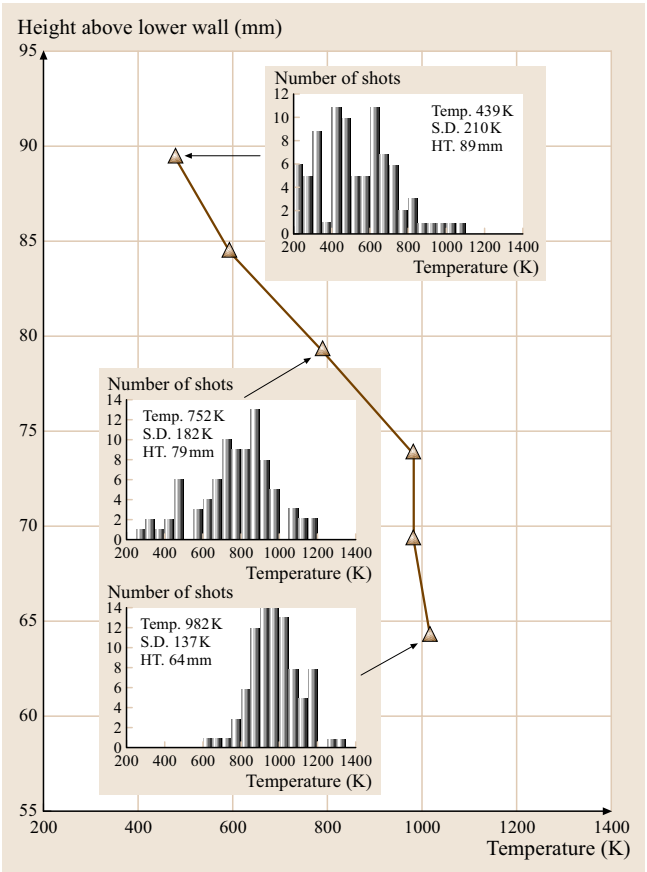

Fig. 20.6 Temperature distribution deduced from H_2 Q-branch CARS spectra across the shear layer of a supersonic hydrogen-fueled combustor [20.119]

that allows movie-like observation of two-dimensional scalar fields has been developed [20.136–138]. These techniques have become especially interesting since combustion modeling moved beyond the calculation of temporally-averaged quantities. For comparison with the results of large-eddy simulations (LES) and direct numerical simulations (DNS) both structural information and the temporal variation of structures is required.

Simultaneous Multispecies Detection in Turbulent Flames

Multi-Scalar 1-D Raman/Rayleigh Measurements in Turbulent Opposed Jet Flames. Simultaneous Raman/Rayleigh measurements allow the measurement of all main species (concentrations $> \approx 0.5$–1%) and temperature. In hydrocarbon-fueled combustion, inter-

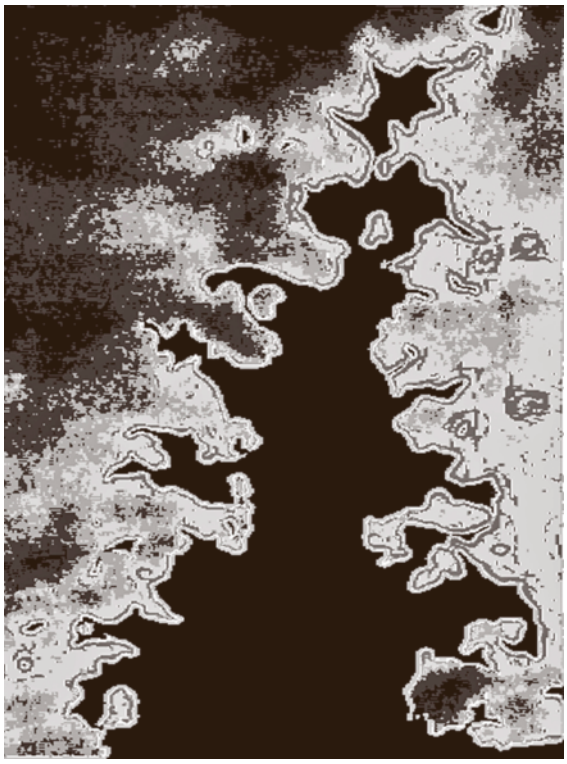

Fig. 20.7 OH-LIF distribution in a turbulent 150 kW flame. Size of the visualized field: $150\,\mathrm{mm}^2 \times 110\,\mathrm{mm}^2$ [20.140]

ference with LIF needs to be avoided. Therefore, the use of intense, pulsed 532 nm radiation from a frequency-doubled neodymium-doped yttrium aluminium garnet (Nd:YAG) laser is beneficial [20.139]. Figure 20.8 shows the experimental setup for multi-scalar measurements in turbulent partially-premixed opposed-jet flames [20.37, 67]. The burner is presented in Fig. 20.2 (Sect. 20.3.3).

A pulsed frequency-doubled Nd:YAG laser with a pulse energy of 900 mJ and a pulse duration of 10 ns was used to excite Raman/Rayleigh scattering. Two pulse stretchers were employed to lower the intensity below the threshold where optical breakdown occurred. The stretched pulse was focused ($f = 1100\,\mathrm{mm}$) from bottom to top along the vertically orientated symmetry axis of the turbulent opposed jet burner, passing through the central holes of the turbulence generating plates. In this arrangement the laser beam intersected the flame front on average perpendicularly and beam-steering effects were mostly avoided.

Perpendicular to the laser beam, inelastically scattered Raman photons within $\pm 1.8\,\mathrm{mm}$ of the focal point were imaged on the entrance slit of a 310 mm imaging spectrograph. For this purpose, a specially designed achromatic corrected imaging lens system with a diameter of 150 mm and $f_\#$-numbers of 2.0 and 4.0 at the object and image side, respectively, was used. At the exit plane of the imaging spectrometer, rovibrational Raman bands of the main species (H_2, O_2, N_2, CO, CO_2, H_2O, and CH_4) were recorded spectrally and spatially resolved with a Gen IV intensified CCD (ICCD) camera. Rayleigh scattering was imaged onto a second ICCD camera with a perpendicular detector arrangement.

Binning the Raman signals in the spatial direction parallel to the laser beam resulted in a probe volume of $350 \times 360 \times 110\,\mu\mathrm{m}^3$; the first dimension is along the laser beam and thereby across the reaction zone, the second is determined by the measured beam waist of 360 µm at the focal point and the last is due to the 220 µm width of the spectrograph entrance slit. This width is a compromise between the resolution necessary to discriminate the CO from the N_2 Raman signal and maximization of the signal. The overall resolution was limited by the diameter of the beam waist and exceeded the required resolution only slightly. Limitations in resolution are well-known phenomena in time-resolved Raman scattering due to the extremely weak signal of the scattering process.

Exemplarily, a partially-premixed flame is considered here. Air emanates from the upper nozzle and a rich methane/air premixed gas mixture (equivalence ratio 2.0) outside the flammability limit emanates from the lower nozzle. In the transient mixing layer both gas streams form an ignitable mixture and a partially premixed turbulent flame can be stabilized. As the most important quantities, the mixture fraction f and the temperature T along the center line are shown in Fig. 20.9. For comparison, this figure includes the non-reacting (isothermal) and combusting case.

In comparison to non-reacting conditions, the mean mixture fraction is almost unaltered by chemical reactions and heat release. The mixture fraction fluctuations, however, are very high for the non-reacting case and are significantly decreased, most likely by viscous effects, in the combusting case. Very close to the stagnation point a stoichiometric mean mixture fraction of $f_{st} = 0.51$ and a maximum mean temperature of approximately 1250 K were observed. Intense spatial fluctuations of the reaction zone cause the relatively small mean temperature. Depending on the instantaneous flow field with different local strain rates, the maximum temperatures vary between 600 and 2050 K.

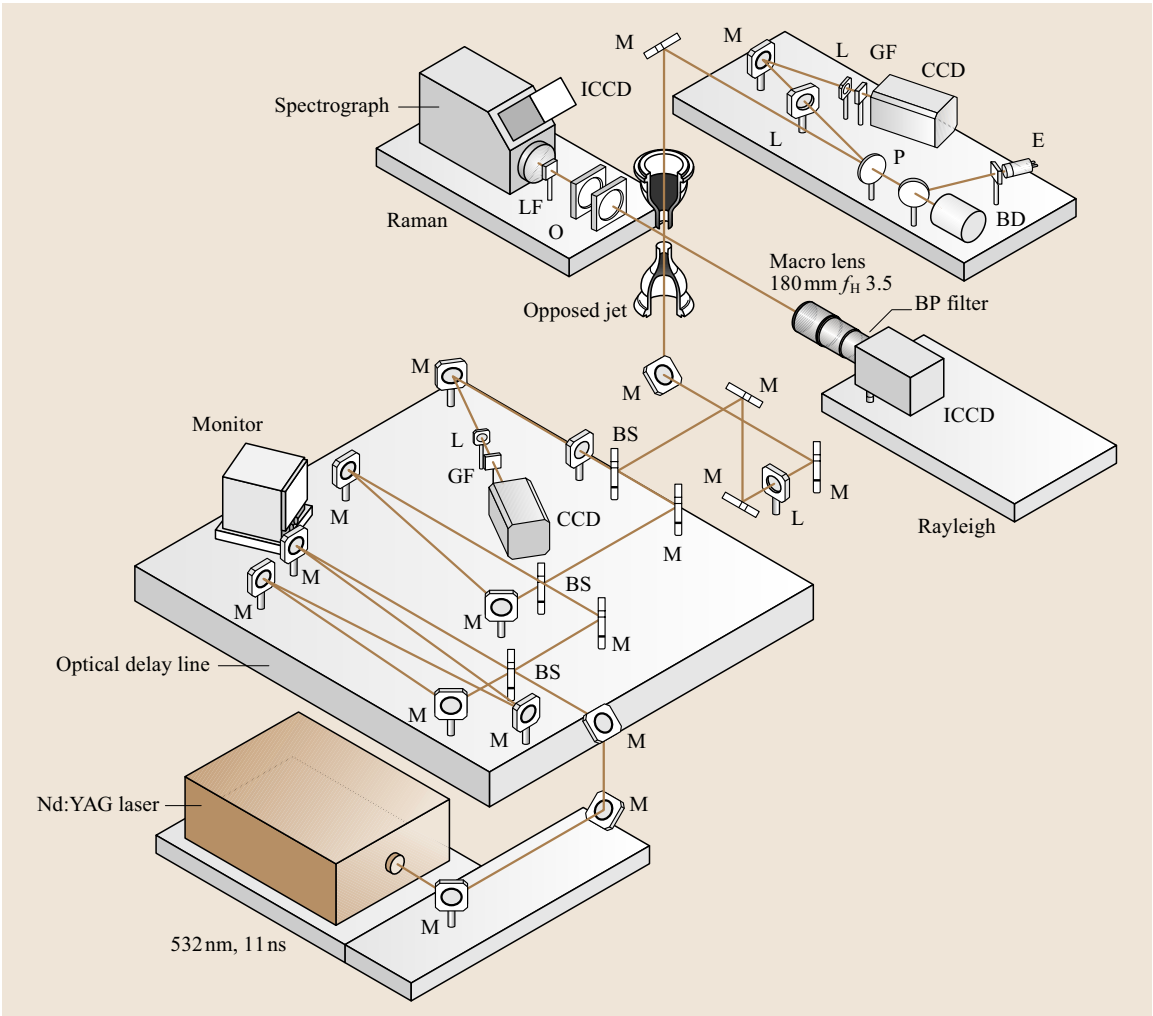

Fig. 20.8 Sketch of the Raman/Rayleigh setup. M: mirror, L: lens, BS: beam splitter, E: energy monitor, BP: band pass

Figure 20.10 shows mole concentrations and the corresponding fluctuations conditioned on mixture fraction for all main species except N_2. In general, the flame shows the typical features of non-premixed combustion as obvious from comparison to flamelet calculations employing a strain rate of 200 s^{-1}. It is clear from the figure that, on the lean side, laminar flamelet calculations are very similar to the results measured in the partially-premixed turbulent flame. At the rich side, however, deviations between the flamelet calculations and the turbulent flame data are apparent, especially for CO, H_2, and H_2O. Note that even small concentrations of CO and H_2 are detectable using the advanced technique applied.

Simultaneous Measurement of OH, HCHO and Temperature in Turbulent Flames. In the past decade much work has been aimed at the visualization of flame-front positions and structures in turbulent flames. Most of this effort has concentrated on measurements of the distribution of OH because of its high abundance in flames and the coincidence of OH transitions with high-power excimer laser wavelengths [20.127]. Measurements of flame front positions using OH, however, can give little information about important chemical reaction paths and fuel consumption rates. Recent investigations indicated that the distribution of HCO correlates well with peak heat-release rates for premixed flames of a certain range of equivalence ratios $\phi = 1.0–1.2$ [20.128, 141]. Due to

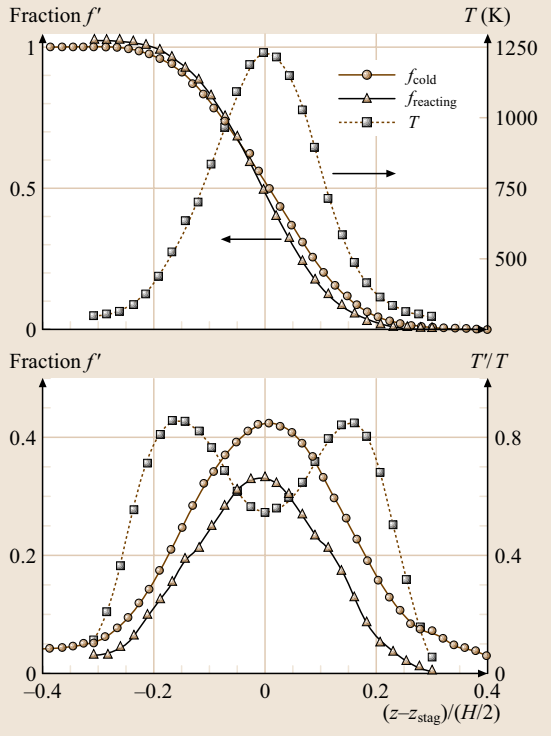

Fig. 20.9 Mean and fluctuation of the mixture fraction f and temperature T along the center line. Temperature fluctuations are normalized by the maximum temperature T = 1250 K

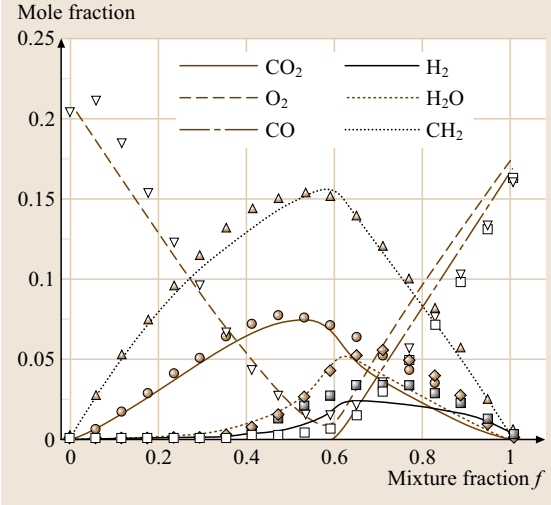

Fig. 20.10 Mole fraction conditioned on mixture fraction. *Symbols* represent experimental values obtained by Raman/Rayleigh spectroscopy in the turbulent opposed-jet burner, *lines* represent laminar flamelet calculations using a strain rate of 200 s^{-1}

its low abundance, measurements of the HCO distribution via LIF have to apply phase sampling in acoustically forced unsteady flows to increase signal-to-noise ratios. Single-shot LIF measurements of HCO distributions in turbulent flows, however, do not seem to be feasible. Instead, *Paul* et al. [20.128] showed that the product of OH and HCHO concentrations is directly proportional to the reaction rate of $HCHO + OH \rightarrow H_2O + HCO$ and therefore yields an estimate for the production rate of HCO. The established link between HCO mole fraction and heat release therefore makes the product $I_{LIF}(OH) \times I_{LIF}(HCHO)$ a good choice for flame front determination. Due to the high abundance of HCHO and OH in the flame-front region and their large fluorescence cross-sections, this approach enables single-shot measurements in highly turbulent reactive flows.

Whereas OH-LIF is frequently applied for measurements in different combustion media [20.142], efficient HCHO imaging have suffered from the lack of suitable high-power laser sources. As well as dye laser systems [20.143], broadband XeF and frequency-tripled Nd:YAG lasers have been used, which, however, access only weak transitions [20.144]. We took advantage of a coincidence of the side band of the XeF excimer laser at 353 nm with the strong 4_0^1 vibronic transition of formaldehyde [20.145, 146]. By combining two tunable excimer lasers (KrF and XeF), simultaneous measurements of OH and HCHO distributions by LIF are feasible on a single-shot basis. Rayleigh-scattered light provides information about the temperature distribution, which will be useful when addressing the quantification of LIF signal intensities.

Figure 20.11 shows an experiment in which a field measuring $20 \times 16\,mm^2$ a distance of 2 mm above the burner exit in a turbulent natural gas/air Bunsen flame was investigated. A plane centered along the axis of the Bunsen flame is illuminated with the light of two tunable excimer lasers operated with KrF (248 nm) and XeF (353 nm). The LIF and scattering signal were detected with three ICCD cameras.

The results (Fig. 20.12) show strong OH LIF intensities throughout the burned gases within the observed area. Separate regions of burned gases are found within the fresh-gas zone, which might be separated from the flame front by the turbulent flow. The HCHO-LIF signal on the other hand is found within the fresh-gas

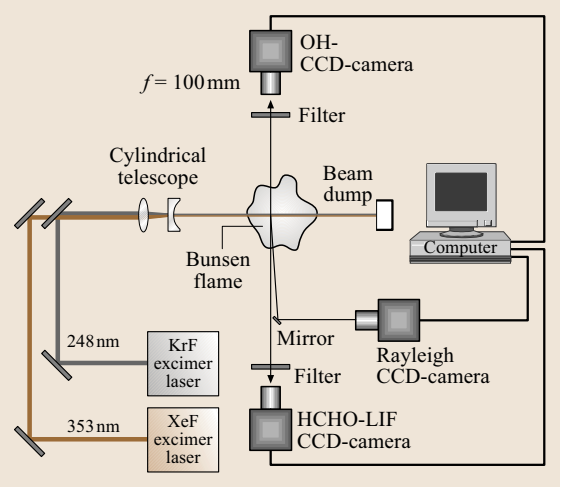

Fig. 20.11 Experimental setup for simultaneous measurements of HCHO and OH LIF and temperature in a turbulent flame

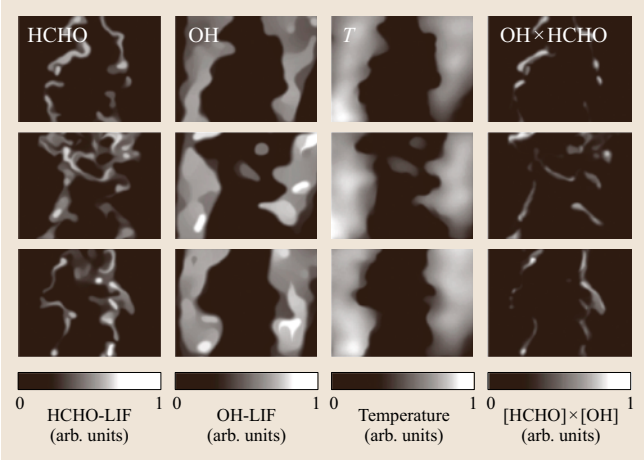

Fig. 20.12 Simultaneous measurement of formaldehyde (HCHO), OH LIF and temperature via Rayleigh scattering. The three *rows* show independent sets of images. The *right column* shows the linear combination of OH and HCHO LIF [20.132]

zone close to the flame front with little overlap with the OH distribution. Extended areas within the fresh gases showing increased HCHO signal levels were also found in areas with elevated temperatures. Here, several millimeters away from the flame front, cool-flame chemistry producing formaldehyde has already started. The H, CHO and OH images show reasonably good signal-to-noise ratio, allowing for the calculation of the product of the OH- and HCHO-LIF distributions as suggested by *Paul* et al. [20.128]. To reduce the influence of shot noise when calculating the LIF product images a nonlinear anisotropic diffusion algorithm was applied [20.147, 148]. The results are shown in the right column in Fig. 20.12 for three typical single-shot situations. The resulting images show sharp contours within the flame-front region. Extended areas with OH-LIF signal, as found on the hot side of the flame front as well as larger areas with HCHO-LIF signal within the fresh gases are suppressed. When comparing the resulting flame-front images to the temperature fields it is found that the product of the OH- and HCHO-LIF signals closely follows iso-lines within the temperature field.

Simultaneous Measurements of OH and NO Concentrations and Temperature in a Swirl Flame. The highly turbulent reactive flow field in practical-scale swirl flames is a challenge for both experiments and numerical simulations. Experiments aim to provide accurate data for model validation. The subject of the investigation described in this paragraph is the TECFLAM standard swirl burner [20.142]. Figure 20.13 shows the burner geometry and the position of the planes observed by laser imaging. The annular slot of the central fuel nozzle of the burner has an inner diameter of 20 mm, whereas its annulus is 3 mm wide. Swirl is provided to the air flow by a movable block swirl generator [20.149], which is set to an effective swirl number of $S = 0.9$. The burner is operated with a thermal load of $P = 150$ kW burning natural gas at an equivalence ratio of $\phi = 0.83$, which corresponds to a flow of 15 m^3/h natural gas and 180 m^3/h air. The Reynolds numbers of fuel and airstream, based on the exit bulk velocity,

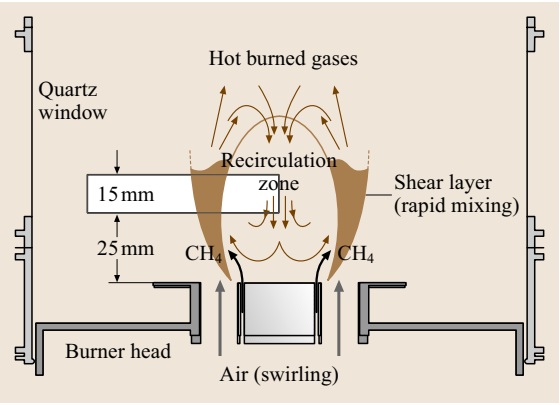

Fig. 20.13 Flow field and measurement position in the TECFLAM swirl flame [20.132, 133]

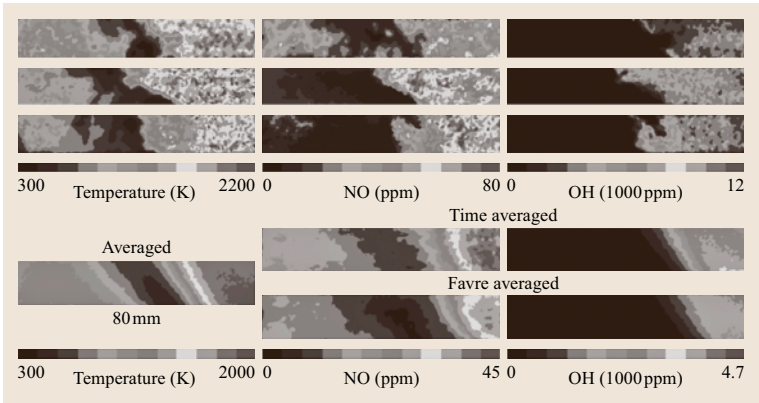

Fig. 20.14 Simultaneous measurements of temperature and NO and OH concentration in the reactive flow field of the TECFLAM swirl burner. *Upper frames*: instantaneous measurements, *lower frames*: averages [20.133]

are $Re_{gas} = 8000$ and $Re_{air} = 42\,900$, respectively. The combustion chamber is confined by a water-cooled housing (72–88 °C) to ensure constant boundary conditions. Optical access to the chamber is realized by four quartz windows ($100 \times 100\,mm^2$).

In the swirl flame a similar setup as in Fig. 20.11 was used to assess OH and NO concentration and the temperature distribution. One of the laser beams is frequency-converted in a hydrogen Raman shift cell [20.150] to provide 225.25 nm radiation for the excitation of the NO A-X(0,0) band at energy densities of $2 \times 10^6\,W/cm^2$. The NO-LIF signal is separated via a reflection band-pass filter (transmission: 248 ± 10 nm) to detect light emitted from the A-X(0,1), (0,2) and (0,3) transitions. The second laser is triggered with a short delay (200 ns) to prevent crosstalk between the NO-LIF and Rayleigh signals. Rayleigh-scattered light is separated via a dielectric mirror (high reflectance at 248 nm at 45°). Achromatic UV lenses are used to focus the signal onto the chips of ICCD cameras. For simultaneous measurements of OH concentration and temperature the laser used for Rayleigh scattering was tuned to the OH transition ($P_2(8)$ within the OH A-X(3,0) band, laser energy density: $5 \times 10^7\,W/cm^2$) and the OH-LIF signal was detected using reflection band-pass filters centered at 295 nm. Since OH is a strongly diagonal molecule the strongest emission occurs from the (3,3) vibrational band (and after vibrational relaxation from the (2,2), (1,1), and (0,0) bands). The fluorescence contribution of OH LIF detected at 248 nm together with Rayleigh-scattered light is generally negligible compared to the Rayleigh signal [20.151]. However, in peak temperature zones where total number densities and hence Rayleigh signal are low OH LIF contributes to the overall signal, resulting in additional uncertainties of −5% in the temperature images.

The measurements presented here were carried out 25–40 mm (Fig. 20.13) above the burner exit. For calibration of the LIF signal intensities a *McKenna* burner was installed in the burner housing and investigated with an identical optical setup. The burner was operated on stoichiometric methane/air mixtures where resulting OH concentrations and temperatures are documented [20.152]. Additional calibration measurements have been carried out in lean flames ($\phi = 0.83$) doping known quantities of NO (300–800 ppm) into the fresh gases. The increase in signal intensities provided the necessary data for calibrating the NO-LIF measurements [20.153] in the swirl burner measurements.

Simultaneous measurements of temperature, OH and NO concentration allow one to quantify the LIF signal intensities by correcting for the temperature dependence of the ground-state population and collisional energy-transfer processes on a single-shot basis. Furthermore, by correcting for local total number densities, local concentrations can be calculated from number densities, allowing the computation of time-averaged concentration fields. In Fig. 20.14, three sets of simultaneously recorded temperature, NO and OH distribution fields are shown. The position of the observed area is depicted in Fig. 20.13. It can be seen that NO is present throughout the whole burned gas area. NO is formed within the hot burned gases on both sides of the fresh-gas intake and accumulated by recirculation. In the outer recirculation zone (the left part of the figure) peak NO concentrations are around 35 ppm, whereas in the inner recirculation zone peak NO concentrations in the range of 70–80 ppm are reached due to the higher temperatures. OH on the other hand is mainly found on the inner side of the fresh-gas intake. Due to the lean air–fuel mixture and the strong turbulence, OH is distributed across a relatively broad zone behind the flame front. Local

peak OH concentrations are found to be 8000 ppm in the super-equilibrium range. Below the single-shot images, averaged images for the same measurement position are presented. For the NO and OH concentration fields, both, Favre- and time-averaged images are shown. Since both species are mainly present within the hot burned gases, the influence of density variations is restricted. However, in the burned gases, the time-averaged concentrations are higher than the Favre averages by up to 15%.

Three-Dimensional LIF Diagnostics

Two-dimensional images yield information about cross sections in turbulent combustion media. They can therefore not distinguish between isolated areas (i. e., *islands* of burning gases) and structures that are connected via the third dimension. Information on the propagation of a structure perpendicular to the measured plane is missing. Furthermore, gradients measured by these planar techniques are only a projection of the real gradients onto the observed line or plane.

Time-Averaged Three-Dimensional Measurement of Fuel Distribution. In isobaric, isothermal systems the use of tracer LIF is straightforward. When seeding acetone into the gas flow, the local LIF intensity is a direct measure of the local concentration. In later chapters we will describe how temperature and pressure effects must be corrected for more-general applications.

Figure 20.15 shows the setup for a measurement of fuel distributions in the combustion chamber of a stationary gas turbine (thermal power of the investigated segment ≈ 1 MW). The gaseous fuel flow was simulated with air, seeded with acetone and the fluorescence was successively measured in three adjacent planes. Instantaneous and time-averaged images are shown in Fig. 20.16. The time-averaged concentration distributions from the adjacent planes were then used to reconstruct the average three-dimensional fuel distribution (Fig. 20.17) assuming cylindrical geometry. The strong variation in local concentrations (upper row in Fig. 20.16) indicates, however, that an instantaneous view into the three-dimensional structure would deviate significantly from the average distribution.

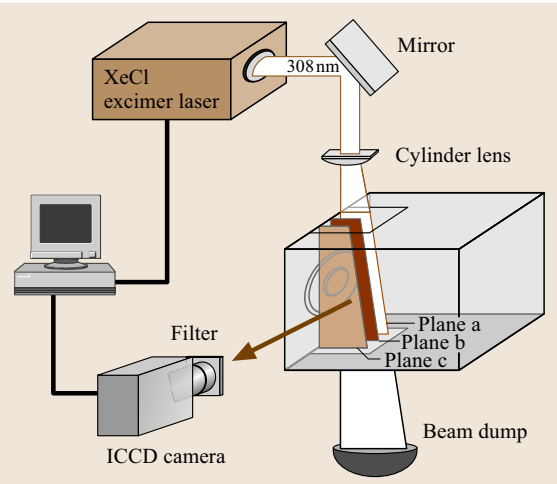

Fig. 20.15 Experimental setup for the time-averaged measurements of fuel–air mixing in a swirl burner of a stationary gas turbine [20.11]

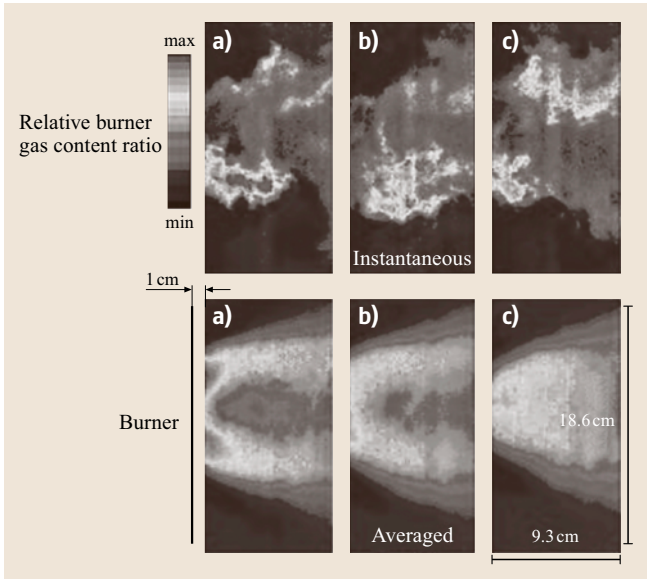

Fig. 20.16 Measurements of the fuel distribution (doped with acetone) in three parallel planes in the mixing chamber. The fuel nozzle is 1 cm to the left end of the images. *Upper row*: randomly chosen single-shot images, *lower row*: averaged fuel distribution [20.11]

Instantaneous 3-D Measurement of Temperature and Flame-Front Position. For instantaneous observation of three-dimensional structures in turbulent flows several approaches have been developed and applied to turbulent mixing processes and flames. Parallel alignment of multiple detection planes either using subsequent detection of the imaged planes with a single camera and a long sweeping pulse or CW laser beams and scanning mirrors, or using high-repetition-rate imaging with the need for laser and camera *clusters* are the methods that have been used to observe extended volumes within turbulent flows [20.142, 154–156]. The spatial resolution in

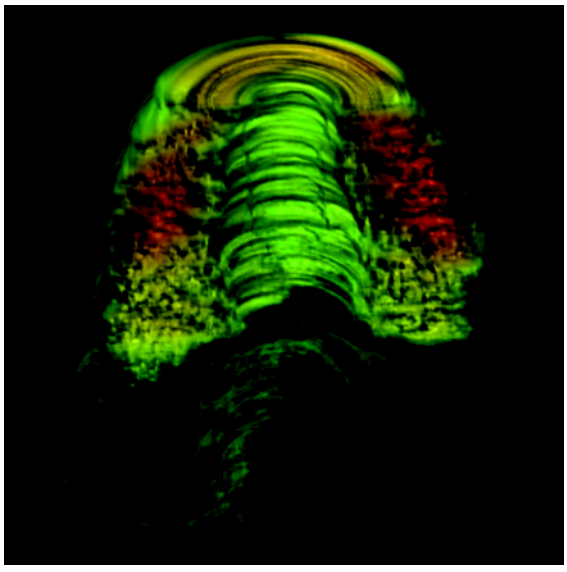

Fig. 20.17 Visualization of the averaged three-dimensional fuel distribution in the nonreactive swirl flow [20.157]

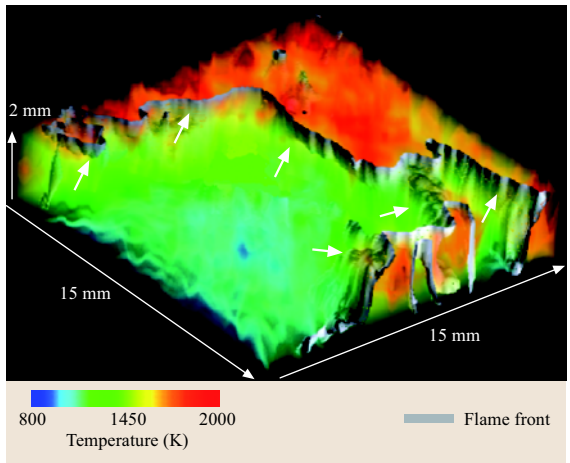

Fig. 20.19 Three-dimensional visualization of the temperature field and the flame front position (gray surface marked with *arrows*) in the reactive flow of a technical scale swirl flame at a swirl number of $S_0 = 0.9$ and an equivalence ratio of 0.83 [20.142]

the z-dimension (perpendicular to the observed planes), however, is restricted. Figure 20.18 shows the setup for instantaneous measurements of OH-LIF and temperature in three parallel planes within the reactive flow field of the TECFLAM swirl flame (Fig. 20.13).

The beams of two tunable excimer (tuned to an OH A-X(0,3) transition at 248.45 nm) are directed through the flame. Via a beam splitter a third beam is generated from one of the lasers, optically delayed and used to illuminate the third plane. Three cameras are aimed to detect the Rayleigh signal with dielectric mirrors as bandpass filters ((248±10) nm). Three additional cameras record the OH-LIF signal, which is spectrally separated from scattered light by WG280 long-pass filters.

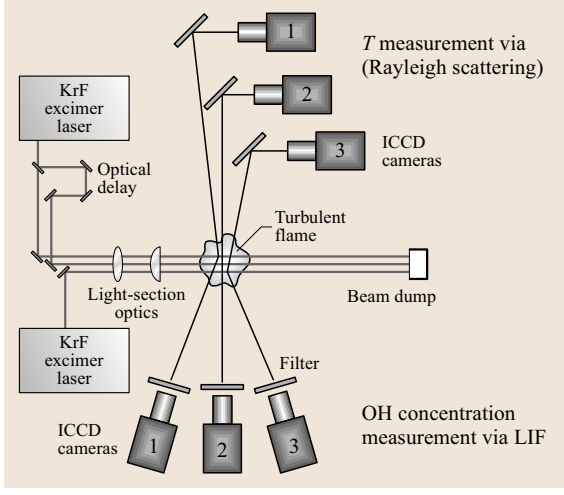

Fig. 20.18 Experimental setup of instantaneous 3-D measurements of OH LIF and temperature in a turbulent flame

Figure 20.19 presents a three-dimensional visualization of the flame front embedded in the turbulent temperature field of size $15 \times 15\,\mathrm{mm}^2$ at $x/D = 1.5$ and $r/D = 0.5$. The visualization is based on ray-tracing algorithms (in collaboration with IWR, Heidelberg). The flame-front position is evaluated for each individually measured OH concentration field by determining the position with the steepest gradient in OH concentration. Between the three adjacent planes the flame-front positions and temperatures are interpolated to obtain a 3-D representation.

Instantaneous 3-D Measurement of OH LIF with Crossed Light Sheets. An alternative attempt to image three-dimensional volume elements is the use of crossed detection planes (Fig. 20.20) [20.158–160]. A quasi-instantaneous detection is provided with two cameras [20.157]. In special mirror arrangements detection is possible with a single laser and camera [20.161]. One of the benefits of this method is the increasing resolution towards the crossing line and a small cylindrical volume of several hundred micrometers to approximately 1 mm around it. This geometry is ideal

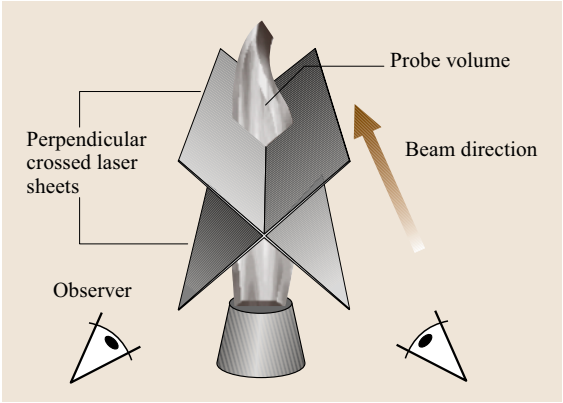

Fig. 20.20 Arrangement of the crossed light sheets for instantaneous three-dimensional observation of OH LIF around the crossing line

for the combination with one-dimensional (1-D) Raman line measurements which can provide temperature profiles and multispecies distributions in a limited part of the crossing line [20.162]. The resulting three-dimensional data matrix can also be visualized using a 3-D visualization tool that assigns not only color but also transparency values to the given intensity values [20.163]. The results for OH-LIF measurement in a lean Bunsen flame are presented in Fig. 20.21. To the left of the reactive zone is the unburned fresh gas in the center of the burner above the nozzle, while the right side shows the surrounding air around the flame cone. The depth of the visualized 3-D volume is 2 mm.

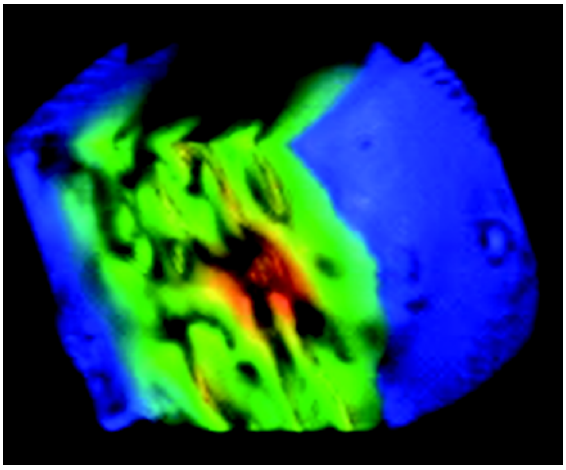

Fig. 20.21 Volume visualization of OH LIF intensity in a lean Bunsen flame [20.129, 161]

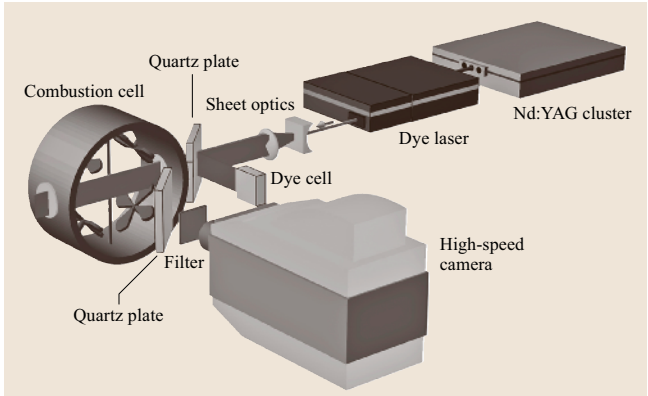

Fig. 20.22 Experimental setup for high-repetition-rate OH PLIF in the turbulent combustion cell

Multiple-Timestep Imaging

Tracking of Flame Kernel Development After Spark Ignition. Many practical combustion processes rely on electrical spark ignition in their initial phase. During the breakdown, arc and glow phases of an electrical discharge, a plasma is formed. At the interface of the plasma kernel and the ambient fuel–air mixture transfer of heat and radicals causes the formation of an initial flame kernel. Depending on the local fuel–air ratio and the turbulence levels the flame kernel may either grow in time, leading to a successful ignition, or be extinguished. To understand and predict the fate of an initial flame kernel requires the flame kernel development to be tracked temporally. This can be achieved by sequential OH LIF imaging.

A multiple laser and detector system [20.136] was used to record time sequences of OH-LIF images from single combustion events in a closed vessel using premixed methane/air mixtures [20.164]. The laser source of the high-repetition-rate imaging system is a cluster of four Nd:YAG lasers (BMI/CSF-Thomson) that are fired in series with a short time delay to generate a burst of four laser pulses. The separation between pulses was varied between 250 µs and 3 ms, depending on the fuel and turbulence intensity used in the experiment. The output from the four Nd:YAG lasers are combined to a single beam and frequency doubled to 532 nm. The pulse energy from each of the lasers was around 500 mJ. The Nd:YAG lasers pumped a dye laser (Continuum ND60) operating near 566 nm on rhodamine 590 dye. The output from the dye laser was frequency doubled to 283 nm and tuned to excite OH at the $Q_1(8)$ transition in the (1,0) band of the $A^2\Sigma^+ \leftarrow X^2\Pi$ system. The laser energy at 283 nm was around 2 mJ/pulse for a pump pulse

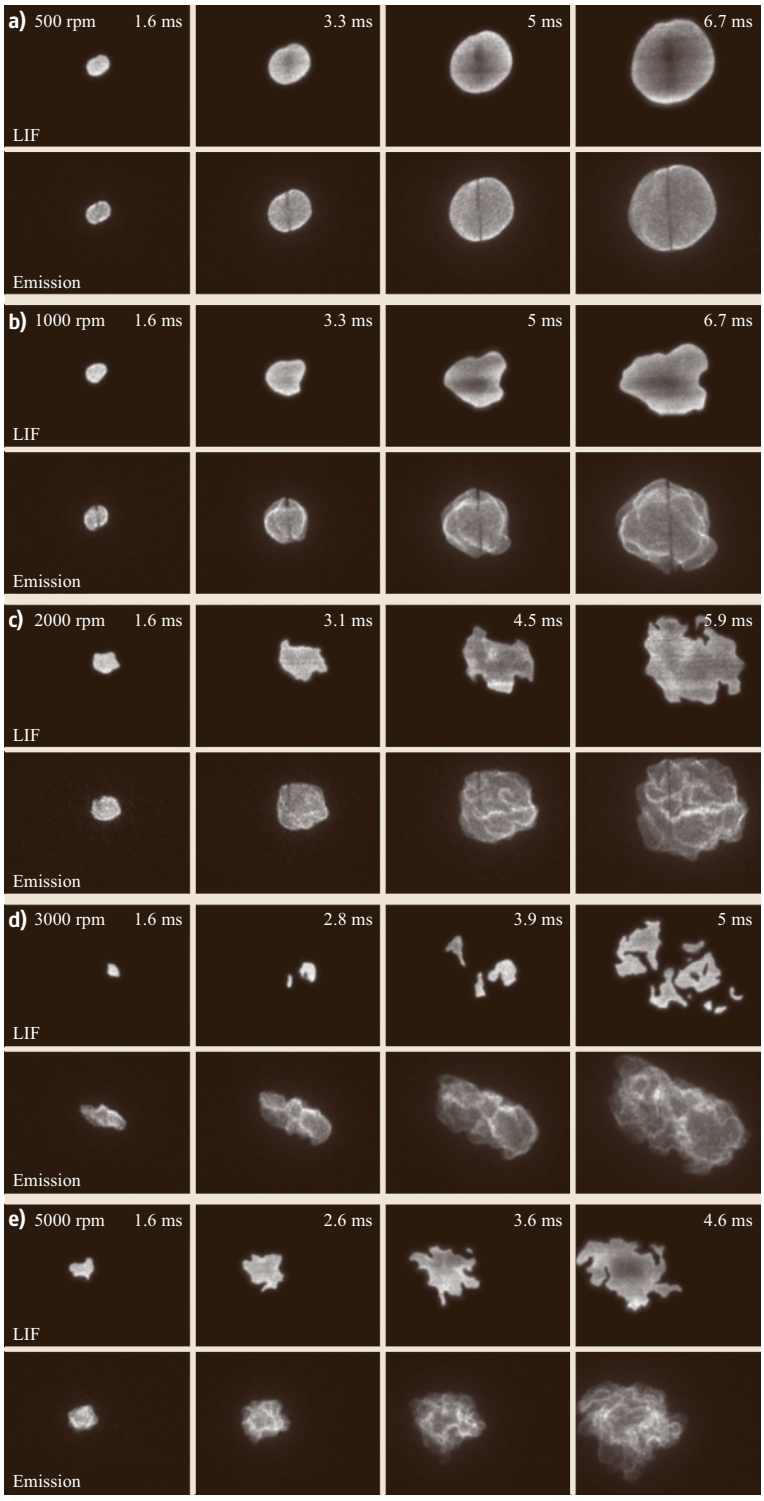

Fig. 20.23 Flame propagation for individual events measured by OH PLIF and flame emission for various rotor speeds as indicated in each row and stoichiometric methane/air mixtures. Times in each image denote the time after ignition. Turbulence intensities associated with the increasing rpm as stated in the figures are 0.31, 0.62, 1.3, 2.01, and 3.31 m/s

separation of 2 ms. The laser light was formed to a sheet, 50 mm in height and 0.2 mm in width, using a cylindrical telescope, and passed through the cell 1 mm in front of the electrodes (Fig. 20.22).

A high-speed camera consisting of eight individual intensified CCD units coupled to a single optical input (Imacon 468, DRS Hadland) was used to detect the fluorescence. An additional image intensifier was fitted to the optical input to achieve UV sensitivity. The first four CCD units were triggered by the individual lasers, and used to capture the four OH LIF images. The remaining four CCD units were used to capture flame chemiluminescence shortly after each LIF exposure. The delay between the LIF and chemiluminescence exposures was 2 µs, which can be considered simultaneous on the time scale of the studied process. An achromatic quartz lens ($f = 100$ mm, $f_\# = 2$) was fitted to the camera. A UG11 filter was used in combination with a long-pass filter, transmitting above 295 nm, was used to reject scattered laser light and transmitting fluorescence in the (1,1) and (1,0) bands of OH.

An external pulse generator synchronized the ignition system to the laser and detector system, while allowing the laser system to operate continuously at 10 Hz, to maintain stable operation. The ignition system consists of two units: the first unit produces an electrical breakdown between two electrodes (1 mm diameter Tungsten wire, conically shaped, 1 mm gap) and thereby an electrically conducting plasma channel. The energy of the breakdown was kept as low as possible and the released energy in this phase is below the minimum ignition energy. The second unit is a constant-current power supply giving rise to currents and voltages of approximately 1 A and 100 V, respectively, typical for an arc phase. In this study, an arc-phase duration of 200 µs is chosen. To achieve a constant current, the voltage is adjusted adaptively, leading to a reproducibility in energy deposition of better than 2%. Therefore, conditions for initially spherical flame kernels generated by the ignition system are highly reproducible as proven in [20.165] for initially quiescent gas mixtures.

The cylindrical constant-volume combustion vessel has a diameter of 39 cm and a height of 51 cm, resulting in a volume of approximately 55 l. Three optical access ports allow for LIF measurements. Four high-speed rotors of 144 mm in diameter are situated 200 mm from the electrode gap. Rotor axes are perpendicular to their respective neighbors. Rotor speeds are synchronized and can be varied between 0 and 5000 rpm. In the vicinity of the electrode gap a homogeneous isotropic turbulent flow field of variable intensity is generated.

Figure 20.23 shows data corresponding to single ignition events in stoichiometric CH_4/air mixtures subjected to different degrees of turbulence. The sequences were obtained using four consecutive laser shots fired in rapid succession with stated timings referring to time after ignition. The top rows of pictures are two-dimensional (2-D) LIF images of OH; the bottom rows are OH chemiluminescence images. Figure 20.23a corresponds to moderate levels of turbulence ($u' = 0.62$ m/s). It can be seen that first wrinkling (deviations from a spherical kernel) appears around 1.6 ms, which is a consequence of turbulence chemistry interaction although essentially the flame retains its near-laminar character. On the regime diagram [20.44] this corresponds to the laminar wrinkled flame front region. On the emission images a shadow appears indicating the position of the electrodes. Increasing turbulence levels to $u' = 2.01$ m/s (3000 rpm) results in a large change of flame shape. The flame now shows significant internal structure due to distortion by vortices. Here, the advantage of a planar light-scattering technique to assess flame structure is clearly seen: whereas emission images may still be interpreted as compact and connected flames the LIF images on the other hand show formation of cusps and handles or possibly islands.

From OH sequences, as shown in Fig. 20.23, a variety of parameters can be deduced to characterize the temporal evolution of the flame kernel. Here only the degree of wrinkling as a consequence of the turbulence–

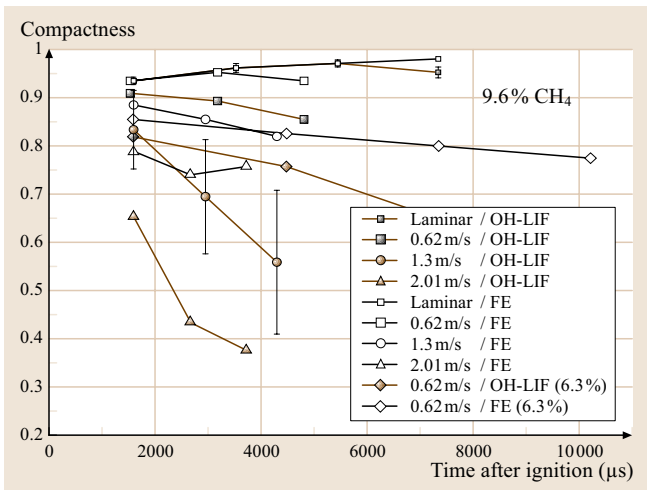

Fig. 20.24 Temporal evolution of compactness for stoichiometric methane–air mixtures subjected to various degrees of turbulence. FE: flame emission

chemistry interaction is briefly discussed. The degree of wrinkling and its effect on flame propagation can be quantified using the flame compactness factor K, which is defined as

$$K = \frac{4\pi A_t}{C_t^2} = \frac{C_s^2}{C_t^2}\,, \tag{20.1}$$

where A_t is the area. OH LIF is detected within the observed cross section, and C_t is its circumference. C_s is the circumference of a spherical laminar flame of the same area A_t as the turbulent kernel. In this definition, spherical flame kernels have a compactness factor of $K = 1$ whereas wrinkled flames have $K < 1$. For example $K = 0.5$ would increase the circumference of the flame by a factor of 1.41. Figure 20.24 shows the temporal evolution of K for stoichiometric CH_4/air mixtures at various degrees of turbulence where K is calculated both from emission and from PLIF measurements. It is evident that line-of-sight-averaged chemiluminescence measurement is not a suitable tool to assess flame wrinkling: taking the $v' = 2.01$ m/s case as an example (3000 rpm rotor speed), large discrepancies between the two measurement techniques are visible. The LIF data indicate how strongly K is affected by turbulence and is especially strongly influenced if the mixture is lean. In contrast, in the laminar case (black line) both the emission data and the LIF data yield essentially the same results as expected. Note that the apparent increase in K for the laminar case is due to the decreasing effect of heat conduction to the electrodes as the flame kernel grows in size. The standard deviations of 30 individual measurements per point is indicated for the $v' = 0$ and $v' = 1.3$ m/s cases.

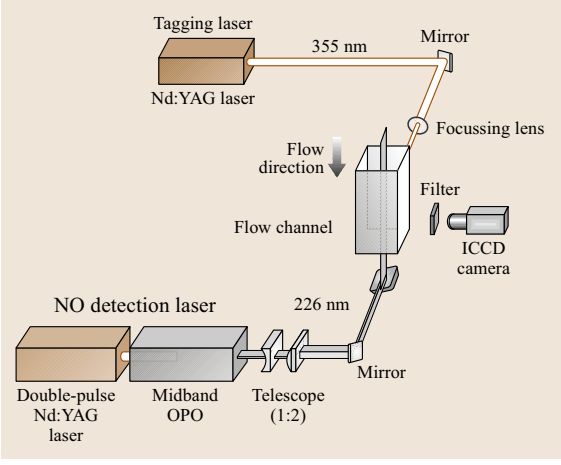

Fig. 20.25 Optical setup for the laser-based investigations in the flow channel

Flow Diagnostics Close to the Wall with Two-Time-Step Imaging. Flow-field imaging is most frequently carried out via particle imaging velocimetry (PIV) or laser Doppler velocimetry where particles are added to the flow. Close to surfaces, these techniques, however, fail due to the interaction of the particles with the surface. Different flow-tagging techniques have been proposed to overcome these problems. They are based either on Doppler shifts of molecular tracers [20.166] or on the laser-induced generation of a molecular tracer within the flow that can be observed for a certain time after its generation (tagging). This tagging is based on photodissociation of vibrationally hot H_2O [20.167], vibrationally excited O_2 [20.168, 169], NO formed from photodissociation of *tert*-butyl nitrate [20.170] or from photolytically generated oxygen atoms with subsequent reaction with nitrogen [20.171]. We discuss here photodissociation of NO_2 with subsequent LIF imaging of nitric oxide and expand this technique to allow the investigation of the temporal development of the turbulent flows by either photolytically tagging in two subsequent time steps with a single detection of both marked volumes or with one tagging and subsequent detection of each individual flow situation after two variable delays.

In an optically accessible flow channel (60×5 mm^2 cross-section, mean flow velocities of $v = 74$ m/s associated with a Reynolds number of $\mathrm{Re} = 24\,500$ at room temperature, the flow seeded with 1200 ppm NO_2) a frequency-tripled Nd:YAG laser is focused to a line where the NO tag is generated. The resulting *line* of NO is then observed at two time steps with various delays (up to 300 µs) with LIF imaging. The frequency-tripled laser light of a double-cavity Nd:YAG laser is used to pump a midband optical parametric oscillator (OPO). It is tuned to generate a signal wavelength at 450 nm which is then extra-cavity frequency-doubled in a beta barium borate (BBO) crystal. The resulting UV beam has a pulse energy of approximately 1 mJ and a spectral width of $\approx 4\,\mathrm{cm}^{-1}$. It therefore excites a large portion of the NO $A - X(0, 0)$ band head. NO-LIF signals are discriminated against scattered light by a UG5 filter and focused onto the chip of an CCD-intensified interline camera. The image intensifier ensures short detection gate times for both frames. The maximum repetition rate of 200 ns of the double-frame camera is no restriction for our experiments. The optical setup is shown in Fig. 20.25.

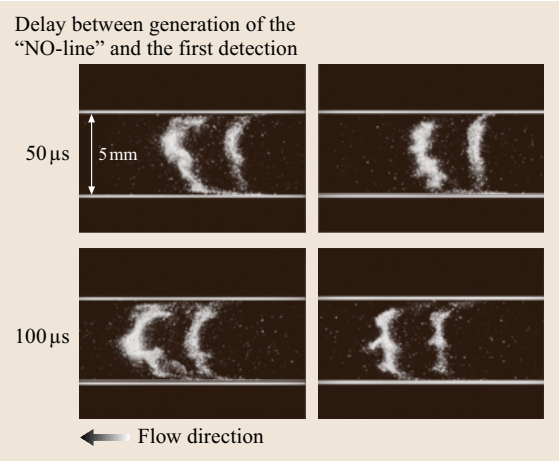

Fig. 20.26 Observation of a photolytically generated structure at two time steps after generation. Delay between generation and first detection: 50–100 µs, delay to the second detection: 75 µs. The flow is from *right to left*, the *horizontal lines* mark the position of the channel walls

Figure 20.26 shows the result of the double-frame imaging for NO lines generated at the right side of the frames (the flow is towards the left). The interaction of the flow with the boundary layer at the walls (horizontal lines) and with turbulence elements in the main flow is clearly seen.

Multiple-Timestep Imaging in Spray Diagnostics. Techniques using simultaneous detection of Mie scattering and LIF signals have been used successfully for two-dimensional drop-size imaging in practical spray configurations. The fluorescence tracers commonly used, however, prevent the application in realistic fuels like gasoline and diesel because of strong interference with fluorescing compounds of the fuels. Therefore, the use of a fluorescent tracer is proposed that can be excited in the red spectral range, where the absorption by commercial fuels is minimized. We use a frequency-doubled diode-pumped Nd:$YAlO_3$ laser-oscillator power-amplifier system to generate pulse bursts at 671 nm with 30 ns pulses ($\approx$ 1 mJ each) and a 30 kHz repetition rate. At this wavelength an organic tracer (rhodamine 800) with high fluorescence quantum yield is excited. Fluorescence and elastically scattered light is separated via dielectric filters and detected on two slow streak cameras. The fluorescence emitted at around 700 nm originates from the liquid phase only and the LIF/Mie signal ratio is a measure of the local Sauter mean diameter.

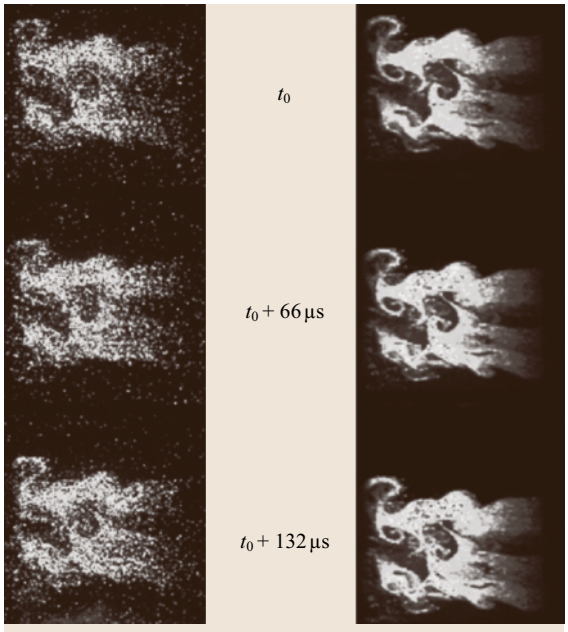

Fig. 20.27 LIF and Mie signal distributions in the spray of a nebulizer. Three images with a temporal separation of 66 µs are shown

Figure 20.27 shows a time series of Mie and LIF signal in the spray field of a medical nebulizer. The high-repetition-rate pulse bursts of the laser allow the observation of the spray development and evaporation. Further experiments will be carried out in diesel sprays. First measurements show that the tracer system with excitation in the red can be used in commercial diesel fuel without any significant fluorescent background from the fuel [20.172].

20.4.4 Engine Combustion

In-cylinder laser-based combustion diagnostics in internal combustion (IC) engines focus on three main fields:

1. the observation of the mixture preparation before ignition, which includes fuel injection and evaporation, fuel–air mixing, pre-combustion temperature distributions, and the distribution of residual inert gases from the previous engine cycle and intentionally recirculated exhaust gas
2. the observation of the ignition and combustion process including flame propagation and potential flame

quenching, also considering post-flame temperatures
3. the observation of pollutant formation, namely nitrogen oxides (NO_x) and soot

In the following paragraphs these different topics are treated separately.

Different strategies for optically accessible IC engines have been used over the last years. The design of optical engines requires compromises between the needs of the diagnostics and the level of comparability to production-line engines. Best optical accessibility is obtained with transparent cylinders and extended windows that are inserted into the piston (Fig. 20.28). The thickness of pressure-resistant quartz windows, however, usually prevents the operation of the neighboring cylinder and changes in-cylinder heat transfer considerably due to the extended quartz surfaces. More-advanced concepts sacrifice optical access by using smaller optical sapphire windows that can be thin enough to fit into a multi-cylinder engine block with minor modifications (Fig. 20.29). Recently, micro-optical laser-based probes using endoscope optics and fibers have been developed for in-cylinder investigation in IC engines [20.175–177].

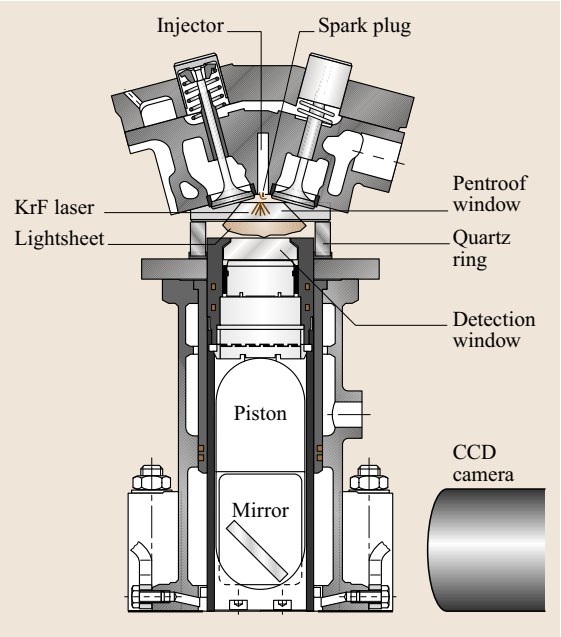

Fig. 20.28 Basic setup of an optical engine with access to the combustion chamber through a quartz cylinder and a piston window [20.173]

Analysis of Mixture Formation

There are a number of quantities that would be desirable to measure with non-intrusive in-situ techniques to characterize the mixing process in the fresh gas completely. These quantities include:

- Fuel concentration
- Fuel–air ratio
- Temperature
- Fuel composition (i. e., the concentration of individual components)
- Residual gas concentration

To visualize the mixing process and to facilitate the interpretation of the results these quantities should be imaged in at least two dimensions with temporal resolution faster than the time scale of mixing and chemical reaction. A recent review summarizes the state of the art [20.11].

Mixing processes of interest can be categorized according to the level of difficulty in terms of quantitative imaging measurements. They are listed here in order of increasing complexity.

- Constant pressure versus temporally fluctuating pressure
- Constant temperature versus temporally fluctuating (spatially homogeneous) temperature
- Homogeneous temperature versus spatially varying temperature
- Temperature approaches the stability limit of the tracer

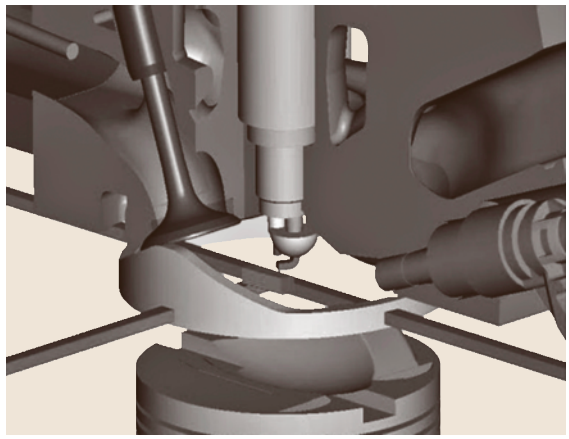

Fig. 20.29 Advanced concept for an optical engine with narrow sapphire ring that allows the operation of full quasi-production-line four-cylinder engines [20.174]

- Homogeneous versus inhomogeneous bath gas composition (mainly oxygen concentration is relevant)
- Single-component fuel versus multicomponent fuel
- Non-fluorescing versus fluorescing fuel
- Homogeneous (gas phase) versus heterogeneous (two-phase flows)

The ideal tracer should behave exactly like the fluid it is added to (i. e., the fuel or the desired component of a multicomponent fuel) in terms of droplet formation, evaporation, convection, diffusion, reactivity, and reaction rate. It is obvious that these requirements can not be met in full. However, practical tracers are often very similar to the fuel or are components that are present in commercial fuels. Therefore, in some situations, tracers must not be understood as being *added* to the fuel. Rather, the other fluorescing substances are replaced by non-fluorescing compounds. The modification of the system must be kept to a minimum and the influence of the tracers on a given experimental situation must be critically reviewed.

Ideally, the tracer should yield LIF signal intensities that are directly proportional to the desired quantity and should not be influenced by the ambient conditions. Unfortunately, signals from all fluorescent tracers show at least some dependence on local temperature, pressure and bath gas variation. Therefore, in experiments where ambient conditions change in time or space, the underlying interdependencies with the tracer signal must be understood in order to obtain quantitative results.

Tracers for Homogeneous Gas-Phase Systems. Tracer-based LIF techniques have been used for experimental studies in fluid mechanics and combustion for several years. Tracers are single components (molecules or atoms) with highly defined spectral behavior that represents the local concentration of the fluid of interest or that allow to remotely measure a quantity of interest (i. e., temperature or pressure). Typically, compounds are chosen that yield strong enough LIF signal intensities to allow two- (or even three-)dimensional visualization of the desired quantity with sufficient temporal resolution to freeze the motion.

There are two opposite cases that require the application of tracers for the measurement in fluids. First, the components of the fluid *do not (or only weakly) fluoresce*. This is the case for air and typical exhaust gases (H_2O [20.178], CO_2 [20.179]). At room temperature these species are only excited in the vacuum-UV region and only at high temperatures do their spectra extend into the spectral range that is of practical use for combustion diagnostics. The resulting signal in O_2 [20.180] and CO_2 [20.179] is then strongly temperature dependent and the practical use for concentration measurements is limited. In the second case the fuel contains *too many fluorescing compounds*. This is true for commercial fuels. Their fluorescence has been used to obtain qualitative and semiquantitative measurements of fuel vapor concentrations [20.181]. However, because all these compounds have different physical properties in terms of volatility and transport as well as in terms of their spectral response on variations in ambient conditions, the overall signal cannot be quantified. In both situations it is desirable to add a single tracer that can be selectively observed within the fluid. In the case of fuels (gasoline or Diesel-type fuels) this often means replacing the fluorescing compounds of the fuel by non-fluorescing compounds leaving only one, or adding an additional compound that was not part of the original mixture.

Different *classes* of molecules have been used as tracers. The choice of potential tracers is driven by the desire to add a minimum concentration of foreign material that yields a maximum LIF signal intensity while not perturbing the system under study. To provide high enough seeding concentrations especially at low temperatures (room temperature) the tracer must have a sufficient vapor pressure. While the main part of the following section focuses on the fuel-like hydrocarbon-based tracers, we include other concepts in the following overview.

Atoms have large absorption cross sections and are candidates that emit strong fluorescence upon excitation in the UV and the visible. The atomization of the material, however, requires the high temperatures that are present in flames. Some metal salts (such as thallium or indium chloride) can be dissolved in the fuel. In the flame front metal atoms are then generated that can be used to measure temperature in the burned gas [20.182, 183]. The strong transition moments in atoms allow the use of extremely low (and therefore non-perturbing) seeding levels. The strong transitions, in turn, are easily saturated. Excitation laser intensities are therefore limited and signals are weak, despite their favorable spectroscopic properties. For the observation of fuel distributions prior to combustion this class of fluorescing species is not suitable.

Small Inorganic Molecules. Di- and triatomic inorganic molecules are frequently used in combustion diagnostics. While unstable radicals such as OH, CH, C_2 that appear during the combustion process can be used

for flame-front localization and combustion diagnostics [20.10], they are not suitable for observations in the mixing process prior to ignition. Strongly fluorescing stable species, however, are potentially interesting as tracers for the airflow. NO has been used despite its toxicity for studies in gaseous mixing processes [20.184,185] and its spectroscopy is well understood for a wide range of possible applications [20.186]. OH and NO can also be photolytically generated in flow systems. While not suited for studying mixing on a large scale, these flow-tagging techniques give detailed insight into the fluid motion within the lifetime of the generated species. OH has been generated following photodissociation of vibrationally hot water [20.167], NO has been produced from NO_2 photolysis [20.187] and from O_2 photolysis in air [20.188].

Molecular oxygen has been used to *trace* the air flow [20.189] and to measure temperatures during mixture formation in a Diesel engine [20.180]. It was also used for flow tagging following the excitation of higher vibrational states by stimulated Raman scattering [known as Raman excitation plus laser-induced electronic fluorescence (RELIEF) [20.169]].

Iodine was applied as a fluorescing tracer that can be excited and detected in the visible spectral range [20.190]. Its toxicity, corrosiveness and the difficulty of seeding iodine at constant rates limits its practical applicability. SO_2 can be excited at various wavelengths below 390 nm and subsequently emits fluorescence from the UV to the violet [20.191–193]. The (corrosive and toxic) gas (boiling point: $-10\,^{\circ}C$) can either be doped into the flow or generated in a flame from sulfur-containing precursors [20.194]. The latter application was suggested to mark residual burned gases in internal engine combustion and to visualize their mixing with fresh air and fuel. SO_2 fluorescence is strongly quenched by many molecules, including N_2 [20.192, 195–198]. Its applicability in high-pressure environments is therefore restricted. The LIF properties of high-temperature CO_2 upon excitation in the UV [20.179] offer the potential for new diagnostics for the observation of mixing of hot burned gases with air and fuel.

Organic Molecules. In contrast to the excitation of atoms and di- and several triatomic molecules, polyatomic organic molecules have a high density of states and therefore show broadband absorption spectra with excitation possible at various wavelengths that are often accessible with standard laser sources. The organic tracers are chemically close relatives of hydrocarbon fuels. Some of the molecules that are attractive tracers are present in commercial fuels at the few percent level. Therefore, relatively high tracer concentrations can be applied without significantly disturbing the combustion process.

The chemical similarity between tracer and fuel has the additional advantage that the tracer disappears (burns) together with the fuel close to the flame front. In measurements with limited spatial resolution (≈ 1 mm) this is a good match to identify and visualize the position of reactive zones. However, since the reaction kinetics of the tracer is not perfectly identical to that of the fuel, tracers are not in general suitable for high-resolution measurements close to the flame front, because their concentration may not represent the fuel concentration accurately in this zone.

Fluorescing organic tracers come in different sizes and structures with different volatilities. According to their boiling points as a first criterion they can be used to represent different volatility classes of multicomponent fuels [20.199]. At the same time, care must be taken to avoid distillation processes that separate fuel and tracer due to non-ideal boiling behavior during the fuel evaporation [20.200–202].

Aromatic hydrocarbons are typical components of commercial fuels. These species are responsible for the strong absorption in the UV and the subsequently emitted fluorescence [20.203]. Single-ring aromatics such as benzene, toluene and xylene are part of gasoline fuels on the percent level while two-ring aromatics such as naphthalene and its derivatives are present in Diesel fuels. They typically have high fluorescence quantum yields (toluene: $\phi = 0.17$, benzene: $\phi = 0.22$, fluorene: $\phi = 0.66$, dimethyl anthracene: $\phi = 0.82$) and their absorption and emission spectra shift towards the red with increasing size of the aromatic system. The wide variety of molecular sizes (and therefore boiling points) makes this class of molecules attractive as tracers that can be adjusted to the boiling behavior of the fuel or that are representative for boiling classes in multicomponent fuels. For seeding room-temperature gas flows compounds larger than benzene and toluene have too low vapor pressures.

A major drawback of aromatic tracers is the strong quenching by oxygen. The signal intensities therefore do not only depend on the tracer but also (inversely) on the oxygen concentration. This effect was taken advantage of by interpreting the signal as proportional to fuel–air ratios, which are of major practical interest.

The aromatic compounds in commercial fuels have been used for qualitative and semiquantitative

measurements, both in the vapor [20.204] and liquid phase [20.205, 206]. Benzene as a fuel tracer is typically avoided because of its carcinogenic effects. Toluene is less toxic and not considered carcinogenic. Therefore, it has been most frequently chosen as a fuel tracer [20.207] and recent publications have shed more light on the dependence of its fluorescence on p, T and n_{O_2} [20.208, 209]; α-methyl naphthalene was investigated by LIF, see e.g. [20.210], because it is part of a model two-component fuel that is used in experimental and numerical studies as a substitute for diesel or JP8 fuel. Like naphthalene, it is used in combination with N,N,N',N'-tetra-methyl-p-phenylenediamine (TMPD) in exciplex studies to visualize liquid and vapor phases simultaneously [20.211].

Aliphatic Compounds. Typical saturated aliphatic hydrocarbons such as alkanes and saturated alcohols do not fluoresce. They have their first absorption bands in the vacuum-UV region and excitation typically leads to photodissociation. Nonsaturated hydrocarbons with extended conjugated systems that would have useful spectroscopic properties are unstable and tend to polymerize.

Fluorescing aliphatic candidates contain chromophores that allow excitation into stable states that subsequently fluoresce. This class of molecules includes ketones (R_2CO), aldehydes (R−CHO) and amines (R_3N, where R is a saturated aliphatic hydrocarbon chain). The (conjugated) combination of chromophores (as in diketones R−CO−CO−R) typically shifts the absorption and fluorescence spectra to the red.

Ketones are the most frequently used class of fluorescent tracers. Their properties have been extensively studied [20.212–218] and they have been applied to various practical situations [20.219–222]. The high vapor pressure makes acetone (bp: 56 °C) an ideal tracer for gaseous flows [20.223, 224]. 3-pentanone (bp: 100 °C) [20.213, 225, 226] or mixtures of 3-pentanone and 3-hexanone [20.200] have been suggested as tracers that mimic the boiling and transport properties of gasoline. In most of those cases, *iso*-octane was substituting gasoline. This has the advantage that *iso*-octane is non-fluorescent and as a single component is more amenable to detailed modeling studies. For Diesel fuels, the use of even larger ketones was suggested, although they turned out to have limited stability at high temperatures. The larger aliphatic chains enhance the reactivity of the carbonyl group.

The smallest aldehyde, formaldehyde (HCHO), tends to polymerize and is therefore difficult to handle as a dopant. The next largest homologous molecule, acetaldehyde (CH_3CHO), has been used as a tracer in internal combustion engines [20.227]. Its low boiling point (21 °C) allows high seeding concentrations. Its spectral properties are comparable to those of acetone. Because acetone is considered less harmful, acetaldehyde is not frequently used as a tracer substance. Aldehydes with different molecular weight have been used to trace different boiling fractions in multicomponent fuels [20.228].

The fluorescence quantum yields ($\phi = 0.0008-0.0018$ for acetaldehyde depending on the excitation wavelength and $\phi = 0.002$ for acetone [20.229, 230]) are small compared to those of aromatic compounds in the absence of oxygen. In realistic situations where fuel is mixed with air, however, the resulting signals are comparable. Hexafluoroacetone has been suggested as an alternative that has fluorescence quantum yields about an order of magnitude stronger than in acetone [20.231, 232]. Because of its toxicity, however, this substance has not been further considered as a tracer for practical applications.

Biacetyl ($CH_3-CO-CO-CH_3$) is frequently used as a fluorescent tracer. With a boiling point of 88 °C the room-temperature vapor pressure is too low for many applications. On the other hand, the boiling point is significantly below that of typical fuels. This intermediate position, its stability and its strong odor might be the reasons why biacetyl, despite its attractive spectroscopic properties and its extensively studied photophysics [20.233–235], is less popular than ketones. For seeding oxygen-free flows, biacetyl is especially attractive because of its high phosphorescence quantum yield (15%, but strongly quenched by O_2).

Amines do fluoresce upon UV excitation. Some studies have covered ethylamine [20.236], and N,N-dimethylaniline [20.237]. Strong quenching by oxygen often hinders practical applications and an unpleasant (fish-like) smell and toxicity may deter people from using this class of tracers. Amines have found some attention as part of exciplex systems TMPD [20.211, 238], triethylamine (TEA) [20.239], and diethylmethylamine (DEMA) [20.240]. TEA and DEMA do not contribute significantly to the overall gas-phase signal but play an important role in forming the excited complex that is responsible for a shift of the liquid-phase fluorescence relative to that of the monomers.

Analysis of Air–Fuel Ratio. Depending on the system under study various approaches have been used for determining the local fuel–air equivalence ratio

ϕ. In situations where the local oxygen concentration can be predicted, the standard procedure relies on the application of a fluorescent tracer that is considered independent of oxygen (i. e., acetone or 3-pentanone). As long as the fuel concentration is reasonably low (not close to a directly-injected fuel spray) and as long as oxygen is homogeneously distributed in the fresh air (no exhaust gas recirculation) and as long as temperature is known, air–fuel ratios can be determined directly [20.220, 225, 241]. With a simultaneous measurement of temperature the results are less dependent on these assumptions [20.134]. In areas with high fuel concentration, the air partial pressure is reduced by the presence of fuel vapor. An iterative data evaluation can then be applied.

Another approach relies on the measurement of a single LIF signal that depends on both the fuel and the oxygen concentration [fuel–air ratio by laser-induced fluorescence (FARLIF)] [20.207]). FARLIF takes advantage of the strong quenching of toluene (or other tracer) LIF by O_2 in order to use toluene as a fluorescent tracer to measure ϕ directly [20.207]. Toluene fluorescence in air at room temperature is proportional to ϕ for $p > 3$ bar with 248 nm excitation. In IC engine applications the decrease of total fluorescence with increasing crank angle (i. e., increasing p and T) has been observed using excitation at 248 nm [20.242, 243]. Recent studies at elevated temperatures revealed a strong T dependence of the fluorescence quantum yield, which changes by more than two orders of magnitude within the temperature range of the compression stroke in engines, while the relative strength of O_2 quenching depends on the O_2 number density itself [20.208, 244, 245]. With these new findings FARLIF must be reconsidered and can only be applied within a limited range of conditions [20.246].

Further measurement strategies rely on the measurement of a number of signals (typically two) that depend on the fuel and the oxygen concentration. Mixtures of two fluorescent tracers, one of which is strongly quenched by O_2, have been applied in isothermal flows [20.135] and in an IC engine [20.242]. The combinative effects of oxygen and temperature variation are not yet fully understood. Therefore, measurements in systems with an inhomogeneous temperature distribution may be problematic. Additional information is currently being obtained [20.208, 209].

Finally, Raman scattering has been used for fuel–air measurements in pointwise measurements [20.241], line [20.247–249] and imaging measurements [20.250, 251]. These measurements require a detailed knowledge of the temperature-dependent shape of the Raman spectra and therefore require detailed calibration experiments or a detailed understanding of the underlying spectroscopy [20.252]. The influence of liquid droplets has been evaluated [20.248].

Multispecies Measurements during Mixture Formation in IC Engines. Knowledge of the spatial distribution of temperature and local fuel–air equivalence ratios in the combustion chamber in IC engines prior to ignition is of major interest when modeling engine combustion and modifying combustion chamber geometries. Especially in modern engines with stratified load and systems with exhaust gas recirculation that both strongly influence ignition and flame development, temperature and fuel concentration inhomogeneities are present.

2-D temperature distributions between 300 and 1000 K relevant for pre-combustion conditions can barely be assessed with other laser spectroscopic techniques developed for two-dimensional combustion thermometry so far. Rayleigh scattering has been employed for the determination of temperature fields in flames [20.140]. Engine measurements have been performed as well [20.253] but problems might occur in realistic engine geometries due to strong elastic scattering off surfaces. Since Rayleigh signal intensities are a function of a species-dependent scattering cross-section this method is not applicable in non-homogeneous systems where local effective Rayleigh cross-sections are unknown. Techniques based on atomic fluorescence [20.182, 254] and OH LIF [20.255] are only applicable to post-flame gases. NO-LIF thermometry [20.184, 185] would be an alternative because NO, when doped into the fresh gases, is present in both unburned and burned gases. This requires, however, an additional dopant and some uncertainty is induced in the fresh gases by the presence of NO_2 formed by reaction of NO with air.

For quantitative measurements of fuel vapor concentrations ketones such as 3-pentanone are frequently used because their evaporation properties are similar to those of common model fuels such as *iso*-octane [20.237]. Furthermore, the influence of collisional quenching, mainly by molecular oxygen, is greatly reduced compared to aromatic compounds since the lifetime of the excited states is limited by rapid intersystem crossing. 3-pentanone possesses an absorption feature at 220–340 nm with the peak near 280 nm at room temperature [20.213]. The absorption spectrum exhibits a temperature-induced shift towards longer wavelengths

of about 10 nm per increase of 100 K (Fig. 20.30). Upon excitation in this region, fluorescence is emitted between 330 and 550 nm, with a spectral distribution that is almost independent of the absorbed wavelength. This spectral shift of the absorption, albeit undesired for concentration measurements with single-wavelength excitation, can be used for measuring temperature, e.g., when 3-pentanone is seeded to non-fluorescing model fuels, as the fluorescence intensity is a function of the absorption coefficient for a given excitation wavelength, and thus, of temperature. After excitation at two different wavelengths the ratio of the fluorescence signal intensities reflects the local temperature. This was first described by *Großmann* et al. [20.213] and later applied to temperature measurements using acetone as a tracer [20.256]. Since this temperature measurement is based on the ratio of signal intensities it is independent of local tracer concentrations and therefore allows measurements of 2-D temperature distributions in nonhomogeneous systems.

For the organic tracers the fluorescence signal S for weak laser excitation is given by the following equation:

$$S_{\mathrm{fl}}(\lambda, p, c, T) = cI_{\mathrm{Laser}}(\lambda)VN\sigma(\lambda, p, x, T) \times\phi(\lambda, p, x, T)\,, \qquad (20.2)$$

where I_{Laser} is the local laser pulse energy in the detection volume V, N is the number density and σ the molecular absorption cross section of the marker, and

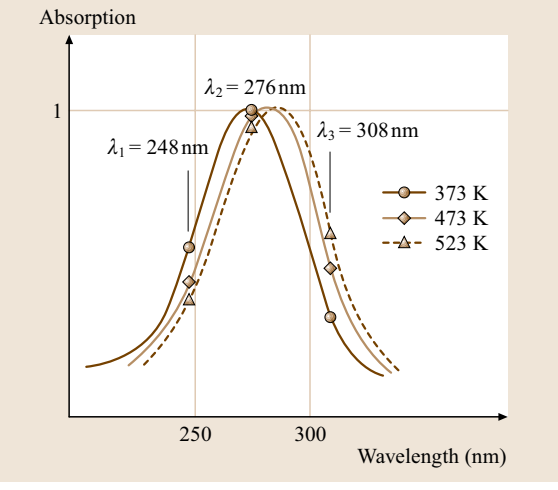

Fig. 20.30 Temperature dependence of the absorption spectra of 3-pentanone. The spectra are normalized, and the total integral increases with temperature [20.213]

ϕ its fluorescence quantum yield. σ and ϕ depend on the excitation wavelength λ, the pressure p, the mixture composition x, and the temperature T. The factor c captures geometrical arrangements and detection optics properties. If the same volume V is excited by two laser pulses of different wavelengths (with a short temporal delay to ensure separate detection of the induced fluorescence), the ratio

$$\frac{S_1(\lambda_1, p, T)}{S_2(\lambda_2, p, T)} = \frac{I_{\mathrm{Laser_1}}(\lambda_1)}{I_{\mathrm{Laser_2}}(\lambda_2)} \frac{\sigma_1(\lambda_1, p, x, T)}{\sigma_2(\lambda_2, p, x, T)} \times \frac{\phi_1(\lambda_1, p, x, T)}{\phi_2(\lambda_2, p, x, T)} \qquad (20.3)$$

depends on the pressure- and temperature-induced variation in absorption cross-sections and fluorescence quantum yields whereas it is independent of the observed volume V, the number density N of the detected species and the detection efficiency c. Pressure and possible composition effects can be corrected for using data provided by *Großmann* [20.213] and *Ossler* [20.215] by including a pressure-dependent ratio π_1/π_2 that includes effects on σ and ϕ. Then, the remaining ratio of both signals normalized to the respective laser energy is a function $F(T)$ of temperature only.

$$\frac{S_1(\lambda_1, p, T)/I_{\mathrm{Laser_1}}(\lambda_1)}{S_2(\lambda_2, p, T)/I_{\mathrm{Laser_2}}(\lambda_2)} \frac{\pi_2}{\pi_1} = \frac{\sigma_1(\lambda_1, T)}{\sigma_2(\lambda_2, T)} \frac{\phi_1(\lambda_1, T)}{\phi_2(\lambda_2, T)} = F(T)\,. \qquad (20.4)$$

A strong temperature dependence of the ratio, and hence high accuracy, can be expected when λ_1 and λ_2 are selected on opposite sides of the absorption maximum. We apply a combination of 248 and 308 nm excitation. The temperature dependence of the ratio $F(T)$ for these conditions is shown in Fig. 20.31 [20.257]. With the local

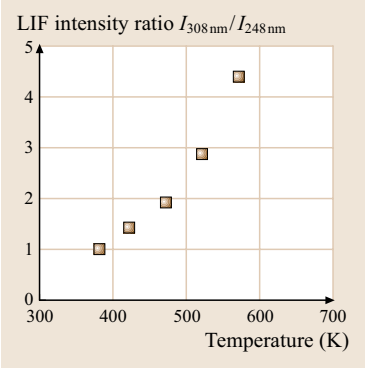

Fig. 20.31 Temperature dependence of the ratio of LIF intensities in 3-pentanone with 308 and 248 nm excitation [20.134]

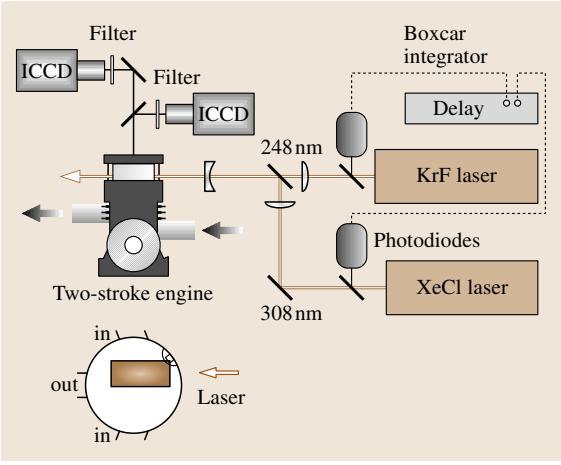

Fig. 20.32 Experimental setup for the simultaneous measurements of fuel concentration, temperature and air–fuel ratio in a two-stroke engine. The *lower figure* shows the position of the measurements displayed in Fig. 20.33

temperatures now determined from the signal ratio the fluorescence signals from either excitation wavelength can be corrected for temperature effects to calculate the number density N of tracer molecules. A calibration with a known number density of tracer molecules at a known temperature allows one to scale N to absolute number densities. With the ideal gas law the local *mole fraction* can then be calculated. The fuel–air equivalence ratio can then be determined based on the assumption that the cylinder contains fuel and air only and that the oxygen concentration is homogeneous within the air. There are limitations to these assumptions in systems with lots of recirculated exhaust gases. Techniques to overcome this problem will be discussed below.

The engine measurements [20.134] (Fig. 20.32) were conducted in a modified production-line single-cylinder two-stroke engine (bore: 80 mm, stroke: 74 mm, compression ratio: 8.6). The original cylinder head was replaced by a quartz ring with a height of 4 mm to allow for the entrance and exit of the laser sheets, and a full-size cylindrical quartz window on top through which fluorescence was monitored. The engine was carburetor-fueled with *iso*-octane doped with 10% (v/v) 3-pentanone. For the measurements described here the equivalence ratio was kept at $\phi = 0.62$ with an ignition timing at $-20°$ crank angle (CA) with respect to top dead center (TDC) at a speed of 1000 rpm. Two excimer lasers, operated with KrF (248 nm) and XeCl (308 nm), were fired with a fixed delay of 150 ns to prevent crosstalk between the LIF signals. The laser pulse energies were adjusted to no more than 50 mJ within a $20 \times 0.5\ \text{mm}^2$ light sheet. The signals were directed via a metal-coated beam splitter to two ICCD cameras that were equipped with $f_{\#} = 2$, $f = 100$ mm achromatic UV lenses.

Figure 20.33 shows the LIF intensities upon 308 nm excitation for three single-shot images (18° CA after

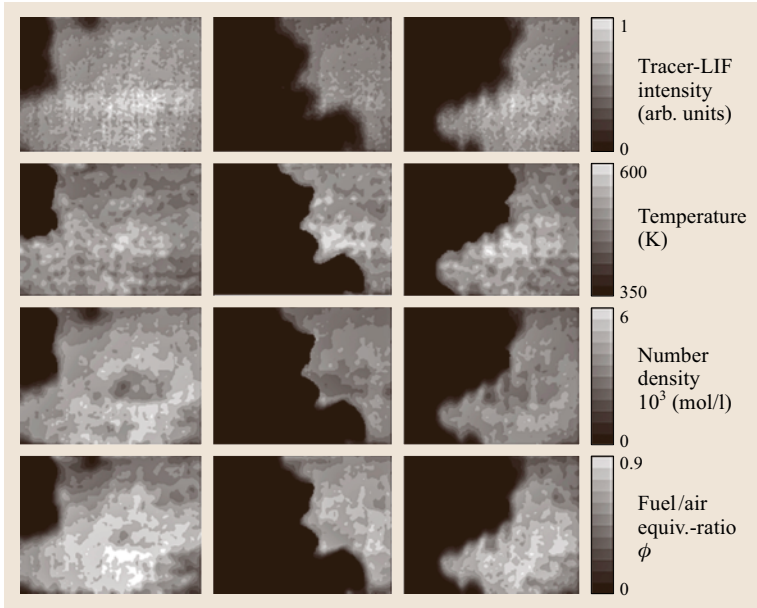

Fig. 20.33 Measurements of the tracer LIF intensity (first row), temperature (second row), fuel number density (third row) and fuel–air equivalence ratio (fourth row) in a two stroke engine. The columns show three randomly chosen data sets for instantaneous measurements [20.134]

TDC). The correction for temperature effects was performed on a per-pixel basis. The temperature-corrected LIF images were then calibrated to absolute number densities using the measurements under perfectly mixed conditions where the fuel concentration was calculated from the ratio of measured air flow and fuel consumption. The resulting images give absolute fuel number densities (third row). Since pressure gradients within the cylinder can be safely neglected temperature images allow the calculation of total number densities, which enable the calculation of fuel–air equivalence ratio distributions (fourth row). This series of images shows how the actual equivalence ratio corresponds to the measured LIF intensity.

Simultaneous Measurement of Fuel and Oxygen Concentration. In future highly energy-efficient combustion systems such as stratified-charge engines or homogeneous-charge compression-ignition (HCCI) engines, high concentrations of recycled exhaust gases strongly dilute the fuel–air mixture. In these situations, ignitability, flame speed, and auto-ignition susceptibility are governed by fuel and oxygen concentrations (number densities) rather than equivalence ratios. Whereas several techniques for measuring fuel concentrations and equivalence ratios are available (measurements for example based on the assumption that for tracers that are strongly quenched by oxygen – within a limited range [20.258] – the LIF signal is proportional to the equivalence ratio [20.207]. For the limitations of this assumptions under combustion-engine conditions see [20.246, 259]), we report here a technique that allows the simultaneous measurement of oxygen concentrations with a suitable tracer combination of aromatic and ketonic tracers. Aromatic molecules are efficiently quenched by molecular oxygen [20.260]. The influence of O_2 quenching on aliphatic ketones on the other hand is greatly reduced [20.213]. Aromatic and ketonic compounds have different LIF emission spectra upon excitation in the UV. Whereas single-ring aromatic compounds such as toluene display a narrow emission band peaking around 280 nm, the emission of ketones like 3-pentanone appears between 320 and 450 nm with a broad maximum at around 370 nm (Fig. 20.34). This difference has been used previously for the detection of the two different tracers when simultaneously observing the distribution of different volatility classes of multicomponent fuels [20.199]. Here, we use this two-tracer approach for measuring oxygen concentrations.

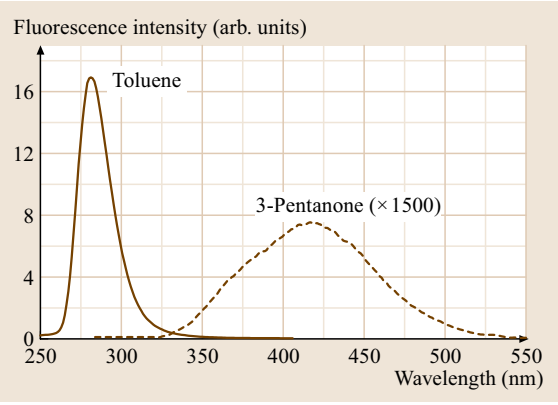

Fig. 20.34 Emission spectra of toluene and 3-pentanone with excitation at 248 nm. The signal of both species can be separated with appropriate filters. In pure nitrogen (shown here) the toluene signal dominates by far (3-pentanone signal enhanced by a factor of 1500) [20.135]

For weak excitation the LIF signal intensity S_{fl} is given above. Molecular oxygen is regarded as the only relevant species quenching toluene fluorescence, while 3-pentanone fluorescence is considered independent of oxygen concentration. For a mixture of 3-pentanone (3P) and toluene (tol) the ratio of signal intensities S_{fl}^{R} (20.5) is a function of the oxygen concentration only [$f(n_{O_2})$] since all the other factors are either constant (like absorption cross sections due to constant pressure and temperature) or cancel (like the local laser intensity and detection volume):

$$S_{fl}^{R} = \frac{S_{fl}^{3P}}{S_{fl}^{tol}} = \text{const} \times \frac{\phi_{fl}^{3P}}{\phi_{fl}^{tol}} = f(n_{O_2}) \,. \tag{20.5}$$

The fluorescence quantum yield ϕ_{fl}^{i} for species i is

$$\phi_{fl}^{i} = \frac{k_{fl}^{i}}{k_{tot}^{i} + \tilde{k}_{q}^{i} n_q} \tag{20.6}$$

with the rate coefficient for spontaneous emission k_{fl}^{i} and the sum rate of all collision-independent de-excitation processes k_{tot}^{i}. $\tilde{k}_{q}^{i}$ is the rate coefficient for collisional quenching with the quencher (i. e., O_2) number density n_q.

For atmospheric pressure in 3-pentanone, as in all aliphatic ketones, quenching by O_2 can be neglected (because $\tilde{k}_{q}^{3P} n_q \ll k_{tot}^{3P}$). With the Stern–Volmer coefficient for toluene quenched by O_2 ($k_{SV}^{tol,O_2} = \tilde{k}_{q}^{tol,O_2} / k_{tot}^{tol}$) the above equation can be rewritten [20.135]:

$$S_{fl}^{R} = \text{const} \frac{k_{fl}^{3P} (k_{tot}^{tol} + \tilde{k}_{q}^{tol} n_q)}{k_{tot}^{3P} k_{fl}^{tol}} = c_1 \left(1 + k_{SV}^{tol,O_2} n_q\right) \,. \tag{20.7}$$

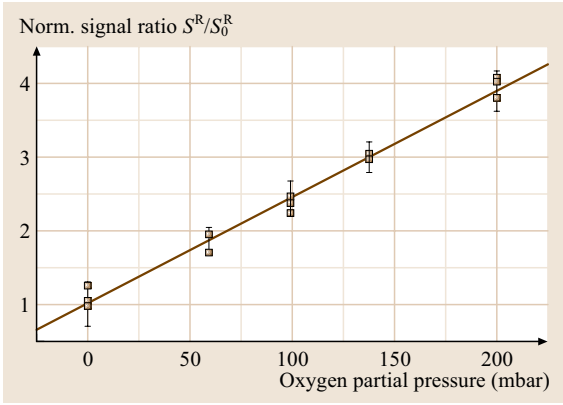

Fig. 20.35 Signal ratio of 3-pentanone and toluene LIF normalized to the ratio measured in pure nitrogen [20.135]

The signal ratio of 3-pentanone versus toluene LIF therefore increases linearly with the oxygen number density. The offset, given by c_1, can be obtained from a single-point calibration. An experimental validation is shown in Fig. 20.35. This simple approach assumes that the toluene and 3-pentanone signals are detected independently without any spectral overlap and that oxygen is the only quenching species. Further corrections may be added in order to reduce the systematic errors caused by these assumptions [20.135].

The Stern–Volmer coefficients and absorption and fluorescence spectra have been measured in a static cell where evaporated tracers were combined with various pressures of air and nitrogen. The imaging experiments were carried out in an optically accessible quartz cell with square cross section ($40\,\text{mm}^2 \times 40\,\text{mm}^2$). Two metal tubes (exit diameter 1 mm) were inserted 5 mm apart with the gas streams mixing at an angle of approximately 30°. The tubes were supplied with various mixtures of nitrogen and oxygen controlled by mass-flow controllers. The gas mixtures were bubbled through a blend of the liquid tracers (3-pentanone and toluene, 50 : 50 per volume), which were kept at a constant temperature of 293 K. The gaseous tracer concentration was therefore constant in both gas streams with a fixed ratio of both tracer compounds determined by the vapor pressure of the binary mixture. The volume of the liquid mixture was large enough to ensure negligible changes in its composition over time. For the experiments presented here one stream was supplied with pure nitrogen and the other contained variable oxygen concentrations. The gas exit velocities were set to 5–15 m/s. The mixing cell was purged with an additional nitrogen flow that was quiescent compared to the velocities of the other two gas streams. For calibration of the LIF signal ratio, a single gas stream with identical tracer concentrations but at various well-known oxygen concentrations was used. For imaging, the 248 nm laser beam was expanded to a light sheet 0.4 mm thick and 30 mm high and directed through the quartz cell 2 mm below the tube exits. The LIF signal was detected simultaneously with two ICCD cameras equipped with appropriate filters for observing each tracer separately.

Results of the two-tracer imaging technique in an arrangement of interacting N_2 and air gas jets within a quiescent N_2 atmosphere are shown in Fig. 20.36. The first box Fig. 20.36a shows the individual pictures taken in the toluene and 3-pentanone spectral region in the

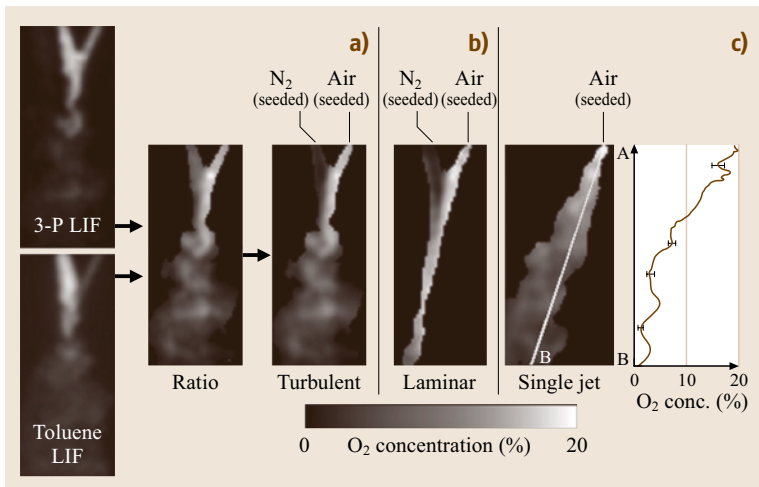

Fig. 20.36 Results of the O_2 imaging measurements in the mixing chamber [20.135]. For details see the text

two interacting turbulent gas jets. The 3P-LIF image shows increased signal intensities in the nitrogen jet due to some spectral overlap from the strong toluene signal. This error is corrected for by quantifying the relative contribution of toluene LIF to the 3-pentanone detection channel in additional experiments where the flow is seeded with toluene only. The second image shows that the ratio of signal intensities is not directly a function of oxygen number density [according to (20.7)] since the left jet (containing no O_2) yields higher signal intensities compared to the mixing region. After correcting for energy transfer processes [20.135], this artifact disappears (right image in Fig. 20.36a) and the resulting signal is calibrated using a measurement in pure air. Figure 20.36b shows the oxygen distribution in similar flows at a slower exit velocity at which the two laminar gas flows stay mostly separated. Figure 20.36c shows the O_2 distribution in an air jet injected into a quiescent N_2 atmosphere where the dilution of O_2 by entrainment of N_2 is clearly visible. The line plot shows the oxygen concentration along the line in the 2-D image including error bars to demonstrate the sensitivity of the technique. Since only the incoming jets were seeded by tracers, the outer region does not yield any information in these measurements and is shown in black.

Quantitative Nitric Oxide Diagnostics in High-Pressure Combustion

Detection of nitric oxide using LIF is of particular interest because NO is one of the most important combustion-generated pollutants. Oxides of nitrogen in the atmosphere contribute to photochemical smog and are precursors to acid rain. Exhaust from aircraft engines can add to the destruction of stratospheric ozone while automobile exhaust adds NO/NO_2 to our urban atmosphere. A significant amount of this nitrogen oxide is directly caused by combustion of biomass and fossil fuels [20.262]. As regulations for the restriction of NO become more stringent, much effort and research is underway to develop new and improved combustion systems that meet these standards. To optimize the combustion processes involved, a coupled understanding of physical and chemical processes and empirical diagnostic methods to map out the formation of the pollutants are required.

Choice of NO Detection Schemes for High-Pressure Flames. Two-dimensional LIF measurements of trace species require the coincidence of strong electronic transitions with the emitted wavelength of intense light

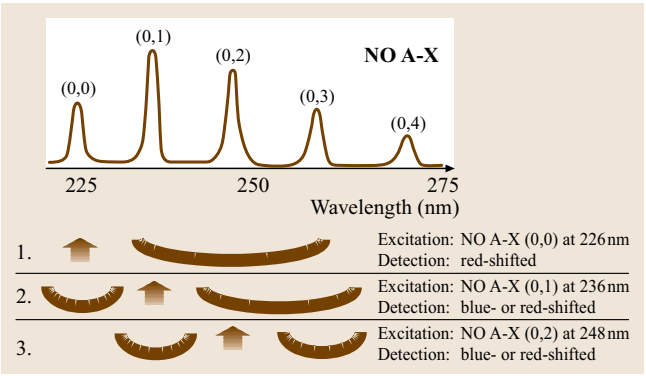

Fig. 20.37 Different options for NO LIF detection with excitation in the A – X band

sources; therefore, excimer lasers are a convenient source for NO excitation, but the limited wavelength tuning enables only a few excitation schemes. The NO D-X(0,1) system can be probed with 193 nm radiation, e.g., from an ArF excimer laser [20.263], the A-X(0,0)

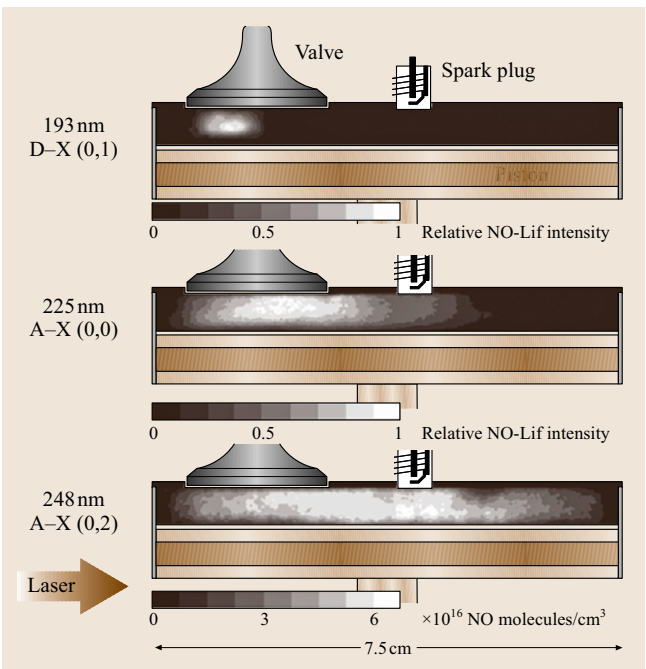

Fig. 20.38 Attenuation of laser light at different wavelengths during NO imaging with 193, 225 and 248 nm excitation. All three frames show the engine under identical operating conditions. Only with the longest wavelength (248 nm) was the expected symmetrical distribution of NO in the cylinder observed ($\phi = 1$ propane/air flame, actual pressure: 13 bar) [20.253, 261]

band at 225 nm with a H_2 Raman-shifted KrF excimer laser [20.150], or the A-X(0,2) band at 248 nm with a tunable KrF excimer laser [20.264]. Other measurements have been carried out with dye lasers and OPO systems in the (0,0) [20.265,266] and (0,1) [20.267,268] bands.

The NO D-X(0,1) system at 193 nm works for combustion processes where strongly absorbing species are present at low number densities only. In high-pressure combustion systems drastic attenuation of laser and signal light by hot CO_2, H_2O and O_2 limits their applicability [20.261,270]. Therefore, we focus here on three NO detection schemes with A-X excitation, as depicted in Fig. 20.37.

In lean and stoichiometric high-pressure flames the selectivity of NO detection is perturbed by interfering hot-bands of O_2 that overlap the NO excitations. At pressures of a few bar, the quantum yield of O_2 LIF is dominated by predissociation, and the NO quantum yield decreases with increasing pressure due to collisional quenching while the O_2-LIF quantum yields remains constant. It is therefore crucial to choose NO excitation schemes that minimize the simultaneous excitation of O_2.

The NO A-X(0,0) system at 225 nm has been successfully used for measurements in high-pressure methane/air flames [20.271] and in engines fueled with propane under conditions up to 20 bar [20.272]. Three different strategies have been studied and applied to combustion diagnostics. Whereas *DiRosa* et al. [20.265] uses the combined $P_1(23.5)$, $Q_1+R_{12}(14.5)$, $Q_2+R_{12}(20.5)$ feature at 226.03 nm, *Laurendeau* et al. [20.266] prefer the $Q_2(26.5)$ transition at 225.58 nm. Within the tuning range of the Raman-shifted KrF excimer *Sick* [20.272] chooses the $R_1+Q_1(21.5)$ line at 225.25 nm. We use measurements in a methane/air flames at 1–60 bar to compare the O_2 LIF interference and signal intensities of these three approaches.

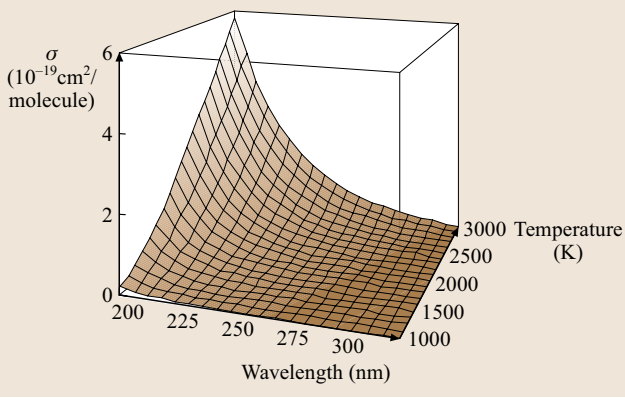

Fig. 20.39 Wavelength and temperature dependence of the CO_2 absorption cross sections [20.269]. A parameter fit to this data for the calculation of temperature- and wavelength-dependent absorption cross sections can be found in [20.261]

Optical absorption in high-pressure combustion environments increases strongly at short wavelengths [20.261, 270] as a result of the transmission properties of hot CO_2 and H_2O [20.269, 273]. In high-pressure media, where the number density of absorbers is high, it is therefore desirable to use the longest possible wavelengths for excitation and detection. Excitation of the NO $A-X(0,2)$ near 248 nm [20.264, 274] exploits the strong KrF laser sources and has significantly less optical absorption in the engine; the feasibility of this approach is demonstrated with detailed spectroscopic studies [20.153, 274] and in-cylinder engine measurements (Fig. 20.38) [20.253, 275, 276]. In addition, this strategy allows the detection of NO fluorescence in the $A-X(0,1)$ band, which is blue of the excitation light. This is a significant advantage as it suppresses LIF interference from intermediate hydrocarbon compounds. Unfortunately, the thermal population of the $v''=2$ level at post-flame temperatures is small, leading to a rather weak LIF signal intensity.

The availability of optical parametric oscillator systems (OPOs) which provide high laser pulse energies throughout the UV (up to 30 mJ/pulse) allows convenient excitation of the NO $A-X(0,1)$ transition, and *Jamette* et al. applied this scheme to measurements in an spark ignition (SI) engine [20.267].

A detailed analysis of the properties of the different excitation/emission schemes in the NO $A-X$ has been performed based on spectroscopic measurements in laminar high-pressure flames [20.153, 186, 277–280]. The results were used to develop the *LIFSim* spectral simulation code that allows the simulation of absorption and emission spectra as well as the pressure and temperature influence in user-specified gas mixtures [20.174, 281].

Influence of Attenuation by Hot CO_2. Experiments in engines and high-pressure flames showed that hot exhaust gases strongly attenuate UV laser and signal light [20.261]. Figure 20.39 shows the strong wavelength dependence of the transmission of laser light in hot combustion gases. It was shown that this effect is mainly due to the shift of vacuum-UV absorption features of CO_2 towards longer wavelengths with increasing temperature [20.269]. For H_2O a similar

Table 20.2a,b Transmission at NO excitation wavelengths in two typical high-pressure combustion situations due to hot CO_2 (CO_2 and H_2O) absorption: **(a)** high-pressure flame: diameter 8 mm, 40 bar, 2300 K and **(b)** engine cylinder: diameter 7 cm, 13 bar, 2400 K [20.261]

	High-pressure flame, diameter: 8 mm	Engine cylinder, diameter: 7 cm
193 nm	13.7% (0.4%)	0.02% (10^{-6}%)
226 nm	62.4% (58.1%)	11.5% (9.1%)
237 nm	75.4% (73.8%)	26.6% (24.8%)
248 nm	84.4% (83.9%)	44.3% (43.4%)

behavior can be found at short wavelengths. It is, however, negligible at $\lambda > 230$ nm [20.269]. Transmission in typical high-pressure combustion situations is calculated (based on an empirical fit to the data in Fig. 20.40 [20.261]) for the different NO excitation wavelengths and summarized in Table 20.2. These data show that in many practical applications the longest possible wavelengths must be used for NO excitation despite the relatively weak fluorescence intensity that can be expected upon excitation from the excited vibrational levels.

Temperature Dependence of the Different NO Excitation Strategies. LIF diagnostics of practical systems are greatly simplified if the signal is relatively insensitive to the local gas temperature. The Boltzmann population of each of the vibrational manifolds produces quite different temperature sensitivities. In the temperature range relevant to post-flame gases (1500–2500 K) the signal intensity after excitation in the (0,0) band decreases with increasing temperature whereas in the (0,1) and (0,2) bands signals are strongly increasing. Minimal variation of the ro-vibrational population with temperature is found for the intermediate rotational levels in the (0,0) band. The (0,1) band has minimal pressure dependence since the chosen excitation line is within a very dense part of the spectrum where at elevated pressures neighboring lines contribute significantly to the overall signal. The simulated temperature dependence of the NO-LIF signal is shown in Fig. 20.40 for $p = 10$ bar for the candidates with minimal O_2 LIF interference for

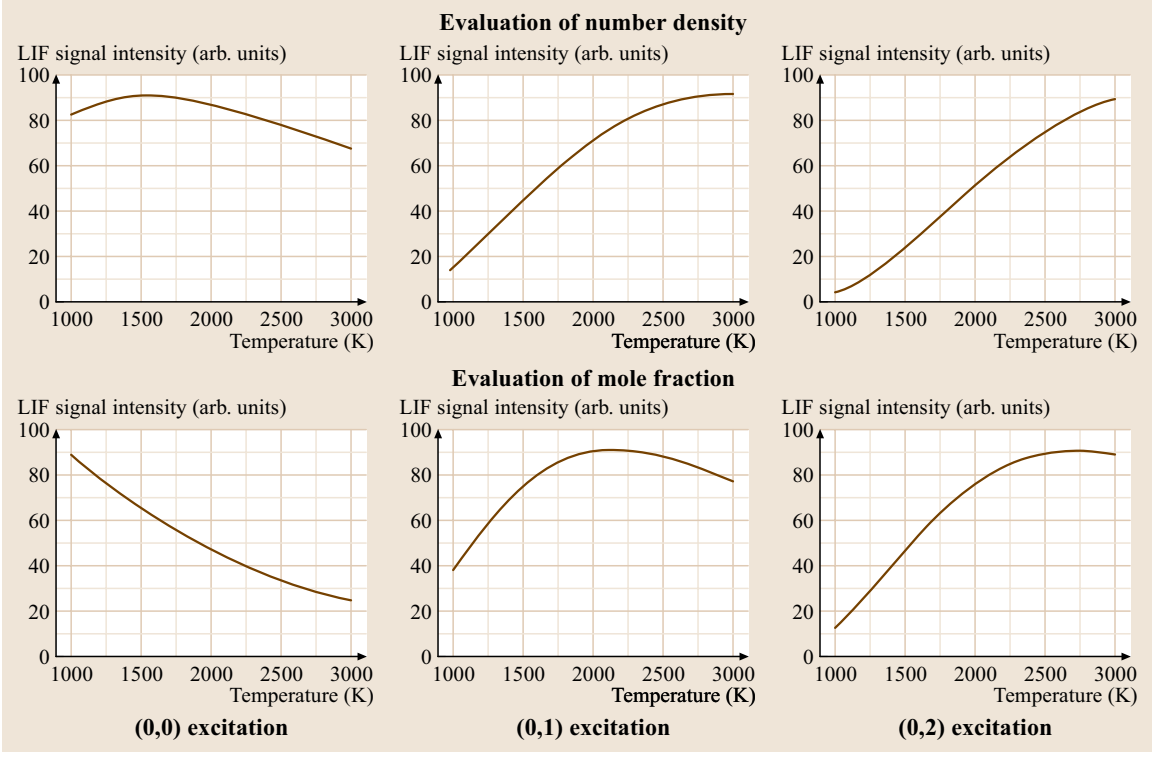

Fig. 20.40 Simulated variation of NO LIF signal with temperature for three excitation strategies. Rotational transitions with minimal O_2 LIF interference have been chosen [20.186]. $p = 10$ bar

each vibrational band. The data in Fig. 20.40 include the temperature dependence of Boltzmann population, spectral overlap of laser and NO transition, and collisional quenching. Note this temperature dependence can be mitigated with the judicious choice of measuring either number density or mole fraction. Excitation in the (0,0) band has weak temperature dependence of *number density*; however, excitation of the (0,1) or (0,2) bands can provide *mole fraction* measurements that are weakly temperature dependent at combustion temperatures.

There are three practical schemes for NO A – X LIF, which involve exciting transitions in the (0,0), (0,1) and (0,2) bands. In systems where excitation in the NO A – X(0, 0) band is not hindered by laser and signal absorption an NO absorption feature at 226.03 nm was found to be the best choice in terms of spectral purity and signal intensity. A – X(0, 1) excitation with (0,0) detection provides strong signal, small variation of signal with gas temperature when evaluating mole fraction, and good suppression of O_2-LIF interference. Any scheme exciting or detecting (0,0) in high-pressure hydrocarbon combustion, however, is plagued by attenuation of the excitation or fluorescence light. Excitation of A – X(0, 1) with (0,2) detection provides significantly stronger signals with less temperature variation than strategies using (0,2) excitation, and the interference from O_2 LIF is comparable for (0,1) and (0,2) excitation. However, practical engine diagnostics have hydrocarbon fluorescence interference red of the excitation light. The strategy of exciting NO A – X(0, 2) and detection of (0,1) provides LIF signal blue-shifted compared to the excitation light. This advantage may outweigh the lower signal and greater temperature sensitivity for practical diagnostics applications.

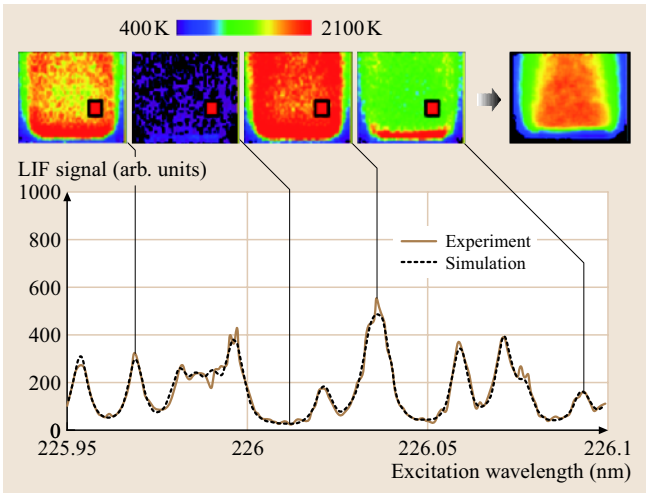

Fig. 20.41 Schematic of multi-line 2-D temperature measurement strategy based on a single point. NO A – X(0, 0) excitation at 5 bar. The images show an area of 11 mm² × 13 mm² above the burner exit [20.185]

Quantitative Multi-Line Temperature Imaging. Temperature imaging is often performed as a two-line technique that probes the relative population of two ro-vibrational ground states in molecules such as NO [20.282, 283] or OH [20.255, 284]. This technique typically requires a calibration with measurements in an environment with known temperature and is affected by background signal. With simultaneous application of two excitation wavelengths, instantaneous temperature imaging is possible. Alternatively, scanning techniques have been applied that record the fluorescence excitation spectrum over an extended range of excitation wavelengths and evaluates absolute temperatures – independent of signal background – from the shape of the spectra [20.271]. We use the latter approach to measure temperature fields in stationary flames [20.185]. For the multi-line temperature imaging, 2-D LIF excitation scans were performed over a broad spectral range in the NO A – X(0, 0) band. For each individual pixel, LIF intensities were extracted versus excitation wavelengths, yielding experimental excitation spectra (Fig. 20.41).

The LIFSim spectral simulation code [20.281, 285] was then used to fit simulated spectra to the experimental data for each pixel. This yields absolute temperatures without the requirement for calibration. Simultaneous fit of background signal and LIF strength makes this technique robust against both broadband interference and laser and signal attenuation. This evaluation therefore yields temperature and semiquantitative NO concentrations that then can be calibrated by adding known amounts of NO to the fresh gases according to [20.153]. The broadband background that was recently attributed to CO_2 LIF [20.179] is measured at the same time yielding spatial distributions of CO_2 LIF intensities [20.179, 286]. The temperature information in turn can be used to calculate the local laser and signal attenuation due to hot CO_2 based on the data shown in Fig. 20.39 assuming a homogeneous concentration of CO_2 in the burned gases. These corrections have been applied for the measurement of quantitative NO concentration distributions in the (unseeded) methane/air high-pressure flame.

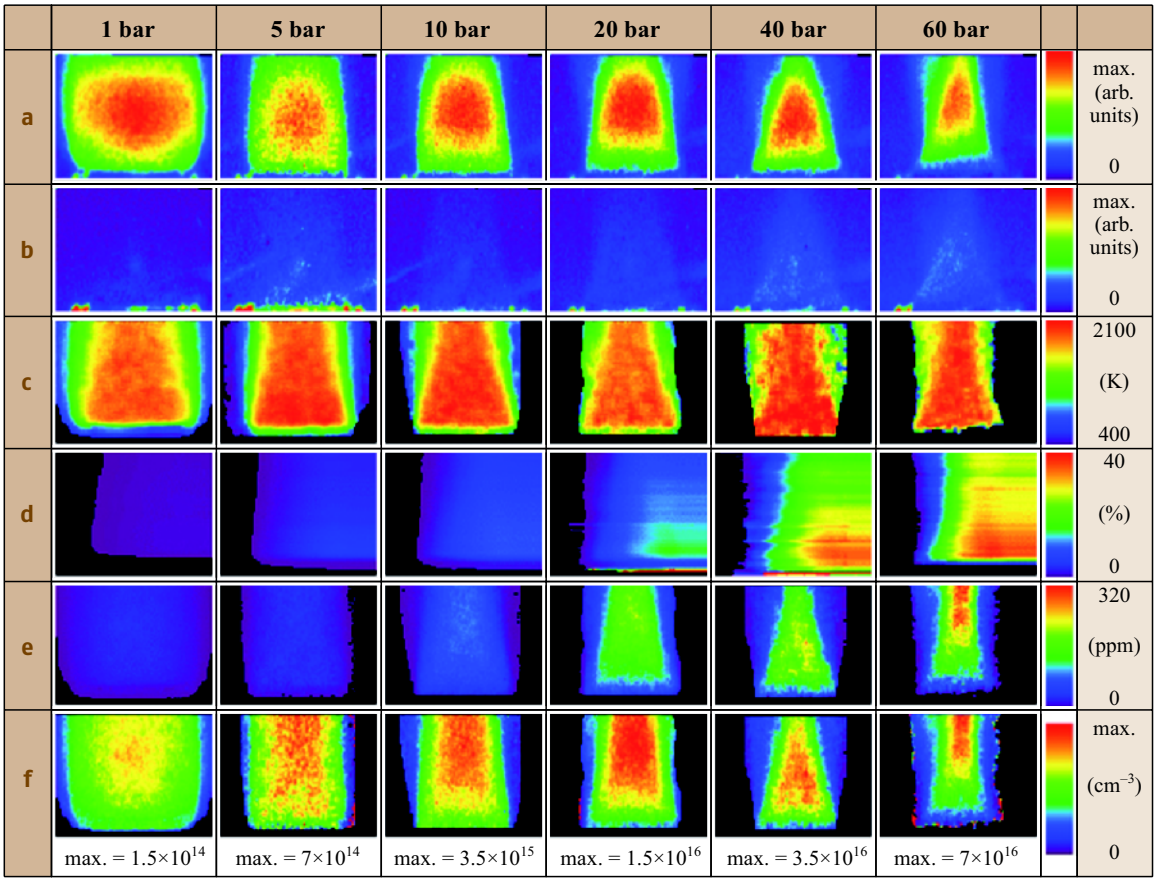

Fig. 20.42a–f Imaging results from a methane/air flame ($\phi = 0.95$, without seeding). **(a)** Raw NO-LIF images (not corrected for laser sheet inhomogeneities) **(b)** Raw off-resonant images **(c)** Absolute temperatures **(d)** Total attenuation due to laser and signal absorption by CO_2 and H_2O **(e)** Quantitative NO mole fractions (calibrated by NO-addition) **(f)** Quantitative NO number densities (calibrated by NO-addition method)

Figure 20.42 shows raw NO-LIF images, corrections performed for quantification, and evaluated NO concentrations. For maximum selectivity (i. e., minimum O_2 LIF interference), excitation was performed at 226.03 nm as discussed in the introduction section (Fig. 20.42a). Remaining interference was assessed by tuning the laser off-resonance to 224.78 nm (Fig. 20.42b). The temperature-sensitivity of the LIF signal was accounted for by using LIFSim. In many cases, temperature insensitivity is advantageous when conducting concentration imaging because of fluctuation of temperature within the view of the image. The temperature fields that were acquired using the multi-line technique are shown in Fig. 20.42c. A correction for collisional quenching was applied. Collisional quenching scales linearly with pressure when the gas composition is unchanged; however, due to the fact that gas composition and collisional cross-section are all temperature dependent, correction for this temperature effect is required. Figure 20.42d shows the corrections applied for signal and laser beam attenuation. Recent experiments have shown that in high-pressure and high-temperature combustion environments, the UV transmission is reduced by absorption from major species such as CO_2 and H_2O. The attenuation of both the laser beam and the LIF signal due to CO_2 and H_2O require calibration and have been accounted for in the imaging processing stage. The corrected and calibrated NO concentrations are shown in Fig. 20.42e (mole fractions) and f (number densities). Recent measurements report the application of multi-

line NO-LIF thermometry also to sooting high-pressure flames and spray flames [20.276, 287–289].

Quantitative NO Diagnostics in Engines. Minimizing the generation of the pollutant nitric oxide is of particular interest when improving the environmental acceptance of internal combustion engines. While the release of many unwanted exhaust compounds like unburned hydrocarbons and carbon monoxide has been drastically reduced within the last years, additional effort is necessary to further reduce the NO release in order to meet future legislative regulations. Especially in modern lean-burning engines, inhomogeneous combustion conditions make it difficult to control the pollutant formation. Furthermore, standard catalytic converters can not be used since the overall air–fuel ratio deviates significantly from unity. Exhaust gas recirculation (EGR) has been used successfully in diesel and in gasoline engines to reduce the raw NO formation mainly due to decreased combustion temperatures. A detailed understanding of the elementary physical and chemical steps involved as well as their coupling is necessary to allow a mathematical description of the combustion process. Models with the ability of predicting optimized operating conditions, however, need input and feedback from preferably quantitative in-cylinder experiments.

For in-cylinder NO imaging diagnostics we use NO excitation in the $A-X(0, 2)$ band with a tunable KrF excimer laser at 247.94 nm and subsequent detection of the fluorescence light emitted from the $A-X(0, 1)$ transition around 237 nm. This technique allows the effective suppression of interfering LIF signals due to hot O_2 and CO_2 and partially burned hydrocarbons [20.274, 291, 292]. Therefore, selective detection of NO is possible even in inhomogeneous combustion environments like in direct injecting gasoline [20.275] and Diesel engines [20.293]. Furthermore, with this scheme the influence of laser beam attenuation is minimized [20.261, 270] (Fig. 20.38).

Figure 20.43 shows experimental and numerical results for the NO concentration distribution in a single-cylinder engine fueled with *iso*-octane air equipped with a production-type Volvo cylinder head [20.173, 294]. Care is taken to provide a homogeneous air/fuel mixture in these cases. Figure 20.44 shows results of spatially averaged NO concentration versus detection time in crank angle in a direct-injection engine with variable amounts of synthetic recirculated exhaust gases (variable mixtures and concentrations of N_2, CO_2, H_2O added to the intake air) [20.275, 290]. The experiments presented here were carried out in an optically accessible gasoline engine featuring a direct-injection cylinder head (BMW) and a Bosch injection system. A significant reduction of peak NO concentrations from 1200 ppm to 200 ppm with increasing EGR rate can be observed. A significant influence on the composition of the *synthetic exhaust gas* added to the fresh in-cylinder gases was found that correlates well with the heat capacity of the gas mixture [20.290]. For comparison with exhaust gas NO_x concentrations, results from the chemiluminescence (CLD) measurements

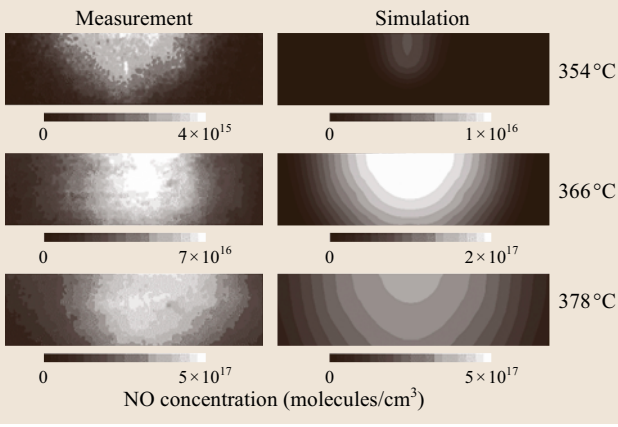

Fig. 20.43 Comparison of measured an simulated NO concentration distributions in an IC engine fueled with iso-octane/air [20.173]

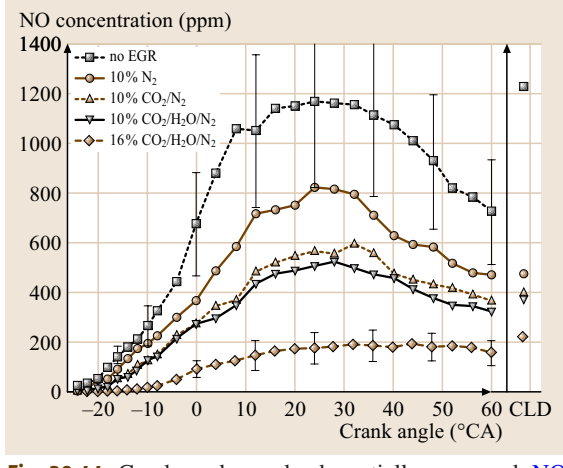

Fig. 20.44 Crank-angle-resolved spatially averaged NO concentrations for the different EGR conditions (see legend) in the BMW engine with gasoline direct injection. CLD NO_x concentration measurements are included in the graph [20.290]

have been included in Fig. 20.44. It should be kept in mind that the LIF images represent the NO concentration present in the plane defined by the position of the laser beam whereas the exhaust gas measurements represent averaged concentrations after homogeneously mixing the burned gases during the expansion and exhaust stroke. The comparison shows a good agreement of exhaust-gas concentrations and concentrations of the in-cylinder LIF measurements in the observed plane.

Soot Diagnostics

Soot formation has been a major issue in combustion research over the last few decades as soot is emitted by many practical combustion processes, e.g., power plants and IC engines. Soot is the result of incomplete combustion of hydrocarbons if not enough oxygen is locally available for full oxidation. Soot consists mainly of carbon but may have a wide range of properties and composition [20.295]. Transmission electron microscopy (TEM) shows that flame-generated soot consists of primary particles which have a typical size between 5 and 100 nm. Primary particles form aggregates that contain up to several hundred primary particles and have a fractal structure.

Laser-induced incandescence (LII) has proven to be a powerful tool for soot diagnostics. It was observed for the first time by *Week* and *Duley* in 1973 when they heated aerosols of carbon black and alumina with a CO_2 laser [20.296]. They set up the first energy balance describing the heating and cooling of particles and suggested that the method could be used for particle sizing. *Eckbreth* observed the incandescence as an interference in Raman scattering experiments in sooting propane diffusion flames [20.297]. In 1984 *Melton* set up the first detailed energy- and mass balance for LII and suggested to use LII as a tool for quantitative measurements of soot volume fractions [20.298]. Since the early 1990s LII has been used successfully in a variety of systems for measuring volume fractions of soot in laminar diffusion flames [20.299–303], laminar premixed flames [20.22, 304, 305], and turbulent flames [20.299, 306–308]. Particle sizes have been deduced from the temporal behavior of the LII signal taking the ratio of the LII signal at two different delay times after the signal peak [20.309, 310] as well as using the entire decay curve in point measurements [20.311–315]. In exhaust gases particle sizes have been measured with LII as well [20.316, 317]. Particle sizes were obtained assuming monodisperse particles [20.311,313,314] as well as considering a polydisperse lognormal particle-size distribution [20.312, 315].

The LII signal is due to thermal radiation from particles that are heated by an intense pulse laser. Subsequent cooling occurs due to several heat loss channels until, typically after a few hundreds of nanoseconds, the particle temperature reaches ambient gas temperature again. LII is basically used for two applications: Determination of the volume fraction of particles and particle sizing in the submicron region. Though LII has been used to investigate non-carbon particles [20.318–320] with increasing interest in recent years with the upcoming nanosciences, the main focus has been in the field of soot diagnostics. In the following overview LII will be discussed with respect to soot.

Soot volume fractions measured with LII are based on the detection of the temporally integrated LII signal over a certain range of wavelengths. This allows the expansion of the laser beam into a sheet and the detection of the signal light with a fast gated intensified CCD camera equipped with appropriate detection filters. In this way two-dimensional images of the soot distribution can be obtained, even in turbulent flames. As the emitted radiation of the laser-heated soot is close to that of a black body, corrected by the emissivity, a wide choice of detection wavelengths is available. Experimental and theoretical studies have shown [20.321,322] that detection towards longer wavelengths minimizes the influence of a variation in particle size and ambient gas temperature. However, in most practical environments a detection in the blue around 400 nm is preferred to obtain a better discrimination of LII signal against flame luminosity.

A large impact on the accuracy is caused by the choice of the temporal detection gate. First, after the laser heating smaller particles cool faster than large ones because small particles have a larger surface-to-volume ratio than large particles. If long or even delayed (relative to the laser pulse) detection gates are used the integrated signal will underestimate small particles [20.299, 321]. Second, with increasing pressure the LII signal decays faster due to an increased heat conduction with increasing pressure [20.323]. If calibration is carried out at one single pressure, long or delayed detection gates should be avoided. Hence, short and prompt, i. e., with the start of the laser pulse, detection gates of 50 ns or less should be used.

In LII, several excitation wavelengths have been used, mainly the fundamental, 1064 nm, and second harmonic, 532 nm, of pulsed Nd:YAG lasers. Light at 532 nm is easier to handle as it is visible and

lower laser fluences are necessary to heat up the soot particles as the absorption cross-section of soot at 532 nm is roughly twice the value at 1064 nm. However, 1064 nm causes less interference from electronically-excited C_2 [20.22, 324] and less broadband interference from PAH [20.325]. For low laser fluences the LII intensity rises monotonically with laser fluence as peak particle temperatures increase. Increasing laser fluence starts to vaporize the soot during the laser pulse and the maximum particle temperature remains constant. In this regime, where maximum particle temperature is reached but only minor vaporization occurs, the variation of LII with laser fluence is small, resulting in a so-called plateau region. This plateau region is preferred in soot volume fraction measurements as the LII signal is relatively independent of laser fluence. This is important in strongly absorbing environments. With higher fluences, the soot concentration is significantly reduced by vaporization resulting in reduced LII signals.

To obtain absolute soot volume fractions LII signals need to be calibrated. Therefore, the accuracy of LII is strongly influenced by the accuracy of the calibration method. A common method is the use of light extinction. However, this technique depends on the knowledge of the refractive index of soot. Different values have been reported for this value [20.326]. A method that is independent of an external calibration is the calibration with absolute light intensity [20.327]. The current status in LII is reviewed in [20.328].

Numerous models have been developed to predict the temporal behavior of the LII signal [20.298, 310, 329–332]. The basis for most models is an energy and mass balance between absorption of laser energy and heat loss due to vaporization of material from the surface, heat conduction to the surrounding gas and radiation:

$$q_{\mathrm{abs}} = q_{\mathrm{int}} + q_{\mathrm{evap}} + q_{\mathrm{cond}} + q_{\mathrm{rad}} \,, \tag{20.8}$$

where q_{abs} is the flux of laser energy absorption, q_{int} the flux of increase of internal energy, q_{evap} the flux of energy loss by evaporation, q_{cond} the flux of heat conduction, and q_{rad} accounts for the cooling due to radiation. Various submodels for the different processes have been suggested in the past. Solving the resulting differential equation numerically yields the particle temperature as a function of time which is then turned into LII signal intensities using Planck's law. A more detailed model for soot particles including thermal annealing and oxidation has been developed by *Michelsen* [20.333]. However, several aspects in modeling LII are still related to large uncertainty. The evaporation term is usually based on equilibrium thermodynamics, e.g., describing the vapor pressure of carbon using the Clausius–Clapeyron equation. Large differences exist between experiment and model results at high laser fluences when significant evaporation of soot particles takes place. Hence, most experiments for obtaining particle sizes are carried out using low laser fluences. Still, if the heat transfer is dominated by conduction, which is the case for conditions at atmospheric and higher pressure, uncertainties remain in the value of the thermal accommodation coefficient. There are different approaches to determine the accommodation coefficient [20.319, 334]. However, in these studies the coefficient is treated more like a general calibration factor than assessing the true value of accommodation for molecular energy transfer. A comparison of the model approches is published in [20.335]. A web-based simulation tool for LII signal, LIISim is available [20.336].

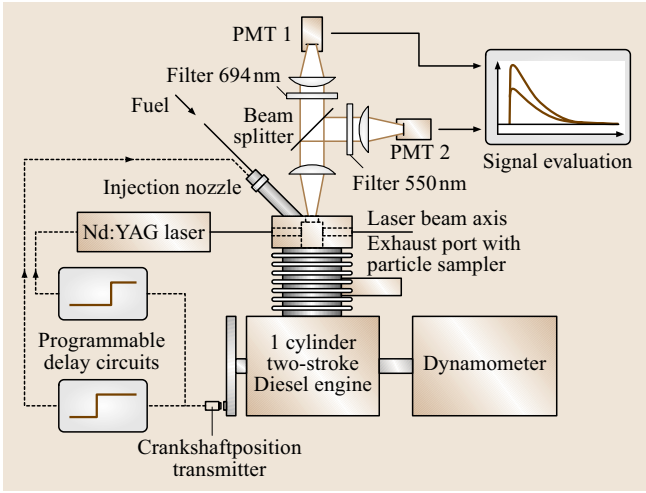

Fig. 20.45 Engine test bench and experimental setup, PMT: Photomultiplier

In-Cylinder Diesel Particle Sizing. The engine used for in-cylinder LII is a single-cylinder, two-stroke Diesel engine with a displacement volume of 250 cm^3. A custom-designed cylinder head provides the required optical access, which can be preheated or cooled, respectively, to a suitable operating temperature of approximately 80 °C. The laser beam axis passes through the center of the combustion chamber through two fused silica windows. The optical axis of the detection system is arranged perpendicular to the laser beam and has access to the combustion chamber by a third window at the top side of the chamber. Time-resolved signals

were detected at 550 and 694 nm. The irradiated test volume resulting from the present geometry is about 0.6 cm^3. The injection nozzle used is a Bosch common rail system, also located in the cylinder head. The engine is motored by an electrical asynchronous motor at a constant speed of 1500 min^{-1}. For time-resolved LII (TiRe-LII) measurements, the engine was fired for some individual cycles only. In this way, the windows could be kept as clean as possible and the thermal load on the cylinder head was low. The Diesel engine was equipped with a pressure transducer and a supplementary crankshaft position transmitter. All experiments were performed at an injection crank angle of 23° CA before TDC and an air/fuel equivalence ratio of $\phi = 0.26$. The particles were heated by an Nd:YAG laser at 1064 nm with a laser fluence of 0.10 J/cm^2. Finally, a thermophoretic particle sampler was located in the exhaust gas manifold to get particle probes for further analysis by transmission electron microscopy (TEM). The system is shown in Fig. 20.45.

In contrast to the laminar and well-defined conditions in the high-pressure burner the LII signals in the Diesel engine were taken in turbulent conditions with strongly varying pressures and temperatures. A series of normalized particle emission signals during cooling obtained from single shot experiments at six different crank angles is shown in Fig. 20.46. Particle cooling strongly depends on the engine crank angle and becomes longer with increasing crank angle. The signals of Fig. 20.46 and others were evaluated in terms of particle size by fitting lognormal distribution functions to the measured curves under the variation of the count mean diameter (CMD) and geometric standard deviation σ_g.

For the evaluation of the particle radiation signals in terms of particle size, it is important to know the respective mean combustion chamber pressure p_g and gas temperature T_g. For the present engine conditions, the pressure varied from nearly 80 bar at 0° CA to close to 1 bar at 100° CA. Gas temperatures changed in this crank angle range from 2000 K to 1500 K, respectively. The pressure was directly measured by a pressure transducer and the temperature was evaluated both from two-color pyrometry without laser heating and by calculating an individual combustion cycle. With these two parameters it was possible to evaluate the TiRe-LII signals shown in Fig. 20.46.

The results are shown in Fig. 20.47. CMD is in the range of 30 to 75 nm, increases up to a crank angle of about 10° CA and decreases again towards a value of about 30 nm at 100° CA after TDC. This behavior can be explained by particle formation and subsequent particle

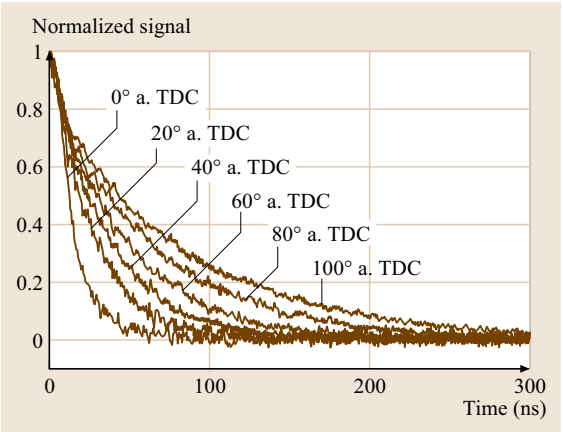

Fig. 20.46 Normalized TR LII signals at six crank angles

oxidation; σ_g is constant at a value of 1.1 up to a crank angle of 70° CA and then increases towards about 1.32. The two circled values of CMD and σ_g, which are shown at the right edge of the diagram, are results of the TEM analysis of the exhaust gas primary particles. The agreement between the TiRe-LII measured sizes at 100° CA after TDC and the TEM determined primary particle sizes in the exhaust gas is quite good.

Additional Species and Techniques for In-Cylinder Measurements

Rayleigh scattering can be used as an alternative method for gas-phase measurements of the distribution of large molecular species (i. e., hydrocarbon fuels) in the presence of small molecular species (i. e., air). Rayleigh scattering has been frequently used to measure gas density (and hence temperature) in homogeneously mixed

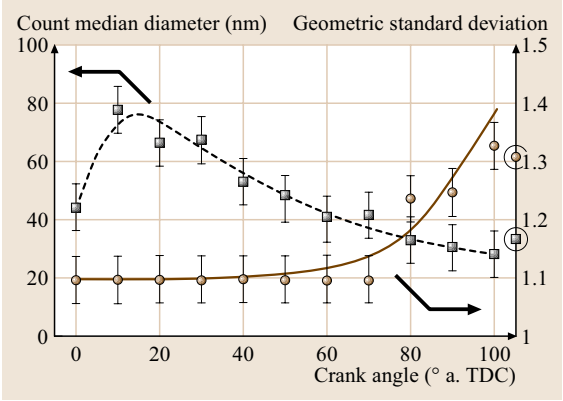

Fig. 20.47 CMD and σ_g evaluated from the signals in Fig. 20.46

systems where the effective cross-section for elastic scattering does not vary spatially [20.337]. It has also been used to measure relative temperature distributions in the post-flame gases in engines with simplified geometry [20.253]. Because of the linear dependence of the Rayleigh signal on number density and laser intensity, the interpretation of the signal is straightforward. As long as a single component dominates the effective Rayleigh cross-section in a mixing system, Rayleigh scattering also allows the measurement of species number densities. Hydrocarbons have a much larger cross-section for elastic scattering than air. Therefore, the overall scattering intensity can be used for measuring the local fuel density. With this technique, fuel vapor density has been measured in internal engine combustion [20.338–341] and in the mixing field of atmospheric-pressure natural gas flames [20.142]. In the case of single-component substitute fuels effects due to preferential evaporation (i. e., spatial separation of different fuel components that might have different scattering cross-sections) are avoided. The cross-sections for elastic scattering can be calculated based on data from [20.342–344] using dispersion relations from [20.345, 346]. Fuel dominates the scattering signal in the case of *n*-decane in air by a factor of $\sigma_{\mathrm{Ray,fuel}}/\sigma_{\mathrm{Ray,air}} = 120$. As long as no background scattering off surfaces and particles is present the total signal can be directly correlated with fuel number densities.

Rayleigh scattering, however, can be strongly influenced by scattering of laser light off walls and particles. It is therefore necessary to assess the background level that comes from these additional processes. In environments with lots of scattering off surfaces or particles (small enclosed housings, presence of fuel droplets, sooting environment) the standard technique fails. Filtered Rayleigh scattering [20.347] has been demonstrated under these conditions. Here, a narrowband laser is used for excitation that overlaps with a narrow line filter. Only slightly frequency-shifted signal (shifted by Doppler broadening due to the thermal velocity of the scattering molecules) is detected.

Raman Scattering. Valuable information for most major species in engines can again be obtained from spontaneous Raman scattering. *Grünefeld* et al. [20.249] performed spontaneous Raman imaging along a line with noise levels of a few per cent in a single shot using the beam of a KrF excimer laser at 248 nm with spectral as well as spatial dispersion of the scattered light accomplished by mounting an intensified CCD (ICCD) camera in the exit plane of a spectrograph. The larger scattering cross-sections in the ultraviolet allow imaging of the scattered light with smaller collection optics and therefore, measurements in technically relevant devices such as engines and boilers. By taking advantage of the highly polarized Raman and Rayleigh scattered light in comparison with unwanted laser excited fluorescence and stray light from enclosure walls, they were able to monitor major species in a *iso*-octane spray flame burner and a four-cylinder in-line engine by subtracting spectra taken with mutually perpendicular polarization of the exciting laser beam.

CARS. The most accurate spatially-resolved temperature measurements in engines can be performed with CARS as long as beam steering effects which severely degrade the CARS signal generation process can be tolerated. Therefore, precise cycle-resolved thermometry is possible in the compression stroke prior to ignition [20.117], in evaporating sprays [20.348] and in the expansion stroke when the flame front has traversed through the focal volume of the beams [20.349]. In any case the unstable resonator enhanced (USED) CARS phase-matching beam geometry [20.118] is preferred in such measurements to minimize beam-steering effects.

20.4.5 Diagnostics for Stationary, Large-Scale Combustion Processes

Efficient control and optimization of large-scale industrial combustion systems such as power plants, incinerators or heavy industries, is of considerable ecological and economical interest. In order to detect and correct deviations from the optimal process conditions detailed physical and chemical information – preferably from within the main process volume – is needed to permit feedback to the process by fast active-control loops. This places high demands on sensors for the gaseous major species and trace species concentrations, gas temperature, gas residence time and other process parameters. An efficient use of feedback loops for process control also requires sensors with sufficient temporal resolution and close coupling of the sensor response to the process of interest. Apart from sufficient sensitivity, selectivity and response times, a sensor for industrial process control applications must offer important additional features like compactness, long sensor life time, good long-term stability, reliable and simple calibration, ease of use, and finally low cost of ownership with respect to the possible savings in the process [20.10, 350].

In power plants and other stationary industrial combustion processes most parameters and especially gas-species concentrations are predominantly measured with extractive sensors. These are based on a multitude of different detection principles ranging from spectrally broadband optical sensors like nondispersive infrared (NDIR) photometers, fluorometric NO detectors, or Fourier transform infrared (FTIR)-based spectrometers to non-optical principles like paramagnetic or ion-conductive O_2 analyzers, metal-oxide-semiconductors and expensive multispecies gas chromatographs or mass spectrometers [20.351]. Common to these devices is that they always require extraction of a gas sample, which is typically done well behind the main reaction zone via a single access point in the flue gas duct. Prior to analysis the gas sample is filtered to remove particulates, usually cooled well below room temperature to remove water, avoid condensation and protect the sensor from the hot gas, and than transported to the main analyzer via a sampling tube that is sometimes up to 100 m long. This sampling process significantly affects the usefulness of the species signal for process control and creates numerous difficulties that can range from slow temporal response, systematic errors due to effects like adsorption, condensation, chemical reaction and fractionation during the sampling process and reduced representativeness due to the local sampling. Furthermore, many of this sensors often suffer – especially in the case of complicated gas mixtures – from a lack of specificity, caused for instance by the low spectral resolution of the optical filters used in some of these instruments. Extractive sensors in general and NDIR in particular also have a rather high cost of ownership due to the requirement for frequent cleaning of the sampling lines and routine calibrations with reference gases. Finally, due to the heterogeneity in the extractive sensor principles and the risk of fractionation during the sampling process it is in most cases impossible to perform a stringent comparison of, e.g., multiple species concentrations with high temporal resolution, which would be most interesting for monitoring and optimization of the combustion chemistry.

Avoidance of these problems requires a single, rather universally applicable, non-intrusive in-situ measurement technique for species concentrations, temperatures and flow parameters, which provides sufficient selectivity, resolution and speed, which completely avoids probe sampling and the need for costly calibration procedures and which is capable of simultaneously measuring nearly unrestricted combinations of process parameters within the same detection volume. Furthermore, in order to facilitate a widespread industrial use, the measurement technique should be rather independent of the type, size, and specific process conditions (temperature, pressure, particulate load of the gas) and, e.g., be applicable to a direct measurement even within large combustion chambers, with lateral dimensions in the order of tens of meters.

High-Resolution Laser-Absorption Spectroscopy

High-resolution laser absorption spectroscopy (LAS) [20.6, 352] is probably the only analytical technique that provides a simultaneous solution to most if not all of the above mentioned requirements. In absorption spectroscopy (AS), one of the oldest techniques of non-intrusive investigation of gaseous media, radiation directed straight through the measurement zone towards a radiation detector is being absorbed and this loss is monitored and analyzed for its dependence on wavelength.

AS is extremely versatile as every species of interest will show internal degrees of freedom which may be optically excited via the absorption process. Atomic species (and homonuclear molecules) maybe detected via electronic transitions in the ultraviolet (UV) and visible (VIS) spectral range, whereas heteronuclear molecules offer several important additional detection pathways via radiative excitation

1. of rotational levels in the far-infrared spectral range (FIR, $\lambda = 0-100\,\mu m$)
2. of vibrational and rotational sublevels in the mid IR (MIR, $\lambda = 10-3\,\mu m$) and
3. via vibrational overtone and combination bands in the near IR (NIR, $\lambda = 1-3\,\mu m$) [20.353–356].

This is a significant advantage to diagnostic techniques based on light emission like fluorescence, phosphorescence or chemiluminescence, which cannot be applied to every analyte as radiative transitions are prerequisite for those techniques [20.357]. Additionally, emission techniques often suffer from problems like radiative quenching, predissociation and other non-radiative de-excitation mechanisms. Thus, even though emission-based sensors are quite simple, inexpensive and robust, extensive pressure-, species- and device-dependent calibration information is needed in order to deliver absolute process data. Especially the low spectral resolution of chemiluminescence techniques provides only limited specificity, making it difficult to separate the signal from fluctuating background radiation.

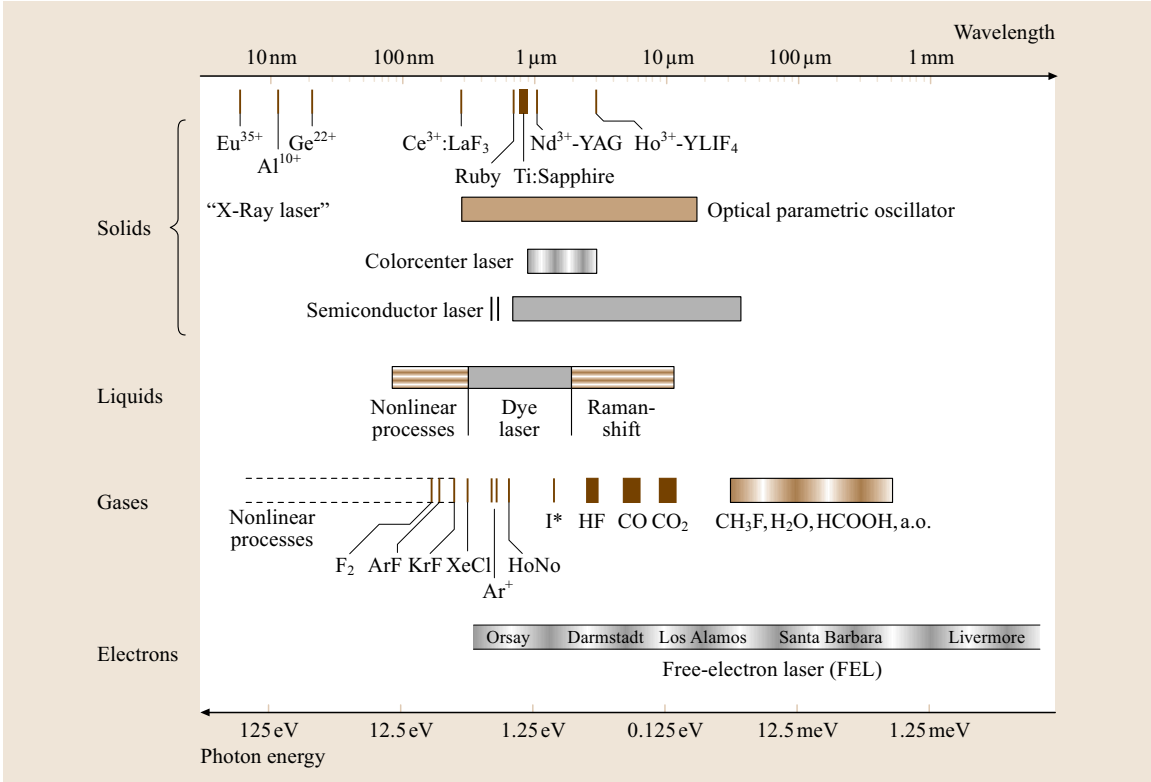

Fig. 20.48 Wavelength range of various available laser light sources

Further unique properties of AS that are important to combustion diagnostics are the possibility to determine absolute absorber densities and temperatures without the need for calibration and the linear sensitivity scaling with absorption path length. The line-of-sight character of AS may be, to a certain extend, a disadvantage compared to laser-induced emission-based techniques, because it prevents spatially resolved measurements in complicated geometries. But on one hand this restriction can be lifted for many cases using tomographic techniques [20.358, 359]. On the other hand this path-averaging effect, as it permits much more representative results than extractive or point-sampling techniques, proves to be very important for the surveillance of the very large measurement volumes frequently found in stationary combustion processes, reaching up to 20 m in diameter [20.10, 350, 357, 360].

Laser Sources for Absorption Spectroscopy

The analytical potential of AS could be significantly enhanced through its combination with laser excitation. The high spectral resolution of a laser light source maximizes the chemical selectivity especially in complex gas mixtures. Its high spectral power density minimizes or even completely removes the influence of detector noise, one of the major limits when working with broadband light sources, thereby significantly enhancing the spectrometer sensitivity. Furthermore, it is the high spectral power density that is an enabling laser feature for non-intrusive diagnostics in strongly luminescent processes, as it often permits one to neglect the influence of the strong thermal emission that occurs in many combustion processes.

Additionally, by taking advantage of the good laser beam quality it is possible to drastically reduce the size of the optical access ports to the process, and even more important, to considerably increase the maximum absorption path lengths, thereby permitting a significant increase in the sensitivity. Using laser sources in combination with simple single-path setups typical in-situ absorption path lengths in the order 1–5 m [20.361, 362] are used in combustion applications, but up to 20 m have been demonstrated in large industrial combustion processes [20.363, 364]. If even longer path lengths are

needed, e.g., for the detection of minor species concentrations, and provided that optical disturbances such as light scattering by particles, are not too strong, it is possible to apply special, ruggedized multipass optics of the *Herriott* [20.365,366] or *White* type [20.367,368] to fold the beam path. Using that approach, path lengths in the order of 100 m and beyond have been achieved and used for gas-phase analysis in multiphase flows, e.g., to study the dynamics of ice cloud formation [20.369, 370]. The same technique is also advantageous if the measurement region has to be spatially confined. Such an approach was realized for the investigation of fire-suppression systems to study the gas-phase composition within water sprays [20.371].

When comparing laser sources for absorption spectroscopy rapid and, if possible, continuous tunability of the laser wavelength [20.10, 372] is one of the key features for combustion diagnostics. Rapid wavelength-tuning capabilities of many laser sources endow LAS with high temporal resolution and simultaneously permit a high degree of robustness against optical disturbances. On the other hand continuous wavelength tuning allows the recovery of entire absorption line shapes. This provides not only enhanced signal stability via suppression of spurious baseline effects, but more importantly the possibility of using line-shape analysis to access all the parameters that affect line area, shape and position (e.g., gas pressure, temperature, velocity, electric and magnetic fields etc. [20.6]) experimentally. Additionally, and most importantly for industrial applications, complete coverage of the absorption profile allows a calibration-free determination of the absolute absorber concentration by extraction of the integrated line strength according to the Lambert–Beer law [20.352, 361, 362, 364, 371].

Laser Selection and Spectral Coverage. Another key feature for laser selection is spectral coverage [20.10]. In general, the impressive versatility of LAS is based upon the very large spectral coverage provided by modern laser technology, spanning nearly seamlessly from the UV-VIS (e.g., via excimer, dye and solid-state lasers), over the mid infrared (e.g., CO_2 and CO gas lasers) [20.372, 373] to the far-infrared and THz region (via masers, quantum-cascade diode lasers) [20.374–376] (Fig. 20.48).

Nevertheless, it must be kept in mind that most individual laser types are limited to a relatively narrow spectral range and that many of them feature only discontinuous or even no tuning capabilities at all. thus having only rather specialized applications.

Typical examples are MIR gas lasers like the CO_2 and the infrared HeNe laser ($\lambda \approx 10.6\,\mu m$ resp. $3.39\,\mu m$). Both are based on quite mature and thus robust technologies, but their applicability for gas sensing relies on accidental coincidences with strong absorption lines. As the single emission line of the IR-HeNe coincidences nicely with the very strong C−H stretch of the ro-vibrational transitions of most hydrocarbons it is quite frequently used for CH_4 monitoring [20.377, 378]. Combined with special IR-transmitting fibers, robust, fast, and sensitive absorption sensors with up to 2 kHz time resolution have been demonstrated and for instance used to study local mixing effects in CH_4 combustion [20.379].

The CO_2 laser is substantially more flexible owing to its high output power (> 1 W) and the multitude of discretely accessible lines. This enabled the realization of important sensing applications of hydrocarbons, ammonia and other species [20.380–382] and led to one of the first commercialized industrial in-situ species sensors for closed-loop control applications in large power plants: a laser in-situ ammonia sensor [20.383, 384] used for optimization of NO_x removal via the selective catalytic reduction (SCR) or selective non-catalytic reduction (SNCR) process [20.358, 385].

Despite these successful applications, only very few laser principles feature the possibility to cover a substantial part of the UV–VIS–IR spectral range with a single lasing mechanism, which is advantageous as the development efforts and cost are substantially lower when new species and hence new laser wavelengths must be incorporated. The two most important members of this laser class are semiconductor diode lasers and solid-state lasers, which provide this special property especially in combination with nonlinear crystal-based wavelength-mixing techniques like optical parametric generation (OPG), as well as second-harmonic, sum-frequency, and difference-frequency generation (SHG, SFG and DFG) [20.386].

However, practical combustion applications impose severe restrictions on the laser choice simultaneously requiring advantageous technical properties like room-temperature operation, long device life time, compactness, high electrical efficiency, and low cost, to name a few. As many of these laser systems are still in a *developmental* stage they have to mature significantly to be routinely applicable to the harsh boundary conditions often found in stationary combustion systems. As a consequence, the use of nonlinear laser-light generation techniques seems currently, despite turbulent developments, due to complexity, robustness, cost and space

restrictions limited to the mid-term future, which leaves the diode laser as the premier choice with regard to general applicability.

The continuously *tunable diode laser* (TDL) is one of the most powerful laser sources for combustion diagnostics. Developed in the 1960s, soon after the first laser demonstration by *Maiman* [20.4], TDLs in the mid IR quickly became an important working horse in analytical basic research because they combined the three most important properties for analytical problems.

- Excellent selectivity due to their very high spectral resolution (10^{-3}–10^{-4} cm^{-1})
- Very good sensitivity,
  - due to the access to the strong absorption lines in the molecular fingerprint region in the mid infrared, in combination with their
  - rapid, versatile and continuous wavelength-tuning properties. Latter permitting the development of advanced noise-reduction techniques [20.387], which provide significant sensitivity enhancement; in some cases even up to the shot-noise limit, the ultimate limit for absorption techniques [20.388].
- Excellent flexibility, due to their near-complete coverage of the MIR ($\lambda = 4$–$20\,\mu$m).

The versatility of MIR-TDL is widely documented in literature [20.389, 390] and first experiments deploying their advantageous spectroscopic properties date back as far as in the 1970s, when a CO detection was first realized for environmental applications [20.391] and then quickly transferred to combustion problems [20.392–394]. However, despite significant long-term development efforts the major drawback of these so-called *lead salt* or IV–VI lasers [20.395] remained their need for cryogenic cooling to liquid-nitrogen or even liquid-helium temperatures, which severely hindered the widespread transfer into industrial combustion diagnostics. Nevertheless, MIR-TDLs are still frequently applied and of significant importance for basic [20.396] and combustion research [20.397].

The availability of room-temperature operated near infrared diode lasers (NIR-DL) in the AlGaAs and InGaAs material system ($\lambda = 780$–1550 nm) with relatively high optical output power (3–200 mW) significantly changed this situation, especially for diagnostics in large stationary combustors, because NIR-DL, which were initially developed and mass-produced for data storage and fiber-based data transmission, for the first time combined wide spectral coverage with superior spectroscopic and technical specifications. As a consequence, the NIR spectral range became quite interesting for absorption-based combustion diagnostics, first, to take advantage of the NIR-DLs high spectral quality, simple operation and low costs, and second, partially because the lower absorption coefficients of molecular overtone and combination bands in the NIR (Fig. 20.49) could be compensated by the longer absorption path commonly available in stationary combustion systems.

In recent years the wavelength coverage and thus the versatility of TDLAS has improved even further. As data storage capacities of optical discs improved, the available wavelength band for room temperature DL was first extended to the red ($\lambda > 630$ nm) and meanwhile even to the blue and near UV (450–350 nm) [20.398], with a small gap remaining in the 460–620 nm range. Simultaneously, the increased interest in industrial sensing applications in combination with a strong growth of the demand for security applications for military countermeasures and public safety provided the driving force for the development of promising new diode lasers in the short wave IR, the mid IR and even the far-infrared (FIR) or Terahertz (THz) spectral ranges. The short wave IR at 1.8–2.8 μm, which is important for combustion diagnostics, as this range is a good compromise between stronger absorption lines without too severe interference from hot water or CO_2, could be very recently accessed with relatively mature room-temperature devices, that are based on the InSb material system [20.362, 399, 400].

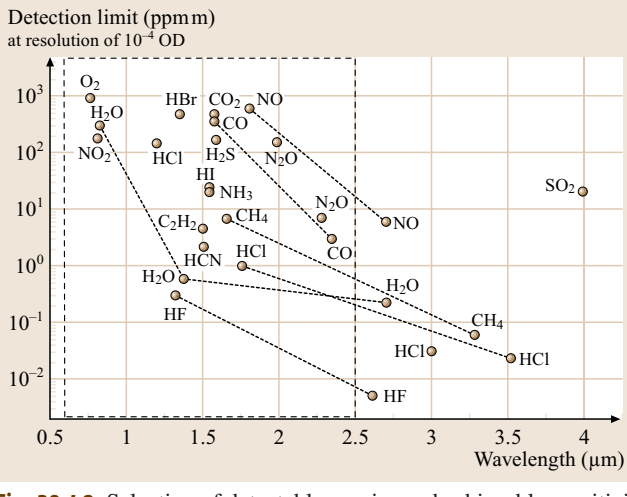

Fig. 20.49 Selection of detectable species and achievable sensitivities using NIR diode lasers. Vibrational overtone transitions of some species are connected with dashed lines. Sensitivities in ppm at one meter absorption path length are calculated assuming a detectable fractional absorption $\Delta I/I_0$ of 10^{-4} OD

Another major wavelength expansion could be derived from the invention of a completely new semiconductor laser type, the so called quantum-cascade lasers (QCL) [20.401]. QCLs permit not only surprisingly high output powers of up to watts, of at least the same if not higher importance is the possibility of operation at or near room temperature in the MIR, as well as the access to the THz region [20.376], though only at cryogenic temperatures.

This increasing flow of new semiconductor developments has already lead to a revival of absorption spectroscopy, which will proceed and expand as THz and especially room-temperature MIR sources will mature and as hybrid technologies like diode laser pumped solid state lasers improve nonlinear wave mixing techniques. This will provide spectroscopic sources with very high spectral resolution, very wide range tunability and a spectral coverage extending from the UV to the THz-region thus encompassing electronic, rovibrational as well as pure rotational transitions, making a TDLAS even more versatile.

In-Situ Tunable Diode-Laser Absorption Spectroscopy (TDLAS)

The development of in-situ laser diagnostics suitable for permanent use in stationary combustion processes impose very high demands on the spectrometer and its components. Currently the NIR spectral region offers the best boundary conditions for such applications, as all components, lasers, (fiber) optics as well as detectors, are highly developed due to their mass production for communication and data-storage technology. Commercial NIR-DL, provide near-complete spectral coverage from 635 to 1650 nm, which was recently expanded to 2600 nm by use of new InSb materials. With regard to industrial sensors NIR-DL offer a unique combination of positive properties like low cost, tiny size, room-temperature operation, very long laser lifetime of 10^5 hours and more, single-mode output power of up to several 100 mW, and excellent spectral resolution of 10^{-3} nm. Their sole disadvantage, to cover only relatively weak transitions in the visible and near infrared range (Fig. 20.49, e.g., overtone and combination vibrational bands, magnetic dipole transitions, line strength 10^{-23} to 10^{-21} cm/molecule), is of minor importance for stationary combustion sensors, as the species concentrations to be monitored are often quite high and the absorption lengths in full-scale combustors are rather large.

The versatile tuning properties of NIR-DL are most important for sensing applications. Monolithic diode lasers provide a wide range but slow tuning by laser temperature (typically 2–5 nm within a few 100 s), as well as a very fast and continuous tunability by laser current modulation (10^3–10^6 cm^{-1}/s over $\Delta\nu = 1$–3 cm^{-1}). Complete absorption line shapes may thus be captured even on µs time scales. The use of entire line shapes improves the stability of the data evaluation as time dependent baseline distortions may be separated. Furthermore by evaluation of the spectral line profile, it is possible to simultaneously extract absorber concentration as well as the physical boundary conditions in the measurement volume. The high tuning speed on the other hand is quite important for in-situ measurements in harsh environments as it permits to *freeze* all disturbances in the measurement volume, which is a prerequisite for their efficient removal [20.362].

Current tuning, however, simultaneously generates an unavoidable side effect: the amplitude modulation (AM) of the laser output power. AM tends to hide the weak molecular absorption signal in a strongly sloping background (Fig. 20.50) and also limits the usable dynamic range of the data acquisition system. The figure of merit, the specific AM, $dP/d\lambda$, i. e., the change in output power per wavelength interval, is usually best for vertical-cavity surface-emitting lasers (VCSELs), and worst for high data rate telecommunication distributed feedback diode lasers (DFB-DL), which on the other hand provide highest spectral purity [20.388]. However, hybrid diode lasers like external cavity diode lasers (XC-DL), which use antireflection-coated laser chips and

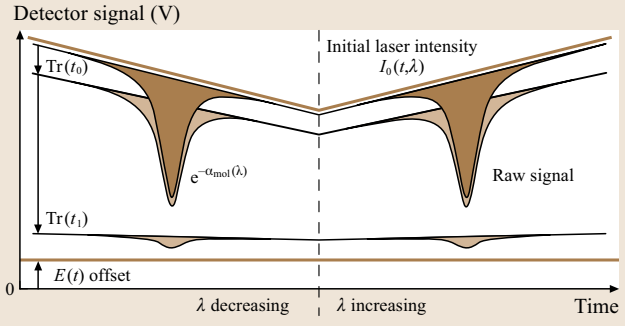

Fig. 20.50 Generic in situ TDLAS signal trace and measurement principle of direct tunable diode-laser spectroscopy. The disturbances [Tr(t), $E(t)$] have to be compensated before applying Beer's law. Tr(t) indicates the unspecific loss of the initial laser light (I_0) due to scattering and refraction, $E(t)$ is the level of background light and gray-body radiation reaching the detector. The *line area* is after disturbance correction proportional to the number density of absorbers

externally mechanically tuned optics to select the laser wavelength, may be used to avoid AM [20.402]. Moreover, XC-DL access the complete gain profile of the semiconductor thus providing the widest tuning ranges (20 nm in the red, up to 200 nm in the NIR) [20.403]. However, increased cost, size, and susceptibility to mechanical instability, and reduced tuning speed, severely hinders their use in combustion applications.

The basic setup of an absorption spectrometer is quite simple: the beam of a diode laser is collimated, directed through the measurement volume, collected by a spherical mirror and projected onto a photo detector. As the laser wavelength is continuously scanned over the absorption line, the photodetector signal is amplified, filtered, digitized by an analog-to-digital (AD) converter, transferred to a computer, and evaluated for narrow band losses by a curve fitting algorithm, which, after removal of the AM and other disturbances, usually extracts the area of the absorption line by applying the Lambert–Beer law, here written for homogeneous conditions along the beam path:

$$I(\lambda) = I_0(\lambda) \exp\left[-S(T) g(\lambda - \lambda_0) NL\right] .$$

The Lambert–Beer law relates the detected intensity $I(\lambda)$ to the initial intensity $I_0(\lambda)$ (describing the current- and thus wavelength-dependent AM) and the molecular absorption signal of a well-resolved individual absorption line. The latter is described by the temperature-dependent line strength $S(T)$ of this line, the number density N of absorbers, the absorption path length L, and an area normalized $(= 1)$ function $g(\lambda - \lambda_0)$, describing only the shape of the absorption line, which is centered at wavelength λ_0. Using this normalization, this equation can be solved to yield the absolute absorber density N,

$$N = \frac{1}{S(T)L} \int \ln\left(\frac{I_0(\lambda)}{I(\lambda)}\right) \mathrm{d}\lambda \rightarrow X = N \frac{k_\mathrm{B} T}{p}$$

or the absorber concentration X by applying the ideal gas law and the measured temperature T and total pressure p.

It is important to note, that this equation does not contain any calibration parameters and that $S(T)$ is a molecular parameter, which is independent of the spectrometer configuration. Thus the absolute absorber density N, respectively the absolute absorber concentration X, can be directly inferred from the measured line area without any calibration. Only L, T and $S(T)$, and the total pressure p, must be known/measured. Furthermore, given a spectrally well-isolated absorption line, the line profile integration yields that N is independent of the line shape, i. e., all line-broadening effects and the total pressure. This property to avoid any calibration as well as pressure-broadening effects, is very advantageous for in-situ measurements in combustion devices or processes with variable pressure or temperature, and is hardly achievable with other measurement principles, thus giving absorption spectroscopy a rather unique position.

However, in order to take advantage these properties, it has to be kept in mind, that the normalization of the line area only holds in wavelength space. Hence, the absorption signal has to be transferred from time space to wavelength space by taking care of the dynamic tuning behavior, $\mathrm{d}\lambda/\mathrm{d}t$, of the diode laser. For very slow, quasistatic current tuning the conversion factor is just a constant. But, for higher tuning speeds, which are needed for fast measurements or, as we will see, under harsh boundary conditions in combustors, the tuning becomes highly nonlinear, which results in asymmetrically distorted line shapes in time space. The line fitting process thus requires that $\mathrm{d}\lambda/\mathrm{d}t$ is determined experimentally and taken into account. This is frequently realized using solid or air-spaced etalons as relative frequency markers [20.402]. As the systematic errors in N or X are dominated by errors in $S(T)$ and $\mathrm{d}\lambda/\mathrm{d}t$, it is most important to determine $\mathrm{d}\lambda/\mathrm{d}t$ at least with the accuracy of $S(T)$. The use of compact, solid etalons, within the instrument, may therefore, despite their robustness, generate too large uncertainties, due to refractive index errors, temperature effects, and reduced resolution. More precise are large air spaced etalons, whose frequency markers depend to a very large extend on the spatial separation of the etalon mirrors only.

In-situ laser absorption spectroscopy in combustion environments requires not only the consideration of the spectroscopic effects of temperature or pressure variations on the molecular signal. Furthermore, great care has to be taken to correct the detector signal for various strong disturbances that are often unavoidable under combustion conditions [20.362, 363, 404]; most important are strong fluctuations of the overall transmission $Tr(t)$ of the measurement path, which are caused by broadband absorption and scattering by particles, or beam steering due to refractive-index fluctuations. Additionally, there is frequently an intense thermal background radiation $E(t)$ from the combustion zone or radiating particles that increases the detector signals. Both effects may be changing rapidly in time and have to be included in an extended version of Beer's

law:

$$I(\lambda) = I_0(\lambda)Tr(t)\exp\left[-S(T)g(\lambda-\lambda_0)NL\right] + E(t)$$

An exaggerated sketch of a typical in-situ TDLAS signal trace is shown in Fig. 20.50, indicating the additive emission and the multiplicative transmission term.

The relative signal-to-disturbance ratio depicted in Fig. 20.50 is however far from reality, as NIR absorption signals only rarely yield more than 5% absorption, while the transmission losses, e.g., in large coal combustors [20.363] or dense water sprays in fire research can [20.371,405] exceed 99.99%, and the thermal background in coal plants may become 10 times stronger than the transmitted laser light. As the disturbances are often orders of magnitudes larger than the molecular absorption signals, they may bury the net signal completely. Effective disturbance suppression, compensation and removal strategies are thus essential in order to extract the narrow-band absorption and compute the desired combustion parameters.

The basic idea to effectively separate and correct the molecular absorption for the transmission and emission effects takes advantage of two important features of diode lasers: their fast wavelength tunability and – taking advantage of a mistake – their simultaneous current-induced output power modulation. By tuning the laser much faster than the transmission and emission fluctuations, both disturbances are effectively *frozen*, thus can be assumed to be constant during the wavelength scan and corrected by subtracting the offsets and dividing the offset-corrected scan through the baseline function [20.362]. The AM thus serves as a *transmission sensor*, while the emission term can be isolated from the DC coupled detector signal by quickly switching off the laser at the beginning of each scan. Hence, it is still possible to avoid calibrations and extract absolute absorber densities directly from the DC coupled detector signal by exploiting the extended Lambert–Beer law, provided that $\mathrm{Tr}(t)$ and $E(t)$ can be extracted from the unprocessed detector signal. Additionally rapid phase-locked averaging of the wavelength scans, equivalent to using a comb filter at the modulation frequency and its overtones, may be used for further noise reduction and improvement of the detection limits [20.362, 406].

The described experimental concept, to directly capture and evaluate the DC coupled detector signal, including all offsets and disturbances, is termed direct absorption spectroscopy (DAS). Though the simplest approach to LAS, it was proved that DAS is capable of routinely achieving fractional optical resolutions, $\Delta I/I_0$, of 10^{-3}–5×10^{-5} in the in-situ signal, depending on the complexity of the disturbances and the measurement environment [20.362, 364, 407, 408]. Other more-complicated double-modulation techniques such as wavelength modulation spectroscopy (WMS) [20.387, 406, 409–414] or frequency modulation spectroscopy (FMS) [20.397,415,416] or dual-path approaches such as balanced detection [20.388,417] are reported to provide one to two orders higher resolution, with $\Delta I/I_0$ better than 10^{-5}–10^{-6} being reported under well-controlled laboratory conditions or in extractive measurements. Application of these techniques to in-situ measurements in combustion scenarios, however, considerably increases their technical complexity and cost, which limits their widespread use. Especially the treatment of pressure and temperature dependent line shape effects, as well as the removal of transmission fluctuations is not straightforward with these techniques, so that sensor calibration if often required and most of the resolution advantage is lost due to incomplete disturbance correction.

In comparison, DAS has a under certain circumstances reduced sensitivity, but it also provides several highly important features, i. e., a relatively simple and robust setup, rapid response, and particularly the possibility to perform a calibration-free measurement of absolute gas concentrations while simultaneously avoiding line broadening effects. Hence, DAS offers a good compromise between sensitivity and complexity, and therefore is of great value for in-situ combustion diagnostics in technical processes.

Application of In Situ TDLAS

TDLAS has been extensively used over the last decades for combustion diagnostics [20.10, 350, 357, 360]. Its versatility can be nicely demonstrated by the long list of *accessible process parameters* using NIR-TDLs. Most important and most frequently employed is the detection of species concentrations, which has been realized for many light molecules (via their molecular overtone and combination bands (Fig. 20.49), and even many atomic species [20.418, 419], (e.g., most alkali [20.402] and earth alkali atoms) via their electronic transitions. Nearly as important to combustion diagnostics is the measurement of gas temperatures, which may be determined either via two-line thermometry [20.364] from the line strength ratio of a suitable line pair or from Doppler broadening [20.420]. Collisional broadening of the line shape has been used for pressure measurements [20.420]. Even the flow speed of the absorber may be extracted using tracer meth-

ods [20.402, 421] or from the Doppler shift of the line profile and combined with the species concentration to derive mass flux or thrust [20.420, 422]. The residence time distribution of the product gases in a reactor [20.402] is another important parameter which in high-temperature flows could only be measured by radioactive tracer methods. Using diode lasers that parameter could be inferred by seeding the flow with a tracer molecule [20.402, 421] and detecting the release of the tracer. Continuous seeding has been used in a pulsed flow [20.421, 423], as well as pulsed seeding in a continuous flow [20.402].

Multi-Parameter Spectrometers. One particular strength of laser absorption spectroscopy is the possibility for multi-parameter sensors with near arbitrary combinations of measurement parameters [20.10, 350, 357]. By optically superimposing the required number of different laser beams, usually one per measurement parameter, a multicolor laser beam is formed and used to enable simultaneous multi-parameter detection in the same detection volume via a single pair of optical access ports. Beam superposition can be realized by free space optics [20.364], or particularly elegant and robust by fiber-multiplexing several diode lasers into a single-mode glass fiber [20.424–427], taking advantage of the high-quality fiber-optical components developed for telecommunication. Depending on the spectral separation of the lasers needed for the individual parameters different wavelength multiplexing schemes maybe used:

- *Spectral wavelength multiplexing* may be used for well-separated wavelength channels. In this case the absorption signals are acquired by simultaneously scanning all lasers and dispersing the multi-wavelength beam after passage of the absorption path onto multiple detectors by use of a grating [20.424–427] or dichroic beam splitters [20.361, 364].
- Alternatively, for insufficient spectral separation, multi-parameter measurements may be realized by *temporal wavelength multiplexing* [20.408, 428], taking advantage of the rapid amplitude modulation possible with diode lasers. Time multiplexing means sequentially scanning each individual laser of a laser array and detecting the transmitted light with a single detector.
- Finally there is the possibility of *modulation frequency multiplexing* [20.410], which has only be demonstrated in combination with double modulation techniques like WMS. Here all lasers are operated simultaneously, but at different modulation frequencies. The light of all the lasers is directed onto a single detector and the respective components are separated by narrow-band electrical filters, e.g., lock-in amplifiers.

Due to the scan range limitations of monolithic lasers multiple-parameter detection has mostly been performed with a combination of several individual diode lasers. However, with the persistent, telecommunication-driven progress in external-cavity diode lasers [20.403, 429] and multi-section distributed-feedback (DFB) and distributed-Bragg-reflector (DBR) lasers [20.428, 430] laser systems continuously scanning up to 100 nm have become available, which will simplify the design of time-multiplexed multi-parameter spectrometers significantly.

Laboratory-Scale Combustion Control Applications. For large stationary combustion systems such as power plants, incinerators and heavy industries, a tight monitoring and control of combustion is of great importance to achieve a high fuel efficiency and reduced pollutant emission. The development of adequate sensors and fast active control loops suffered for a long time from the complex boundary conditions found in full-scale combustors. Thus the first successful TDLAS-based closed-loop combustion control experiments have been realized in well-controlled laboratory environments using small atmospheric burners with a few cm absorption path [20.424, 431]. This first setup consisted of two fiber-coupled wavelength-multiplexed DFB-DLs, which were rapidly scanned (1 kHz) across two water absorption lines in the 1.3 μm overtone band to measure water concentration (from peak height) and gas temperature (from peak ratio) 6 mm above the burner surface with 2 ms time resolution. This permitted a closed-loop temperature control from 900 to 2400 K by adjusting the fuel flow with a proportionally acting voltage-controlled solenoid valve thereby achieving a temperature deviation of only 1% (1σ) between 1800 and 2100 K. The next H_2O/temperature sensor generation [20.432] (with $\Delta l = 10$ cm) used an adaptive controller and acoustic forcing to optimize within 100 ms the performance of an atmospheric 5 kW non-premixed, C_2H_4–air, annular dump combustor (ADC) through improved fuel–air mixing achieved by adjusting amplitude and relative phase between air and fuel flow forcing. System scale-up ended with a 50 kW pulsed ADC waste incinerator, where CO emissions dropped from 2500 ppm to below 200 ppm by active optimization of the relative

phase between primary and secondary air flow based on temperature measurements with 100 μs resolution in a 18 cm-wide flue gas duct [20.433]. Recently TDLAS control was also applied to modern propulsion systems, so-called pulse detonation engines (PDE). PDEs, essentially narrow, few cm-inner-diameter steel tubes, generate thrust by discontinuously igniting premixed gas. To optimize fuel consumption, maximize specific impulse and reduce temporal propulsion fluctuations it is important to avoid overfilling of the PDE and to adapt the ignition timing to the changing boundary conditions in the PDE (i. e. temperature, residual gas). Using fixed-wavelength DFB-DLs and standard lock-in detection C_2H_4 mixture fraction and temperature (for $T = 300–900$ K) was determined (after calibration) from the peak height/peak ratio of the C_2H_4 Q-branch multiplet at 1.62 μm [20.434]. Then, a simple closed-loop on–off controller adapted the fuel loading and ignition timing. This reduced the shot-to-shot thrust fluctuations significantly, clearly demonstrating the advantages of TDL-based control.

TDLAS Application to Stationary Combustion Systems

Sensor scale-up from rather short absorption paths in the order of 10 cm and laboratory-like conditions into industrial combustion environments (i. e. power plants with combustion chambers up to 100 times larger) has long been hampered by the large, quite variable and only rarely characterized disturbances present in large stationary combustors. Careful characterization of the optical and optomechanical properties of the in-situ absorption paths in these combustors has increased the knowledge about these problems in a way that robust and highly efficient correction and data evaluation algorithms for direct absorption spectroscopy could be developed, which can cope with the extreme disturbances levels, and extract weak molecular absorption signals despite severe light losses of more than 99.99% and background radiation signals, which may be more than a 10-fold stronger than the transmitted laser light [20.352, 361, 362, 364, 371]. The development of these procedures extended the working range of in-situ absorption spectroscopy drastically, so that despite the moderate laser output powers of 1–100 mW it became possible to detect and quantify specific absorptions on the order of a few percent with an optical resolution of $10^{-3}–10^{-4}$ and with a temporal resolution of 0.1–30 s.

Another key development which proved indispensable for the realization of industry grade in-situ spectrometers, was the design of a new computer-controlled optomechanical setup, which, in spite of strong disturbances caused by the in-situ path, is able to ensure permanent optical access to the measurement volume by automatically controlling, optimizing, and stabilizing the optical alignment of the spectrometer. Combined with various techniques to suppress the in-situ disturbances, this optomechanical setup could compensate for strong temperature-induced deformations of the combustion chambers, which before prevented continuous measurements during large combustor load changes [20.364]. Further, in cases of extremely poor visibility, this system could also be used to perform an automatic, computer-controlled initial alignment of the in-situ spectrometer [20.363].

All these critical developments are about to change the situation, and to permit the scale-up of TDLAS sensors to full-size combustion processes thus opening up new possibilities to optimize stationary combustion process. As a result of this progress NIR-DL-based in-situ TDLAS has been recently applied to an increasing range of industrial combustion processes (including grate-fired waste incinerators [20.361], rotary kilns [20.362], box-fired power plants [20.363] and even high-pressure coal combustion [20.408]) and an extensive variety of fuel types (encompassing coal, natural gas, biomass, household and special waste) thus impressively demonstrating the versatility and flexibility achievable by TDLAS. In order to give further insight in the potential of NIR-TDLAS for applications in stationary combustion processes, selected example applications will be described in further detail below, which indicate that NIRDL-based absorption sensors are now most promising for real-world applications, ranging from mobile and severely space-restricted sensors to fast, non-intrusive, in-situ species and temperature sensors working in high-temperature and high-pressure environments like full-scale power plants.

Waste Incinerators. The incineration of house hold as well as special waste is in many developed countries the most strictly regulated combustion process, which in combination with the high variability of the calorific value and water content of the waste creates a strong need for active combustion control to adapt the waste feed, the waste mixing or the amount of air/oxygen supplied to the process. To monitor the process conditions, enable process optimization via feedback control and ensure a highly efficient and environmentally safe waste incineration numerous optical techniques have been combined in an advanced combustion control system (CCS) and were applied to an industrial 20 MW_{th} waste

incinerator with a 4 m-diameter combustion chamber, depicted in Fig. 20.51.

Efficient NO reduction according to the SNCR process required the injection of precise amounts of NH_3, which could be effectively monitored by the very first in-situ laser absorption sensor (LISA) based on a $^{13}CO_2$ laser and differential absorption spectroscopy [20.383]. In addition, the primary air injection, grate movement and fuel input are under closed-loop control through a scanning IR camera (TACCOS) [20.435] measuring the waste-bed temperature. Finally in order to control the secondary air injection actively a fast NIR-DL-based in-situ sensor for the simultaneous in-situ detection of O_2 and H_2O directly in the combustion chamber was successfully developed and tested [20.361].

Strong disturbances caused by the in-situ path such as transmission fluctuations and thermal background emission, which interfere with the molecular absorption signal had to be suppressed. The laser signals, which provided a linear response with a sensitivity of about 0.3 vol. % and a temporal resolution of 1 s were verified by extractive reference O_2 and H_2O sensors, which probed the cold flue gas duct. As the laser spectrometer completely avoided gas transport the laser signals were up to 60 s faster than the extractive reference signals, which is of major importance for the combustion control loop. A follow-up version of this sensor could be further improved by fiber-coupling of the laser and by the development of an inexpensive, compact and robust, purely analog data evaluation [20.436], with the potential for low-cost production. In the meantime even fully fiber-coupled TDLAS spectrometers [20.437] have been demonstrated, which enable the important expansion of TDLAS to highly space-restricted applications like internal combustion engines or high-pressure gas turbines.

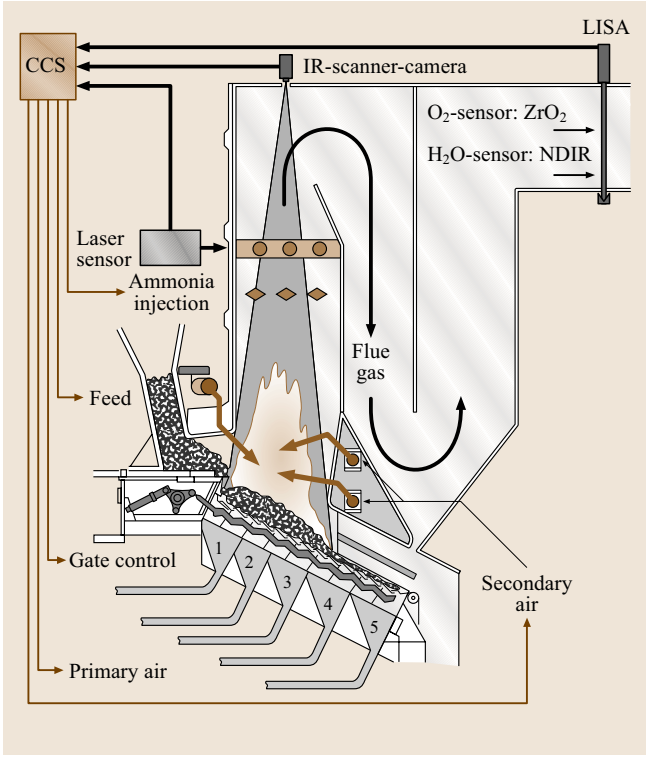

Fig. 20.51 Intersection through a 20 MW incinerator for household waste in which the in situ detection of O_2 and H_2O has been performed. A selection of important sensors (in situ diode-laser sensor, in situ laser ammonia sensor, LISA, and IR-scanner-camera, TACCOS) as well as the possible actors that are connected to the combustion control system (CCS) are indicated (further information in [20.361, 383, 435])

Gas-Fired Power Plants. Owing to their short turn-on time large, gas-fired power plants are frequently used to compensate for demand fluctuations in the power distribution network. But on rare occasions ignition delays in the sequentially ignited multi-burner system, presumably due to excessive humidity levels inside the combustion chamber, are not detected because of a lack of suitable rapid response security sensors for CH_4. In these cases disastrous explosions causing damage of $10 to 100 million dollar have been experienced, even though UV flame sensors and extractive CH_4 detectors have been installed. In the future, such accidents can be avoided with the help of the first laser spectrometer [20.364] for the simultaneous in-situ measurement of the gas temperature and all majority species (CH_4, H_2O, O_2, CO_2) in large stationary combustors which has been developed recently (Fig. 20.52). Employing two DFB-DL at 760 nm and 1.65 µm to detect O_2, CH_4 and CO_2 and a Fabry–Pérot DL at 812 nm to extract absolute H_2O concentrations it is now possible to determine representative, spatially integrated species concentrations from within the main combustion chamber. The temperature signal that is needed to extract absolute species concentrations, which was not available before, is simultaneously derived from the line strength ratios within the group of rotational transitions of H_2O near 0.81 µm via two-line thermometry. These transitions have the advantage of coinciding with high-output-power diode lasers ($\approx$ 35 mW), which increase the spectrometers tolerance to the substantial light losses often found in the large technical combustors.

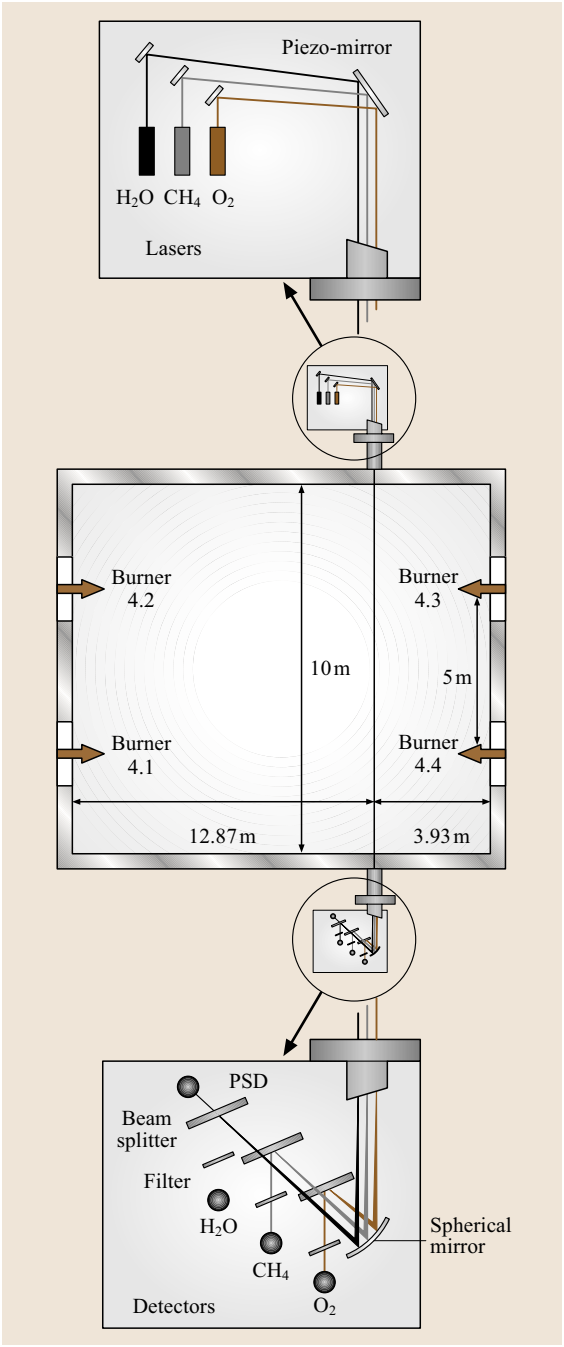

Fig. 20.52 Experimental setup of the spectrally multiplexed multi-parameter in situ diode-laser spectrometer used for the detection of CH_4, H_2O, O_2, CO_2 and gas temperature in the combustion chamber of a 1000 MW gas-fired power plant. Only the four of the 20 burners located in the plane of measurement are indicated. The optical setup containing lasers, optics, and detectors has been enlarged for clarity [20.364]

Further, to allow permanent measurements during start-up conditions it was necessary to compensate for strong temperature-induced wall deformations, which was accomplished with a new active laser beam alignment control loop. Using this multi-parameter spectrometer it was possible to analyze the full start-up and power-down procedure of a 1000 MW gas-fired power plant with 20 50 MW burners and a 10 m furnace diameter and achieve to a time resolution of 1.6 s and a minimum detectable absorption better than 10^{-3} OD. This resulted in a CH_4 detectivity of about 100 ppmV and a dynamic range of more than two orders of magnitude, as well as a relative temperature resolution of ± 10 K and a total temperature range of 300–1300 K. The ability to monitor H_2O as the possible cause, as well as CH_4 as the consequence of an ignition delay offers new possibilities to ensure a safe ignition procedure of large-scale multi-burner gas-fired combustion systems. The device also demonstrates the excellent expandability of multiplexed in-situ diode laser spectrometers and is of high interest to investigate the fuel to air ratio as well as the local chemistry in combustion processes.

Coal-Fired Power Plants. CO, another important combustion species is one of the key control parameters for combustion processes and one of the major pollutants of fossil-fuel combustion. Furthermore it is closely linked to reducing conditions in the combustor, which are responsible for high-temperature corrosion effects as well as fouling and slagging of the combustor containment. CO in-situ sensors are therefore of high interest and intensively studied. In the near-infrared range CO may be detected via two overtone transitions, the 2ν and 3ν vibrational bands at 2.3 and 1.5 μm. The 2.3 μm band has long been inaccessible due to the lack of suitable lasers, while the 1.5 μm band directly coincides with the wavelength range of telecommunication lasers. Using the high optical power (over 20 mW) of the 1.5 μm telecom lasers, the long absorption paths available in full-size power plants and combining it with highly efficient and robust algorithms for the suppression of in-situ disturbances it was recently shown for the first time that CO can be detected even in the very large combustion chamber (20 m diameter) of a 700 MW_{th} lignite-fired power plant. [20.363]. This offers new diagnostic opportunities

to investigate the slagging and fouling process in power plants and their dependence on the composition of the combustion gases. In addition by spectrally multiplexing the 1.5 μm CO laser with a 35 mW 813 nm FP-DL it was possible to access a H_2O overtone transition, which permitted a simultaneous in-situ measurement of H_2O and gas temperature. A major problem which had to be solved was the compensation of beam steering and severe optical losses (Fig. 20.53) of 99.9–99.999% by dust. This zero-visibility condition also required a method to permit the initial spectrometer alignment, which was ensured by an automatic feedback-controlled beam alignment based on motorized bending mirrors and a special phase-locked extraction algorithm to separate the weak laser light from the strong background radiation.

Rotary Kiln Combustors. Batch-fired rotary kilns (Fig. 20.54), used for the combustion of special wastes, are known to generate rapid and strong intermittent CO peaks, which have to be kept below a safety limit, thereby restricting the total waste throughput and the plant efficiency. Advanced control concepts to reduce the CO peaks and improve the throughput demand a very fast CO detection, preferentially directly through the rotary kiln. This could be realized for the first time [20.404] using a modified version of the 1.5 μm CO spectrometer described above. [20.363]. However, first measurements using standard personal computer (PC)-based data-acquisition (DAQ) cards showed that the strong, rapid and burst-like transmission fluctuations lead to saturation and clipping in the detector signal and systematic errors in the measured CO concentration. A new high-speed data-acquisition system based on a fast digital signal processor (DSP) removed these problems by enabling – at modulation frequencies of up to 3 kHz – a real-time evaluation of the individual, unaveraged absorption scans on a ms time scale, so that distorted scans could be rejected. Furthermore the DSP ensured a much higher data throughput close to 100% and allowed the transmission information of each scan to be used to realize an automatic real-time

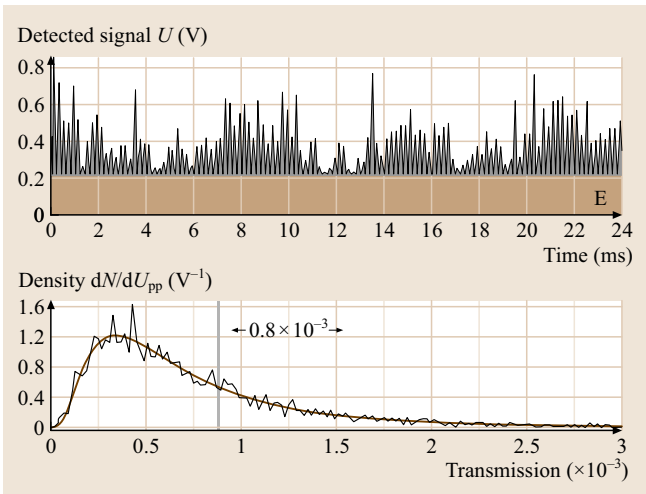

Fig. 20.53 Illustration of the transmission disturbances found in the combustion chamber of a 700 MW coal-fired power plant. *Top*: DC coupled in situ detector signal over a high number of wavelength scans (each sharp spike corresponds to an up and a down scan). The amplitude modulation of the signal is modified by strong transmission losses along the absorption path. In addition, the detector signal is increased by thermal background emission *E*. *Bottom*: distribution of transmission levels found over a longer time period, indicating an average in situ transmission of the measurement path (vertical line) of 8×10^{-4} [20.363]

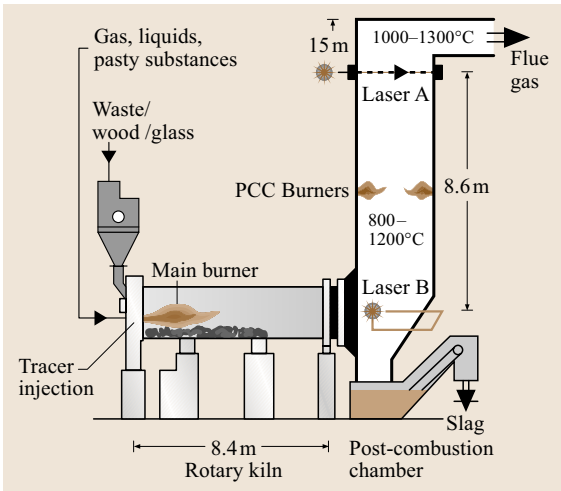

Fig. 20.54 Simplified cross section of the THERESA plant (Thermische Entsorgung spezieller Abfälle) [20.362], a rotary kiln fired incinerator for special waste. A secondary high-temperature combustion section [the post-combustion chamber (PCC)] is attached to the kiln exit. TDLAS was used in the process to realize a simultaneous CO/O_2 detection through the kiln (path A, Fig. 20.55), and at the kiln exit (path B, Fig. 20.56), as well as simultaneous O_2/H_2O/Temperature in the PCC. Multi-section gas residence-time measurements using binary alkali tracers were realized in the same process by injecting the tracer next to the main burner in the kiln and detecting the tracer at the exit of the kiln (path B, Fig. 20.57) and the exit of the PCC (path C, Fig. 20.57)

gain adaptation of the detector amplifiers, which significantly improved the usable dynamic range of the AD converter.

A comparison of both systems revealed that the relative systematic errors, that could be removed completely by the DSP system, can be larger then 1000% under special conditions in the case of a 8 m-long rotary kiln with 3 MW_{th} thermal power. Further enhancement of the DSP-based spectrometer was realized by spectrally multiplexing the 1.5 µm and 760 nm diode laser to access the R23-CO and the R23R23 O_2 transition for the first simultaneous CO/O_2 detection within a rotary kiln [20.404]. A 1.9 s response time yielded an optical resolution of $3-7\times10^{-4}$ and detection limits of 450 ppm CO resp. 2000 ppm O_2, which was sufficient to experimentally reveal the close anti-correlation of the intermittent CO and O_2 peaks (Fig. 20.55).

However, the approach of using the 3ν CO transitions is not feasible in smaller combustors or at low-ppm CO concentrations often found in modern combustion systems. To address this sensor deficiency new 2.3 µm distributed-feedback diode lasers (DFB-DL) that access the R30 line in the CO-2ν-band have been employed recently to develop a fast and highly sensitive in-situ CO absorption spectrometer suitable for hazardous waste incinerators [20.362, 404]. Additionally spectrally multiplexing the 2.3 µm DL with a 760 nm DFB-DL accessing the R17Q18/R19R19 O_2 lines again enabled a simultaneous in-situ detection of CO and O_2, which is most interesting for control strategies requiring the coverage of a wide range of fuel/air ratios. These new spectrometers were successfully tested over periods of up to two weeks in a 3.5 MW_{th} special waste incinerator. The absorption path ($l = 2.5$ m) was located at the rotary kiln exit in the lower part of the post combustion chamber with temperatures of 800–1000 °C (Fig. 20.54). Direct absorption spectroscopy using the DSP-based data evaluation enabled calibration-free species detection. With 1 s data-acquisition time a fractional absorption resolution (1σ) of 1.2×10^{-4} for CO (6×10^{-5} for O_2) could be achieved corresponding to significantly improved detection limits of 6.5 ppm CO (250 ppm O_2) [20.362]. This sensitivity and time resolution was high enough to detect even under lean-fuel conditions and with a relatively short absorption path small quasiperiodic stoichiometry changes of ±15 ppm CO caused by the periodic fuel feed of the rotary kiln (Fig. 20.56), thus nicely demonstrating the great potential of this device to establish an active combustion control system to optimize waste throughput in special waste incinerators.

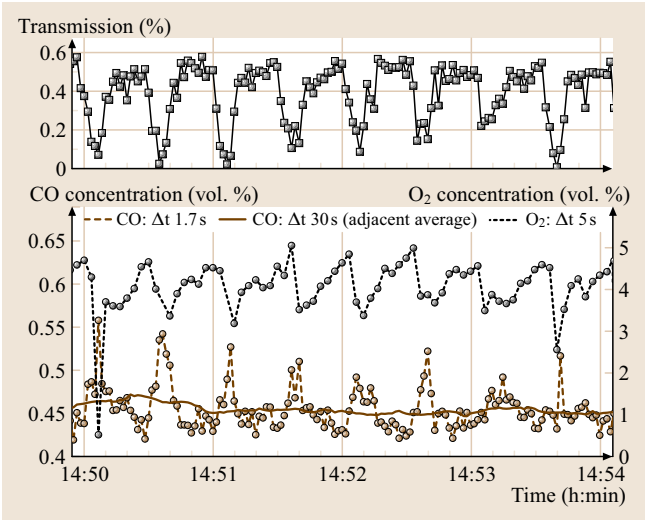

Fig. 20.55 Temporal evolution of the CO and O_2 concentration (*lower* and *middle traces* with *symbols*) and the broadband transmission (*top trace*) within the THERESA rotary kiln (Fig. 20.55) measured with 1.56 and 760 nm DFB-DL. While all signals vary synchronously with the waste feed cycle of 30 s, O_2 and CO are clearly anti-correlated, as expected from combustion chemistry. For comparison the flat *lower line* corresponds to a simulated signal for an extractive CO sensor [20.404]

High-Pressure Coal Combustion. The danger of severe corrosion damage in the high-temperature gas turbines needed for future high-efficiency pressurized coal combustion generates an immediate demand for optical in-situ diagnostic tools that are compatible with high-temperature high-pressure conditions. In particular alkali halide compounds have to be detected, but are spectroscopically difficult to access. ELIF [20.438–440], excimer-laser-induced fragmentation fluorescence is one of very few non-intrusive techniques capable of direct monitoring of alkali compounds in an industrial environment. Here an excimer laser photodissociates gaseous alkali compounds within the flue gas duct and generates electronically excited alkali atoms [Na(3^2P), K(4^2P)], which are then readily detected by their fluorescence in the visible region via a fiber-coupled two species detection system [20.438]. The measured signals are converted to absolute concentrations by a calibration of the complete detection apparatus under known thermodynamic conditions. A detection limit of 0.2 ppb could be established for both alkalis at 10 bar total pressure and 800 °C gas temperature.

As an alternative to the experimentally demanding, costly and calibration dependent, direct detection of

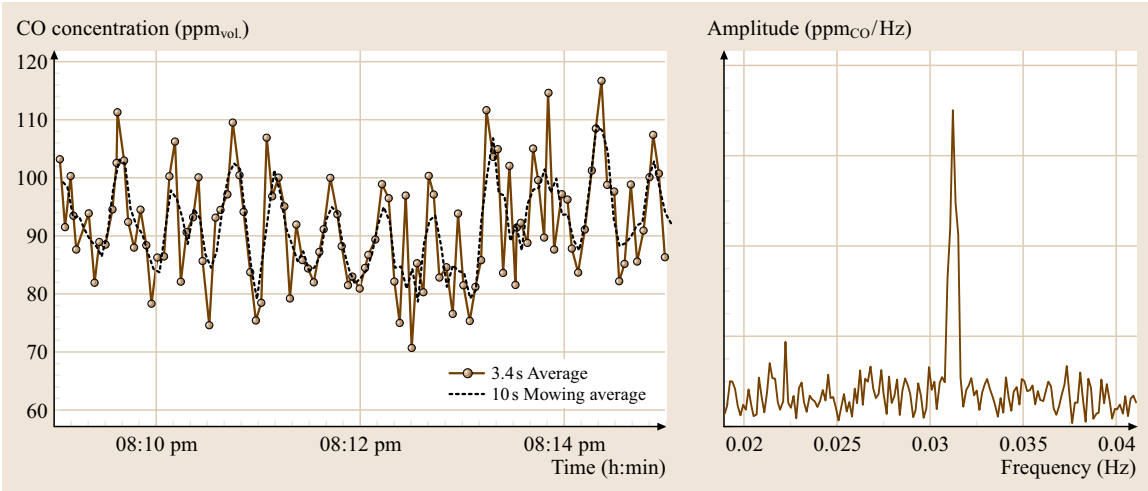

Fig. 20.56 *Left panel*: high-speed detection of fast, periodic CO fluctuations with ±17 ppm amplitude (±10 ppm for 10 s average) measured with 2.3 µm DFB-DL at the rotary kiln exit of the THERESA plant (Fig. 20.54). A fast Fourier transform (FFT) of the fluctuations over a 2 h period (*right panel*) shows a single prominent peak, with the same frequency as the feeding cycle of the incinerator [20.362]

the alkali compounds a diode-laser-based high-pressure compatible in-situ absorption spectrometer to monitor the alkali atoms (Li, K, Rb, Cs), which are produced by thermal dissociation of the compounds, was developed and tested in the flue gas duct of a 1 MW_{th} coal combustor at temperatures of 1400 K and pressures up to 15 bar [20.408]. In spite of severely broadened absorption lines, transmission fluctuations, and strong background emission it was shown for the first time in a practical combustion system that a fast and highly sensitive in-situ detection of alkali atoms is possible via their D-lines in the 670–850 nm spectral range. Crucial to the realization of these spectrometers was the use and detailed characterization of widely tunable vertical-cavity surface-emitting lasers (VCSEL). Despite the low VCSEL output power of only a few 100 µW it was possible to realize the first VCSEL-based in-situ detection of alkali-metal atoms in a technical combustor and achieve detection limits of 1.4 pptm potassium. This demonstrates the applicability of TDLAS to high-pressure in-situ gas analysis and the possibility of low-cost absorption sensors for the surveillance of hot gas filters needed for the protection of flue gas turbines in future coal-fired combined-cycle power plants.

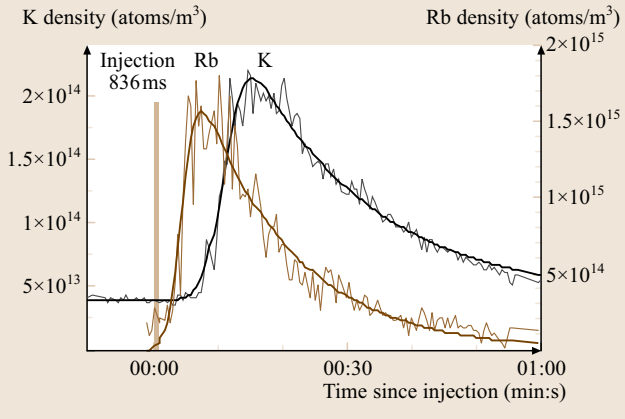

Fig. 20.57 Simultaneous residence-time distribution measurements in different plant segments of the THERESA rotary kiln (Fig. 20.54) using a binary tracer made from a mixture of K and Rb salts; the tracer mixture was injected at $t = 0$ over a period of 836 ms at the head of the rotary kiln (Fig. 20.54). The two species were measured at two locations within the plant: Rb atoms at the exit of the rotary kiln – 8.5 m from the injection site (*left peak* at $t = 9$ s); K atoms at the end of the PCC – 8.6 m downstream of the first measurement location (peak to the *right* at $t = 15$ s). Since K is part of the fuel its signal has – in contrast to Rb – an offset even without a tracer injection. Concentration distribution functions are fitted to the two traces [20.402]

Gas Residence-Time Measurements. Up to now the residence time distribution of the product gases in high-temperature production processes could only be

measured by the use of radioactive tracers. In addition to the complicated regulations that have to be fulfilled for the manipulation of radioactive substances, their use inevitably causes a contamination of the plant and therefore hinders a frequent inspection of this important process parameter. Using the fast-response in-situ spectrometers for alkali atoms [20.408] it was possible to develop a new and promising alternative technique for the in-situ measurement of gas residence time distributions in high-temperature processes (patent pending), which uses cheap and harmless alkali compounds as temperature stable tracer species. These compounds can be effectively monitored via the alkali atoms produced by thermal dissociation near the detection volume after the compounds pass through the process volume. During the first successful demonstration of this technique [20.402] in a 3 MW_{th} rotary kiln followed by a high-temperature post-combustion chamber (PCC; Fig. 20.54) it could be shown that an injection of only 100 mg of the tracer compound near the kiln entrance was sufficient in such a large process to effectively determine the residence time distribution. This high efficiency results from the extremely high detectivity of the laser in-situ absorption spectrometer of 80 ppq potassium (ppq = 1 in 10^{15}) or 4×10^{11} K atoms/m^3 at 1200 K [20.402]. Using binary K/Rb tracer mixtures and a multispecies spectrometer detecting the atoms at different locations in the plant it was possible to realize the simultaneous characterization of the transport properties of two consecutive plant segments (Fig. 20.57) located 8.4 m/17.0 m from the tracer discharge location and determine the mean residence times to (15±1) s and (26±1) s, which met the expected values. With this new technique it is feasible for the first time to realize a permanent online measurement and verification of the residence time distribution of a combustion process, which is particularly important for the optimization of chemical reactors and processes such as waste incinerators with statutory limits for the residence time of the combustion products.

20.5 Conclusions

Despite intensive research for alternative energy sources further economic growth will be closely linked to an extensive use of combustion processes for mobility, energy conversion, and generation of industrial process heat. The drastic increase of combustion fuel consumption has, however, now reached a level where the annual worldwide demand corresponds to amounts of fossil fuel that has been accumulated during a period of 1 million years of the Earth's history. The limited supply of fossil fuels and the detrimental environmental effects of the global use of combustion require pollutant emission to be minimized and total energy conversion efficiency and process performance to be optimized. Demands are similarly important for industrial combustion-based production processes, which are indispensable for high-volume products such as steel, glass, cement, and which require simultaneous optimization of combustion parameters, product quality, and product costs.

After four decades of research and development in the area of laser-based concepts for combustion diagnostics, many of the spectroscopic methods have matured now from qualitative to quantitative techniques. Its capabilities go far beyond the observation of two-dimensional distribution of signal intensities. The instantaneous simultaneous measurement of concentration distribution of several scalars (species concentration and temperature) gives insight in correlation of species, i. e., in turbulent combustion processes. The spatial combination of several observed planes on the other hand allows a visualization of three-dimensional concentration distributions and yields a unique view into turbulent nonreactive and reactive flow systems. The calculation of absolute (three-dimensional) species concentration gradients and scalar dissipation rates is of major importance for combustion modeling. Finally, multiple-time-step imaging yields movie-like insight into fast processes and therefore allows for the first time the investigation of highly dynamic processes in real time.

The interpretation of measured signal intensities in practical combustion situations is not trivial. High pressure, high temperature and a variety of sources of interfering signal and attenuation of laser and signal light hinders the selective and quantitative measurement. The spectroscopic properties of the species under study, therefore, must be well examined. We presented the required studies in high-pressure laminar flames for the example of nitric oxide. This information enables quantitative measurements even in harsh environments such as in-cylinder gasoline and Diesel engine measurements with direct injection. Advanced laser-based imaging diagnostics turns out to be an important tool for the development and optimization of

modern combustion devices that can fulfill the future requirements in terms of energy efficiency and pollutant minimization.

Laser diagnostics techniques similar to those discussed here are also used to study diverse applications beyond combustion, including atmospheric chemistry, plasma chemistry, and chemical vapor deposition and material synthesis. Even biological applications of sophisticated laser techniques are now being pursued in some combustion diagnostics groups since the coupling of elementary chemical reactions with various transport processes is also the basis of living systems.

References

20.1 G.R. Kirchhoff, R.W. Bunsen: Chemische Analyse durch Spectralbeobachtungen, Poggend. Annal. **110**, 161–176 (1860), in German

20.2 A. Einstein: Zur Quantentheorie der Strahlung, Phys. Z. **18**, 21–128 (1917), in German

20.3 J.P. Gordon, H.H. Zeiger, C.H. Townes: The maser – new type of microwave amplifier, frequency standard and spectrometer, Phys. Rev. **99**, 1264–1274 (1955)

20.4 T.H. Maiman: Stimulated optical radiation in ruby, Nature **187**, 493–494 (1960)

20.5 A.G. Gaydon: *The Spectroscopy of Flames* (Chapman Hall, London 1967)

20.6 W. Demtröder: *Laserspektroskopie. Grundlagen und Techniken*, 3rd edn. (Springer, Berlin, Heidelberg 2000), in German

20.7 A.C. Eckbreth: *Laser Diagnostics for Combustion Temperature and Species*, 2nd edn. (Gordon and Breach, Amsterdam 1996)

20.8 K. Kohse-Höinghaus, J.B. Jeffries (Eds.): *Applied Combustion Diagnostics* (Taylor Francis, New York 2002)

20.9 J. Warnatz, U. Maas, R.W. Dibble: *Combustion*, 3rd edn. (Springer, Berlin, Heidelberg 2001)

20.10 J. Wolfrum: Lasers in combustion: From basic theory to practical devices, Proc. Combust. Inst. **27**, 1–42 (1998)

20.11 C. Schulz, V. Sick: Tracer-LIF diagnostics: Quantitative measurement of fuel concentration, temperature and air/fuel ratio in practical combustion situations, Prog. Energy Combust Sci. **31**, 75–121 (2005)

20.12 H. Zhao, N. Ladommatos: Optical diagnostics for in-cylinder mixture formation measurements in IC engines, Prog. Energy Combust. Sci. **24**, 297–336 (1998)

20.13 T. Etzkorn, J. Fitzer, S. Muris, J. Wolfrum: Determination of absolute methyl- and hydroxyl-radical concentrations in a low pressure methane-oxygen flame, Chem. Phys. Lett. **208**, 307–310 (1993)

20.14 D.F. Davidson, A.Y. Chang, M.D. DiRosa, R.K. Hanson: A CW laser absorption diagnostic for methyl radicals, J. Quant. Spectrosc. Radiat. Transfer **49**, 559–571 (1993)

20.15 P. Zalicki, R.N. Zare: Cavity ring-down spectroscopy for quantitative absorption measurements, J. Chem. Phys. **102**, 2708 (1995)

20.16 W.K. Bischel, B.E. Perry, D.R. Crosley: Detection of fluorescence from O and N atoms induced by two-photon absorption, Appl. Opt. **21**, 1419–1429 (1982)

20.17 R.S. Barlow, C.D. Carter, R.W. Pitz: Multi-scalar diagnostics in turbulent flames. In: *Applied Combustion Diagnostics*, ed. by K. Kohse-Höinghaus, J.B. Jeffries (Taylor Francis, London 2003)

20.18 K. Müller-Dethlefs, M. Pealat, J.-P.E. Taran: Temperature and hydrogen concentration measurements by CARS in an ethylene-air bunsen flame, Ber. Bunsenges. Phys. Chem. **85**, 803–807 (1981)

20.19 A. Dreizler, T. Dreier, J. Wolfrum: Thermal grating effects in infrared degenerate four-wave mixing for trace gas detection, Chem. Phys. Lett. **233**, 525–532 (1995)

20.20 A.A. Suvernev, A. Dreizler, T. Dreier, J. Wolfrum: Polarization-spectroscopic measurement and spectral simulation of OH ($A^2\Sigma$-$X^2\Pi$) and NH ($A^3\Pi$-$X^3\Sigma$) transitions, Appl. Phys. B **61**, 421–427 (1995)

20.21 R.W. Pitz, J.A. Wehrmeyer, J.M. Bowling, T.S. Cheng: Single pulse vibrational Raman scattering by a broadband KrFexcimer laser in a hydrogen/air flame, Appl. Opt. **29**, 2325–2332 (1990)

20.22 R.L. Vander Wal: Laser-induced incandescence: Development and characterization towards a measurement of soot-volume fraction, Appl. Phys. B **59**, 445–452 (1994)

20.23 A. Dreizler, J. Janicka: Diagnostic challenges for gas turbine combustor model validation. In: *Applied Combustion Diagnostics*, ed. by K. Kohse-Höinghaus, J.B. Jeffries (Taylor Francis, New York 2002)

20.24 M.D. Smooke: *Reduced Kinetic Mechanisms and Asymptotic Approximations for Methane-Air Flames*, Lecture Notes in Physics (Springer, Berlin, Heidelberg 1991)

20.25 N. Peters, F.A. Williams: The asymptotic structure of stoichiometric methane-air flames, Combust. Flame **68**, 185–207 (1987)

20.26 U. Maas, S.B. Pope: Simplifying chemical kinetics: intrinsic low-dimensional manifolds in composition space, Combust. Flame **88**, 239–264 (1992)

20.27 J.B. Jeffries, G.P. Smith, D.E. Heard, D.R. Crosley: Comparing LIF measurements and computer models of low pressure flame chemistry, Ber. Bunsenges. Phys. Chem. **96**, 1410–1418 (1992)

20.28 U. Meier, U. Kienle, I. Plath, K. Kohse-Höinghaus: Two-dimensional laser-induced fluorescence approaches for the accurate determination of radical concentrations and temperature in combustion, Ber. Bunsenges. Phys. Chem. **96**, 1401–1410 (1992)

20.29 K. Fieweger, R. Blumenthal, G. Adomeit: Shock-tube investigations on the self-ignition of hydrocarbon-air mixtures at high pressures, Proc. Combust. Inst. **25**, 1579–1585 (1994)

20.30 R. Minetti, M. Carlier, M. Ribaucour, E. Therssen, L.R. Sochet: A rapid compression machine investigation of oxidation and auto-ignition of n-heptane: measurements and modelling, Combust. Flame **102**, 298–309 (1995)

20.31 G.P. Smith: Diagnostics for detailed kinetic modeling. In: *Applied Combustion Diagnostics*, ed. by K. Kohse-Höinghaus, J.B. Jeffries (Taylor Francis, New York 2002) pp. 501–517

20.32 K.N.C. Bray: The challenge of turbulent combustion, Proc. Combust. Inst. **26**, 1–26 (1996)

20.33 W.P. Jones, B.E. Launder: The prediction of laminarization with a two-equation model of turbulence, Int. J. Heat Mass Transfer **15**, 301–314 (1972)

20.34 J. Janicka, A. Sadiki: Large eddy simulation of turbulent combustion systems, Proc. Combust. Inst. **30**, 537–548 (2005)

20.35 C. Schneider, A. Dreizler, J. Janicka: Fluid dynamical analysis of atmospheric reacting and isothermal swirling flows, Flow Turbul. Combust. **74**, 103–127 (2005)

20.36 G.H. Wang, N.T. Clemens, P.L. Varghese: High-repetition-rate measurements of temperature and thermal dissipation in nonpremixed turbulent jet flames, Proc. Combust. Inst. **30**, 691–700 (2005)

20.37 D. Geyer, A. Kempf, A. Dreizler, J. Janicka: Scalar dissipation rates in isothermal and reactive turbulent opposed-jets: 1D-Raman/Rayleigh experiments supported by LES, Proc. Combust. Inst. **30**, 681–689 (2005)

20.38 C.S. Barlow, A.N. Karpetis: Scalar length scales and spatial averaging effects in turbulent piloted methans/air jet flames, Proc. Combust. Inst. **30**, 673–680 (2005)

20.39 T.J. Poinsot, D. Veynante: *Theoretical and Numerical Combustion* (Edwards, Philadelphia 2005)

20.40 R.S. Barlow: Laser diagnostics and their interplay with computations to understand turbulent combustion, Proc. Combust. Inst. **31**, 49–76 (2007)

20.41 N. Peters: Laminar flamlet concepts in turbulent combustion, Proc. Combust. Inst. **21**, 1231–1250 (1986)

20.42 R.W. Bilger, S.B. Pope, K.N.C. Bray, J.F. Driscoll: Paradigms in turbulent combustion research, Proc. Combust. Inst. **30**, 21–42 (2004)

20.43 S.B. Pope: Computations of turbulent combustion: Progress and challenges, Proc. Combust. Inst. **23**, 591–612 (1990)

20.44 N. Peters: *Turbulent Combustion* (Cambridge Univ. Press, Cambridge 2000)

20.45 R.S. Barlow, C.D. Carter, R.W. Pitz: Multiscalar diagnostics in turbulent flames. In: *Applied Combustion Diagnostics*, ed. by K. Kohse-Höinghaus, J.B. Jeffries (Taylor Francis, New York 2002) pp. 384–407

20.46 G. Grünefeld, A. Gräber, A. Diekmann, S. Krüger, P. Andresen: Measurement system for simultaneous species densities, temperature and velocity double-pulse measurements in turbulent hydrogen flames, Combust. Sci. Technol. **135**, 135–152 (1998)

20.47 R.B. Miles, W.R. Lempert: Two-dimensional measurement of density, velocity, and temperature in turbulent high-speed air flows by UV Rayleigh scattering, Appl. Phys. B **51**, 1–7 (1990)

20.48 R.W. Dibble, W. Kollmann, R.W. Schefer: Conserved scalar fluxes measured in a turbulent nonpremixed flame by combined laser Doppler velocimetry and laser Raman scattering, Combust. Flame **55**, 307–321 (1984)

20.49 A. Nauert, A. Dreizler: Conditional velocity measurements by simulatenously applied laser Doppler velocimetry and planar laser-induced fluorescence in a swirling natural gas/air flame, Z. Phys. Chem. **219**, 635–648 (2005)

20.50 S. Geiss, A. Dreizler, Z. Stojanovic, A. Sadiki, J. Janicka: Experimental investigation of turbulence modification in a non-reactive two-phase flow, Exp. Fluids **36**, 344–354 (2004)

20.51 H.-E. Albrecht, M. Borys, N. Damaschke, C. Tropea: *Laser Doppler and Phase Doppler Measurement Techniques* (Springer, Berlin, Heidelberg 2003)

20.52 N. Damaschke, H. Nobach, C. Tropea: Optical limits of particle concentration for multidimensional particle sizing techniques in fluid mechanics, Exp. Fluids **32**, 143–152 (2002)

20.53 M.C. Jermy, D.A. Greenalgh: Planar dropsizing by elastic fluorescence scattering in sprays too dense for phase Doppler measurements, Appl. Phys. B **71**, 703–710 (2000)

20.54 I. Düwel, J. Schorr, J. Wolfrum, C. Schulz: Laser-induced fluorescence of tracers dissolved in evaporating droplets, Appl. Phys. B **78**, 127–131 (2004)

20.55 H.C. Hottel, A.F. Sarofim: *Radiative Heat Transfer* (McGraw Hill, New York 1997)

20.56 A.L. Crosbie, J.B. Farrell: Exact formulation of multiple scattering in a three-dimensional cylindrical geometry, J. Quant. Spectrosc. Radiat. Heat Transfer **31**, 397–416 (1984)

20.57 J.T. Farmer, J.R. Howell: Monte Carlo prediction of radiative heat transfer in homogeneous, anisotropic, nongray media, J. Thermophys. Heat Transfer **8**, 133–139 (1994)

20.58 A. Soufiani, E. Djavdan: A comparison between weigthed sum of gray gases and statistical

narrow-band radiation models for combustion applications, Combust. Flame **97**, 240–250 (1994)
20.59 R. Koch, S. Wittig, B. Noll: The harmonic transmission model: A new approach to multidimensional radiative transfer calculation in gases under consideration of pressure broadening, Int. J. Heat Mass Transfer **34**, 1871–1880 (1991)
20.60 J. Brübach, J. Zetterberg, A. Omrane, Z.S. Li, M. Aldén, A. Dreizler: Determination of surface normal temperature gradients using thermographic phosphors and filtered Rayleigh scattering, Appl. Phys. B **84**, 537–541 (2005)
20.61 T. Fuyuto, H. Kronemayer, B. Lewerich, W. Koban, K. Akihama, C. Schulz: Laser-based temperature imaging close to surfaces with toluene and NO-LIF, J. Phys.: Conference Series **45**, 69–76 (2006)
20.62 D. Geyer: 1D Raman/Rayleigh experiments in a turbulent opposed-jet. PhD Thesis (TU Darmstadt, Darmstadt 2004)
20.63 D. Geyer, A. Dreizler, J. Janicka, A.D. Permana, J.-Y. Chen: Finite rate chemistry effects in turbulent opposed flows: comparison of Raman/Rayleigh measurements and Monte Carlo PDF simulation, Proc. Combust. Inst. **30**, 711–718 (2005)
20.64 S.K. Omar, D. Geyer, A. Dreizler, J. Janicka: Investigation of flame structures in turbulent partially premixed counter-flow flames using laser-induced fluorescence, Prog. Comput. Fluid Dyn. **4**, 241–249 (2004)
20.65 B. Böhm, D. Geyer, K.K. Venkatesan, N.M. Laurendeau, M.W. Renfro: Simulatenous PIV/PTV/OH-PLIF imaging: Conditional flow field statistics in partially-premixed turbulent opposed jet flames, Proc. Combust. Inst. **31**, 709–717 (2007)
20.66 K.K. Venkatesan, N.M. Laurendeau, M.W. Renfro, D. Geyer, A. Dreizler: Time-resolved measurements of hydroxyl in stable and extinguishing partially-premixed turbulent opposed-jez flames, Flow Turbulence Combustion **76**, 257–278 (2006)
20.67 D. Geyer, A. Kempf, A. Dreizler, J. Janicka: Turbulent opposed jet flames: a critical benchmark for combustion LES, Combust. Flame **143**, 524–548 (2005)
20.68 K. Shimoda: Limits of sensitivity of laser spectrometers, Appl. Phys. **1**, 77–86 (1973)
20.69 C.A. Taatjes, D.B. Oh: Time-resolved wavelength modulation spectroscopy measurements of HO_2 kinetics, Appl. Opt. **36**, 5817–5821 (1997)
20.70 M.G. Allen: Diode laser absorption sensors for gas dynamic and combustion flows, Meas. Sci. Technol. **9**, 545–562 (1998)
20.71 S. Schäfer, M. Mashni, J. Sneider, A. Miklos, P. Hess, V. Ebert, K.-U. Pleban, H. Pitz: Sensitive detection of methane with 1.65 µm diode laser by photoacoustic and absorption spectroscopy, Appl. Opt. **66**, 511–516 (1998)
20.72 M.S. Chou, A.M. Dean, D. Stern: Laser absorption measurements on OH, NH and NH_2 in NH_3/O_2 flames: Determination of an oscillator strength for NH_2, J. Chem. Phys. **76**, 5334–5340 (1982)
20.73 S. Cheskis, I. Derzy, V.A. Lozovsky, A. Kachanov, D. Romanini: Cavity ring-down spectroscopy of OH radicals in low-pressure flames, Appl. Phys. B **66**, 377 (1998)
20.74 J.J. Scherer, D.J. Rakestraw: Cavity ring-down laser absorption spectroscopy detection of formyl (HCO) radical in a low pressure flame, J. Chem. Phys **265**, 169 (1997)
20.75 J.J. Scherer, D.J. Rakestraw: Cavity ringdown laser absorption spectroscopy detection of formyl (HCO) radical in a low-pressure flame, Chem. Phys. Lett. **265**, 168–176 (1997)
20.76 K. Kohse-Höinghaus, U. Meier, B. Attal-Trétout: Laser-induced fluorescence study of OH in flat flames of 1-10 bar compared with resonance CARS experiments, Appl. Opt. **29**, 1560–1569 (1990)
20.77 C.D. Carter, G.B. King, N.M. Laurendeau: Saturated fluorescence measurements of the hydroxyl radical in laminar high-pressure $C_2H_6/O_2/N_2$ flames, Appl. Opt. **31**, 1511–1522 (1992)
20.78 T. Dreier, D. Rakestraw: Measurement of OH rotational temperatures in a flame using degenerate four wave mixing, Opt. Lett. **15**, 72–74 (1990)
20.79 H. Bervas, B. Attal-Tretout, S. Le Boiteux, J.P. Taran: OH detection and spectroscopy by DFWM in flames: comparison with CARS, J. Phys. B **25**, 949–969 (1992)
20.80 T. Dreier, D.J. Rakestraw: Degenerate four-wave mixing diagnostics on OH and NH radicals in flames, Appl. Phys. B **50**, 479–485 (1990)
20.81 G.J. Germann, R.L. Farrow, D.J. Rakestraw: Infrared degenerate four-wave mixing spectroscopy of polyatomic molecules: CH_4 and C_2H_2, J. Opt. Soc. Am. B **12**, 25–32 (1995)
20.82 R.L. Vander Wal, B.E. Holmes, J.B. Jeffries, P.M. Danehy, R.L. Farrow, D.J. Rakestraw: Detection of HF using infrared degenerate four-wave mixing, Chem. Phys. Lett. **191**, 251–258 (1992)
20.83 R.L. Farrow, M.N. Bui-Pham: Degenerate four-wave mixing measurements of methyl radical distributions in hydrocarbon flames: Comparison with model predictions, Proc. Combust. Inst. **26**, 975–983 (1996)
20.84 C.F. Kaminski, I.G. Hughes, P. Ewart: Degenerate four-wave mixing spectroscopy and spectral simulation of C_2 in an atmospheric pressure oxyacetylene flame, J. Chem. Phys. **106**, 5324–5332 (1997)
20.85 B. Attal, D. Débarre, K. Müller-Dethlefs, J.P.E. Taran: Resonance-enhanced coherent anti-Stokes Raman scattering in C_2, Rev. Phys. Appl. **18**, 39–50 (1983)
20.86 B. Attal-Trétout, P. Berlemont, J.P. Taran: Three-colour CARS spectroscopy of the OH radical at triple resonance, Mol. Phys. **70**, 1–51 (1990)
20.87 L.A. Rahn, P.L. Mattern, R.L. Farrow: A comparison of coherent and spontaneous Raman combus-

tion diagnostics, Proc. Combust. Inst. **18**, 1533–1542 (1981)
20.88 A.C. Eckbreth, R.J. Hall: CARS concentration sensitivity with aqnd without nonresonant background suppression, Combust. Sci. Technol. **25**, 175–192 (1981)
20.89 T. Dreier, J. Wolfrum: Detection of the free OH ($X^2\Pi$) radical by CARS spectroscopy, J. Chem. Phys. **80**, 975–976 (1984)
20.90 T. Dreier, J. Wolfrum: Detection of free NH_2 (X^2B_1) radicals by CARS spectroscopy, Appl. Phys. B **33**, 213–218 (1984)
20.91 T.N. Tanada, J. Velazques, N. Hemmi, T.A. Cool: Detection of toxic emissions from incinerators, Ber. Bunsenges. Phys. Chem. **97**, 1516–1526 (1993)
20.92 C. Weickhard, U. Boesl: Time-resolved trace analysis of exhaust gas by means of laser mass spectrometry, Ber. Bunsenges. Phys. Chem. **97**, 1716–1719 (1993)
20.93 K. Nyholm, M. Kaivola, C.G. Aminoff: Polarization spectroscopy applied to C_2 detection in a flame, Appl. Phys. B **60**, 5–10 (1995)
20.94 K. Nyholm: Measurements of OH rotational temperatures in flames by using polarization spectroscopy, Opt. Commun. **111**, 66–70 (1994)
20.95 R.S. Barlow, A.N. Karpetis: Scalar length scales and spatial averaging effects in turbulent piloted methane/eir jet flames, Proc. Combust. Inst. **30**, 673–680 (2005)
20.96 J.J. Scherer, J.B. Paul, A. O'Keefe, R.J. Saykally: Cavity ringdown laser absorption spectroscopy: History, development, and application to pulsed molecular beams, Chem. Rev. **97**, 25 (1997)
20.97 W. Juchmann, H. Latzel, D.-I. Shin, G. Peiter, T. Dreier, H.-R. Volpp, J. Wolfrum, R.P. Lindstedt, K.M. Leung: Absolute radical concentration measurements and modeling of low pressure $CH_4/O_2/NO$ flames, Proc. Combust. Inst **27**, 469–476 (1998)
20.98 M. Bachmann, J. Griesheimer, K.-H. Homann: Thermal and chemical influences on the soot mass growth, Proc. Combust. Inst. **25**, 635–643 (1994)
20.99 M. Hausmann, K.H. Homann: Scavenging of hydrocarbon radicals from flames with dimethyldisulfide II. Hydrocarbon radicals in fuel-rich low-pressure flames of acetylene, ethylene, 1,3-butadiene and methane with oxygen, Ber. Bunsenges. Phys. Chem. **101**, 651–667 (1997)
20.100 J. Ahrens, A. Keller, R. Kovacs, K.-H. Homann: Large molecules, radicals, ions and soot particles in fuel-rich hydrocarbon flames. Part III: REMPI mass spectrometry of large flame PAHs and fullerenes and their quantitative calibration through sublimation, Ber. Bunsenges. Phys. Chem. **102**, 1823–1839 (1998)
20.101 M. Woyde, W. Stricker: The application of CARS for temperature measurements in high pressure combustion systems, Appl. Phys. B **50**, 519–525 (1990)
20.102 T. Dreier, M. Ridder, G. Schiff, A. Saur, A.A. Suvernev: Determination of temperature from N_2 and O_2 CARS spectra at very high pressure, Proc. Combust. Inst. **25**, 1727–1734 (1994)
20.103 L. Martinsson, P.-E. Bengtsson, M. Aldén, S. Kröll: Applications of rotational CARS for temperature measurements at high pressure and in particle-laden flames. In: *Temperature: Its Measurements and Control in Science and Industry*, ed. by J.F. Schooley (American Institute of Physics, New York 1992) pp. 679–684
20.104 R.L. Vander Wal, R.L. Farrow, Rakestraw: High-resolution investigation of degenerate four-wave mixing in the $\gamma(0,0)$ band of nitric oxide, Proc. Combust. Inst. **24**, 1653–1659 (1992)
20.105 S.J. Tsay, K.G. Owens, K.W. Aniolek, D.L. Miller, N.P. Cernansky: Detection of CN by degenerate four-wave mixing, Opt. Lett. **20**, 1725–1727 (1995)
20.106 S. Williams, R.N. Zare, L.A. Rahn: Reduction of degenerate four-wave mixing spectra to relative populations II. Strong-field limit, J. Chem. Phys. **101**, 1093–1107 (1994)
20.107 A.P. Smith, G. Hall, B.J. Whitaker, A.G. Astill, D.W. Neyer, P.A. Delve: Effect of inert gases on the degenerate four-wave mixing spectrum of NO_2, Appl. Phys. B **60**, 11–18 (1995)
20.108 G. Hall, A.G. Suits, B.J. Whitaker: Resonant degenerate four wave mixing detection of HCO, Chem. Phys. Lett. **203**, 277–282 (1993)
20.109 K. Nyholm, R. Fritzon, M. Aldén: Two-dimensional imaging of OH in flames by use of polarization spectroscopy, Opt. Lett. **18**, 1672–1674 (1993)
20.110 B. Löfstedt, R. Fritzon, M. Aldén: Investigation of NO detection in flames using polarization spectroscopy, Appl. Opt. **35**, 2140–2146 (1996)
20.111 T. Reichardt, R.P. Lucht: Theoretical calculation of line shapes and saturation effects in polarization spectroscopy, J. Chem. Phys. **109**, 5830–5843 (1998)
20.112 J.B. Kelman, A.R. Masri: Reaction zone structure and scalar dissipation rates in turbulent diffusion flames, Appl. Opt. **36**, 3506–3514 (1997)
20.113 Q.V. Nguyen, P.H. Paul: The time evolution of a vortex-flame interaction observed via planar laser-induced fluorescence imaging of CH and OH, Proc. Combust. Inst. **26**, 357–364 (1996)
20.114 A.R. Masri, R.W. Dibble, R.S. Barlow: The structure of turbulent nonpremixed flames revealed by Raman-Rayleigh-LIF measurements, Prog. Energy Combust. Sci. **22**, 307–362 (1996)
20.115 M. Decker, A. Schik, U.E. Meier, W. Stricker: Quantitative Raman imaging investigations of mixing phenomena in high-pressure cryogenic jets, Appl. Opt. **37**, 5620–5627 (1998)
20.116 M. Péalat, P. Bouchardy, M. Lefebvre, J.P. Taran: Precision of multiplex CARS temperature measurements, Appl. Opt. **24**, 1012–1022 (1985)
20.117 R.P. Lucht, D. Dunn-Rankin, T. Walter, T. Dreier, S.C. Bopp: Heat transfer in engines: Comparison of

CARS thermal boundary layer measurements and heat flux measurements, SAE Techn. Paper Ser. 910722 (1991)
20.118 A.C. Eckbreth, G.M. Dobbs, J.H. Stufflebeam, P.A. Tellex: CARS temperature measurements in augmented jet engine exhausts, Appl. Opt. **23**, 1328–1339 (1984)
20.119 A.C. Eckbreth, T.J. Anderson, J.A. Shirley: Laser Raman diagnostics for propulsion systems development, Ber. Bunsenges. Phys. Chem. **97**, 1597–1608 (1993)
20.120 R. Bédué, R. Gastebois, R. Bailly, M. Pealat, J.P. Taran: CARS measurements in a simulated turbomachine combustor, Combust. Flame **57**, 141–153 (1984)
20.121 B. Lavorel, G. Millot, J. Bonamy, D. Robert: Study of rotational relaxation fitting laws from calculation of SRS N_2 Q-branch, Chem. Phys. **115**, 69–78 (1987)
20.122 G. Millot, R. Saint-Loup, S. Santos, R. Chaux, H. Berger, J. Bonamy: Collisional effects in the stimulated Raman Q-branch of O_2 and O_2-N_2, J. Chem. Phys. **96**, 961–971 (1992)
20.123 L.A. Rahn, R.L. Farrow, G.J. Rosasco: Measurement of the self-broadening of the H_2 Q(0–5) Raman transitions from 295 to 1000 K, Phys. Rev. A **43**, 6075–6088 (1991)
20.124 J.P. Looney, G.J. Rosasco, L.A. Rahn, W.S. Hurst, J.W. Hahn: Comparison of rotational relaxation rate laws to characterize the Raman Q-branch spectrum of CO at 295 K, Chem. Phys. Lett. **161**, 232–238 (1989)
20.125 B. Lavorel, G. Millot, G. Fanjoux, R. Saint-Loup: Study of collisional effects on bandshapes of the $\nu_1/2\nu_2$ Fermi dyad in CO_2 gas with stimulated Raman spectroscopy. III. Modeling of collisional narrowing and study of vibrational shifting and broadening at high temperature, J. Chem. Phys. **101**, 174–177 (1994)
20.126 W. Kiefer: Non-linear Raman spectroscopy and its chemical applications. In: *NATO Advanced Study Insitutes Series C: Mathematical and Physical Sciences*, ed. by W. Kiefer, D.A. Long (Reidel, Dordrecht 1982) pp. 241–260
20.127 R. Suntz, H. Becker, P. Monkhouse, J. Wolfrum: Two-dimensional visualization of the flame front in an internal combustion engine by laser-induced fluorescence of OH radicals, Appl. Phys. B **47**, 287–293 (1988)
20.128 P.H. Paul, H.N. Najm: Planar laser-induced fluorescence imaging of flame heat release, Proc. Combust. Inst. **27**, 43–50 (1998)
20.129 A. Hoffmann, C. Schulz, J. Ruckwied, D. Malcherek, T. Dreier, R. Schießl, U. Maas: Three-dimensional measurement of OH-concentration gradients in a turbulent flame by simultaneous laser induced fluorescence and Raman scattering. In: *European Combustion Meeting* (The Combustion Institute, Orléans 2003)
20.130 P.C. Miles: Raman line imaging for spatially and spectrally resolved mole fraction measurements in internal combustion engines, Appl. Opt. **38**, 1714–1732 (1999)
20.131 G. Grünefeld, M. Schütte, P. Andresen: Simultaneous multiple-line Raman/Rayleigh/LIF measurements in combustion, Appl. Phys. B **70**, 309–313 (2000)
20.132 S. Böckle, J. Kazenwadel, T. Kunzelmann, D.-I. Shin, C. Schulz, J. Wolfrum: Simultaneous single-shot laser-based imaging of formaldehyde, OH and temperature in turbulent flames, Proc. Combust. Inst. **28**, 279–286 (2000)
20.133 S. Böckle, J. Kazenwadel, C. Schulz: Laser-diagnostic multi-species imaging in strongly swirling natural gas flames, Appl. Phys. B **71**, 741–746 (2000)
20.134 S. Einecke, C. Schulz, V. Sick: Measurement of temperature, fuel concentration and equivalence ratio fields using tracer LIF in IC engine combustion, Appl. Phys. B **71**, 717–723 (2000)
20.135 W. Koban, J. Schorr, C. Schulz: Oxygen distribution imaging with a novel two-tracer laser-induced fluorescence technique, Appl. Phys. B **74**, 111–114 (2002)
20.136 C.F. Kaminski, J. Hult, M. Aldén: High repetition rate planar laser induced fluorescence of OH in a turbulent non-premixed flame, Appl. Phys. B **68**, 757–760 (1999)
20.137 C.F. Kaminski, M.B. Long: Multidimensional diagnostics in space and time. In: *Applied Combustion Diagnostics*, ed. by K. Kohse-Höinghaus, J.B. Jeffries (Taylor Francis, London 2003) pp. 224–251
20.138 I. Düwel, J. Schorr, P. Peuser, P. Zeller, J. Wolfrum, C. Schulz: Spray diagnostics using an all solid-state Nd:$YAlO_3$ laser and fluorescence tracers in commercial gasoline and Diesel fuels, Appl. Phys. B **79**, 249–254 (2004)
20.139 W. Meier, O. Keck: Laser Raman scattering in fuel-rich flames: background levels at different excitation wavelengths, Meas. Sci. Technol. **13**, 741–749 (2002)
20.140 A. Buschmann, F. Dinkelacker, M. Schäfer, T. Schäfer, J. Wolfrum: Measurement of the instantaneous detailed flame structure in turbulent premixed combustion, Proc. Combust. Inst. **26**, 619 (1996)
20.141 H.B. Najm, P.H. Paul, C.J. Mueller, P. Wyckoff: On the adequacy of certain experimental observables as measurements of flame burning rate, Combust. Flame **113**, 312–322 (1998)
20.142 T. Landenfeld, A. Kremer, E.P. Hassel, J. Janicka, T. Schäfer, J. Kazenwadel, C. Schulz, J. Wolfrum: Laserdiagnostic and numerical studies of strongly swirling natural-gas flames, Proc. Combust. Inst. **27**, 1023–1030 (1998)
20.143 D.I. Shin, G. Peiter, T. Dreier, H.-R. Volpp, J. Wolfrum: Spatially resolved measurements of CN, CH,

NH and H_2CO concentration profiles in a domestic gas boiler, Proc. Combust. Inst. **28**, 319–325 (2000)
20.144 N. Garland: Assignment of formaldehyde laser-induced Fluorescence spectrum from the Sandia engine experiment, SRI International MP **84-033** (1984)
20.145 D. Grebner, J. Hein, W. Triebel, A. Burkert, J. König, C. Eigenbrod: 2D-fast-scan cool-flame diagnostic using formaldehyde-LIF excited by XeF excimer laser radiation. In: *Proc. Joint Meeting of the British German and French sections of the Combustion Institute Nancy* (The Combustion Institute, Nancy 1999) pp. 485–487
20.146 S. Böckle, J. Kazenwadel, T. Kunzelmann, D.-I. Shin, C. Schulz: Single-shot laser-induced fluorescence imaging of formaldehyde with XeF excimer excitation, Appl. Phys. B **70**, 733–735 (2000)
20.147 J. Weickert: *Anisotropic Diffusion in Image Processing* (Teubner, Stuttgart 1998)
20.148 H. Scharr, B. Jähne, S. Böckle, J. Kazenwadel, T. Kunzelmann: Flame front analysis in turbulent combustion. In: *22. DAGM Symposium* (Deutsche Arbeitsgemeinschaft Mustererkennung, Kiel 2000) pp. 325–332
20.149 N. Fricker, W. Leuckel: The characteristics of swirl-stabilized natural gas flames. Part 3: the effect of swirl and burner mouth geometry on flame stability, J. Inst. Fuel **49**, 152–158 (1976)
20.150 T. Dreier, A. Dreizler, J. Wolfrum: The application of a Raman-shifted tunable KrF excimer laser for laser-induced fluorescence combustion diagnostics, Appl. Phys. B **55**, 381–387 (1992)
20.151 W. Ketterle, M. Schäfer, A. Arnold, J. Wolfrum: 2D single shot imaging of OH radicals using tunable excimer lasers, Appl. Phys. B **54**, 109–112 (1992)
20.152 E.W. Kaiser, K. Marko, D. Klick, L. Rimai, C.C. Wang, B. Shirinzadeh, D. Zhou: Measurement of OH density profiles in atmospheric-pressure propane-air flames, Combust. Sci. Tech. **50**, 163–183 (1986)
20.153 C. Schulz, V. Sick, U. Meier, J. Heinze, W. Stricker: Quantification of NO A-X(0,2) LIF: Investigation of calibration and collisional influences in high-pressure flames, Appl. Opt. **38**, 434–1443 (1999)
20.154 B. Yip, D.C. Fourguette, M.B. Long: Three-dimensional gas concentration and gradient measurements in a photoacoustically perturbed jet, Appl. Opt. **25**, 3919–3923 (1986)
20.155 J.H. Frank, K.M. Lyons, M.B. Long: Technique for three-dimensional measurements of the time development of turbulent flames, Opt. Lett. **16**, 958–960 (1991)
20.156 J. Nygren, J. Hult, M. Richter, M. Aldén, M. Christensen, A. Hultqvist, B. Johansson: Three-dimensional laser induced fluorescence of fuel distributions in an HCCI engine, Proc. Combust. Inst. **29**, 679–685 (2002)
20.157 A. Hoffmann, F. Zimmermann, H. Scharr, S. Krömker, C. Schulz: Instantaneous three-dimensional visualization of concentration distributions in turbulent flows with crossed-plane laser-induced fluorescence imaging, Appl. Phys. B **80**, 125–131 (2005)
20.158 S.S. Sattler, F.C. Gouldin, N.T. Boertlein: Combined crossed-plane imaging and stereo-particle image velocimetry. In: *Third Joint Meeting of the U.S. Sections of the Combustion Institute* (The Combustion Institute, Chicago 2003)
20.159 D.A. Knaus, F.C. Gouldin: Measurement of flamelet orientations in premixed flames with positive and negative Markstein numbers, Proc. Combust. Inst. **28**, 367–373 (2000)
20.160 D.A. Knaus, F.C. Gouldin, D.C. Bingham: Assessment of crossed-plane tomography for flamelet surface normal measurements, Combust. Sci. Technol. **174**, 101–134 (2002)
20.161 A. Hoffmann, F. Zimmermann, and C. Schulz: Instantaneous three-dimensional visualization of concentration distributions in turbulent flows with a single laser. In: *First International Conference on Optical and Laser Diagnostics* (London, 2002), in press
20.162 A. Karpetis, R. Barlow: Measurements of flame orintation and scalar dissipation in turbulent hydrocarbon flames. In: *Third Joint Meeting of the U.S. Sections of The Combustion Institute* (The Combustion Institute, Chicago 2003)
20.163 C. Dartu: *Visualization of Volumetric Datasets* (Universität Heidelberg, Heidelberg 2001)
20.164 C. Kaminski, J. Hult, M. Aldén, S. Lindenmaier, A. Dreizler, U. Maas, M. Baum: Spark ignition of turbulent methane/air mixtures revealed by time resolved laser induced fluorescence and direct numerical simulations, Proc. Combust. Inst. **28**, 399–405 (2000)
20.165 A. Dreizler, S. Lindenmaier, U. Maas, J. Hult, M. Aldén, C.F. Kaminski: Characterisation of a spark ignition system by planar laser-induced fluorescence of OH at high repetition rates and comparisons with chemical kinetics calculations, Appl. Phys. B **70**, 287–294 (2000)
20.166 R.B. Williams, P. Ewart, A. Dreizler: Velocimetry of gas flows using degeneratre four-wave mixing, Opt. Lett. **19**, 1486–1488 (1994)
20.167 R.W. Pitz, J.A. Wehrmeyer, L.A. Ribarov, D.A. Oguss, F. Batliwala, P.A. DeBarber, S. Deutsch, P.E. Dimotakis: Unseeded molecular flow tagging in cold and hot flows using ozone and hydroxyl tagging velocimetry, Meas. Sci. Technol. **11**, 1259–1271 (2000)
20.168 R. Miles, C. Cohen, J. Conners, P. Howard, S. Huang, E. Markovitz, G. Russell: Velocity measurements by vibrational tagging and fluorescent probing of oxygen, Opt. Lett. **12**, 861 (1987)
20.169 R.B. Miles, W. Lempert, B. Zhang: Turbulence structure measurement by RELIEF flow tagging, Fluid. Dyn. Res. **8**, 9–17 (1991)

20.170 S. Krüger, G. Grünefeld: Gas-phase velocity field measurements in dense sprays by laser-based flow tagging, Appl. Phys. B **70**, 463–466 (2000)
20.171 T. Elenbaas, N.M. Sijtsema, R.A.L. Tolboom, N.J. Dam, W. van de Water, J.J. ter Meulen: *Characterization of turbulence by air photolysis and recombination tracking (APART)*, AIAA 2002-0694 (American Institute of Aeronautics and Astronautics, Inc., 2002)
20.172 I. Düwel, P. Peuser, P. Zeller, J. Wolfrum, C. Schulz: Laser-based spray diagnostics in commercial fuels using a new all-solid-state laser system. In: *ILASS Europe* (Nottingham 2004)
20.173 G. Josefsson, I. Magnusson, F. Hildenbrand, C. Schulz, V. Sick: Multidimensional laser diagnostic and numerical analysis of NO formation in a gasoline engine, Proc. Combust. Inst. **27**, 2085–2092 (1998)
20.174 W.G. Bessler, M. Hofmann, F. Zimmermann, G. Suck, J. Jakobs, S. Nicklitzsch, T. Lee, J. Wolfrum, C. Schulz: Quantitative in-cylinder NO-LIF imaging in a realistic gasoline engine with spray-guided direct injection, Proc. Combust. Inst. **30**, 2667–2674 (2005)
20.175 M.J. Hall, P. Zuzek, R.W. Anderson: Fiber optic sensor for crank angle resolved measurements of burned gas residual fraction in the cylinder of an SI engine, SAE Techn. Paper Ser. 2001-01-1921 (2001)
20.176 R. Reichle, C. Pruss, W. Osten, H.J. Tiziani, F. Zimmermann, C. Schulz: Acquisition of combustion parameters close to the ignition spark with a fiber optic sensor. In: *Optical measurement systems for industrial inspection IV*, Vol. 5856, ed. by W. Osten, C. Gorecki, E.L. Novak (SPIE-The International Society for Optical Engineering, Bellingham, WA 2005) pp. 158–168
20.177 M. Richter, B. Axelsson, M. Aldén: Engine diagnostics using laser-induced fluorescence signals collected through an endoscopic detection system, SAE Techn. Paper Ser. 982465 (1998)
20.178 H. Neij, M. Aldén: Application of two-photon laser-induced fluorescence for visualization of water vapor on combustion environments, Appl. Opt. **33**, 6514–6523 (1994)
20.179 W.G. Bessler, C. Schulz, T. Lee, J.B. Jeffries, R.K. Hanson: Carbon dioxide UV laser-induced fluorescence in high-pressure flames, Chem. Phys. Lett. **375**, 344–349 (2003)
20.180 A.A. Roller, M. Decker, V. Sick, J. Wolfrum, W. Hentschel, K.-P. Schindler: Non-Intrusive temperature measurements during the compression phase of a DI Diesel engine, SAE Techn. Paper Ser. 952461 (1995)
20.181 M.C. Drake, T.D. Fransler, D.T. French: Crevice flow and combustion visualization in a direct-injection spark-ignition engine using laser imaging techniques, SAE Techn. Paper Ser. 952454 (1995)
20.182 J.E. Dec, J.O. Keller: High speed thermometry using two-line atomic fluorescence, Proc. Combust. Inst. **21**, 1737–1745 (1986)
20.183 C.F. Kaminski, J. Engström, M. Aldén: Quasi-instantaneous two-dimensional temperature measurements in a spark ignition enginge using two-line atomic fluorescence, Proc. Combust. Inst. **27**, 85–93 (1998)
20.184 B.K. McMillin, J.L. Palmer, R.K. Hanson: Temporally resolved, two-line fluorescence imaging of NO temperature in a transverse jet in a supersonic cross flow, Appl. Opt. **32**, 7532–7545 (1993)
20.185 W.G. Bessler, C. Schulz: Quantitative multi-line NO-LIF temperature imaging, Appl. Phys. B **78**, 519–533 (2004)
20.186 W.G. Bessler, C. Schulz, T. Lee, J.B. Jeffries, R.K. Hanson: Strategies for laser-induced fluorescence detection of nitric oxide in high-pressure flames: III. Comparison of A-X strategies, Appl. Opt. **42**, 4922–4936 (2003)
20.187 C. Orlemann, C. Schulz, J. Wolfrum: NO-flow tagging by photodissociation of NO_2. A new approach for measuring small-scale flow structures, Chem. Phys. Lett. **307**, 15–20 (1999)
20.188 N. Dam, R.J.H. Klein-Douwel, N. Sijstema, J. ter Meulen: Nitirc oxide flow tagging in unseeded air, Opt. Lett. **26**, 36–38 (2001)
20.189 M.P. Lee, R.K. Hanson: Calculations of O_2 absorption and fluorescence at elevated temperatures for a broadband argon-fluoride laser source at 193 nm, J. Quant. Spectros. Radiat. Transfer **36**, 425–440 (1986)
20.190 B. Hiller, R. Hanson: Properties of the iodine molecule relevant to laser-induced fluorescence experiments in gaseous flows, Exp. Fluids **10**, 1–11 (1990)
20.191 K. Greenough, A. Duncan: The fluorescence of sulfur dioxide, J. Am. Chem. Soc. **83**, 555–560 (1961)
20.192 H. Mettee: Fluorescence and phosphorescence of SO_2 vapor, J. Chem. Phys. **49**, 1784–1793 (1968)
20.193 S.J. Strickler, D. Howell: Luminescence and radiations transitions in sulfur dioxide gas, J. Chem. Phys. **49**, 1947–1951 (1968)
20.194 V. Sick: Exhaust-gas imaging via planar laser-induced fluorescence of sulfur dioxide, Appl. Phys. B **74**, 461–463 (2002)
20.195 T. Rao, S. Collier, J. Calvert: Primary photophysical processes in the photochemistry of sulfur dioxide at 2875 Å, J. Am. Chem. Soc. **91**, 1609–1615 (1969)
20.196 T. Rao, S. Collier, J.G. Calvert: The quenching reactions of the first excited singlet and triplet states of sulfur dioxide with oxygen and carbon dioxide, J. Am. Chem. Soc. **91**, 1616–1621 (1969)
20.197 R. Caton, A. Duncan: Lifetime of the lowest triplet state of sulfur dioxide, J. Am. Chem. Soc. **90**, 1945–1949 (1968)
20.198 A. Lozano: *Laser-excited luminescent tracers for planar concentration measurements in gaseous*

jets, Ph.D. Thesis (Stanford University, Stanford 1992)

20.199 H. Krämer, S. Einecke, C. Schulz, V. Sick, S.R. Nattrass, J.S. Kitching: Simultaneous mapping of the distribution of different fuel volatility classes using tracer-LIF and NIR tomography in an IC engine, SAE Transactions, J. Fuels Lubricants **107**, 1048–1059 (1998)

20.200 D. Han, R.R. Steeper: An LIF equivalence ratio imaging technique for multicomponent fuels in an IC engine, Proc. Combust. Inst **29**, 727–734 (2002)

20.201 M.-T. Lin, V. Sick: Mixture evaporation characteristics prediction for LIF measurements using PSRK (Predictive Soave-Redlich-Kwong) equation of state, SAE Transactions, J. Fuels Lubricants **111**, 1490–1499 (2002)

20.202 M.-T. Lin, V. Sick: Is toluene a suitable LIF tracer for fuel film measurements?, SAE Techn. Paper Ser. 2004-01-1355 (2004)

20.203 J. F. Le Coz, C. Catalano, T. Baritaud: Application of laser-induced fluorescence for measuring the thickness of liquid films on transparent walls. In: *7th International Symposium on Applications of Laser Techniques to Fluid Mechanics II* (Lisbon 1994)

20.204 T. Fansler, D. French, M.C. Drake: Fuel Distributions in a Firing Direct-injection Spark-ignition Engine Using Laser-Induced Fluorescence Imaging, SAE Techn. Paper Ser. 950110 (1995)

20.205 D. A. Greenhalgh, D. F. Bryce, R. D. Lockett, and S. C. Harding: Development of planar laser induced fluorescence for fuel: Application to gas turbine combustion. In: *AGARD PEP Symposium on Advanced non-intrusive instrumentation for propulsion engines* (Brussels 1997)

20.206 W. Hentschel, B. Block, T. Hovestadt, H. Meyer, G. Ohmstede, V. Richter, B. Stiebels, A. Winkler: Optical diagnostics and CFD-simulations to support the combustion process development of the Volkswagen FSI direct injection gasoline engine, SAE Techn. Paper Ser. 2001-01-3648 (2001)

20.207 J. Reboux, D. Puecheberty: A new approach of PLIF applied to fuel/air ratio measurement in the compressive stroke of an optical SI engine, SAE Techn. Paper Ser. 941988 (1994)

20.208 W. Koban, J.D. Koch, R.K. Hanson, C. Schulz: Oxygen quenching of toluene fluorescence at elevated temperatures, Appl. Phys. B **80**, 777–784 (2005)

20.209 W. Koban, J.D. Koch, V. Sick, N. Wermuth, R.K. Hanson, C. Schulz: Predicting LIF signal strength for toluene and 3-pentanone under engine-related temperature and pressure conditions, Proc. Combust. Inst. **30**, 1545–1553 (2005)

20.210 S.A. Kaiser, M.B. Long: The effect of temperature and quenching on laser-induced fluorescence of naphtalenes as JP-8 tracers. In: *Chemical and Physical Processes in Combustion – Technical Meeting of the Eastern States Section of the Combustion Institute* (Pennsylvania State University, University Park 2003)

20.211 L.A. Melton: Spectrally separated fluorescence emissions for Diesel fuel droplets and vapor, Appl. Opt. **22**, 2224–2226 (1983)

20.212 A. Lozano, B. Yip, R.K. Hanson: Acetone: A tracer for concentration measurements in gaseous flows by planar laser-induced fluorescence, Exp. Fluids **13**, 369–376 (1992)

20.213 F. Großmann, P.B. Monkhouse, M. Ridder, V. Sick, J. Wolfrum: Temperature and pressure dependences of the laser-induced fluorescence of gas-phase acetone and 3-pentanone, Appl. Phys. B **62**, 249–253 (1996)

20.214 L. Yuen, J. Peters, R. Lucht: Pressure dependence of laser-induced fluorescence from acetone, Appl. Opt. **36**, 3271–3277 (1997)

20.215 F. Ossler, M. Alden: Measurements of picosecond laser-induced fluorescence from gas-phase 3-pentanone and acetone: Implications to combustion diagnostics, Appl. Phys. B **64**, 493–502 (1997)

20.216 J.D. Koch, R.K. Hanson: Temperature and excitation wavelength dependencies of 3-pentanone absorption and fluorescence for PLIF applications, Appl. Phys. B **76**, 319–324 (2003)

20.217 J.B. Gandhi, P.G. Felton: On the fluorescent behavior of ketones at high temperatures, Exp. Fluids **21**, 143–144 (1996)

20.218 J.D. Koch, R.K. Hanson: Ketone photophysics for quantitative PLIF imaging, AIAA paper 2001-0413 (2001)

20.219 N.P. Tait, D.A. Greenhalgh: 2D laser induced fluorescence imaging of parent fuel fraction in nonpremixed combustion, Proc. Combust. Inst. **24**, 1621–1628 (1992)

20.220 D. Wolff, H. Schlüter, V. Beushausen, P. Andresen: Quantitative determination of fule air mixture distributions in an internal combustion engine using PLIF of acetone, Ber. Bunsenges. Phys. Chem. **97**, 1738–1741 (1993)

20.221 M. Berckmuller, N. Tait, R. Lockett, D. Greenhalgh: In-cylinder crank-angle-resolved imaging of fuel concentration in a firing spark-ignition engine using planar laser-induced fluorescence, Proc. Combust. Inst. **25**, 151–156 (1994)

20.222 M. Dawson, S. Hochgreb: Liquid Fuel Visualization Using Laser-Induced Fluorescence During Cold Start, SAE Techn. Paper Ser. 982466 (1998)

20.223 R.M. Green, L.D. Cloutman: Planar LIF observations of unburned fuel escaping the upper ring-land crevice in an SI engine, SAE Techn. Paper Ser. 970823 (1997)

20.224 R. Bryant, J.F. Driscoll: Acetone laser induced fluorescence for low pressure, low temperature flow visualization, Exp. Fluids **28**, 417–476 (2000)

20.225 H. Neij, B. Johansson, M. Aldén: Development and demonstration of 2D-LIF for studies of mixture

preparation in SI engines, Combust. Flame **99**, 449–457 (1994)
20.226 A. Arnold, A. Buschmann, B. Cousyn, M. Decker, V. Sick, F. Vannobel, J. Wolfrum: Simultaneous imaging of fuel and hydroxyl radicals in an in-line four cylinder SI engine, SAE Trans. **102**, 1–9 (1993)
20.227 A. Arnold, H. Becker, R. Suntz, P. Monkhouse, J. Wolfrum, R. Maly, W. Pfister: Flame front imaging in an internal-combustion engine simulator by laser-induced fluorescence of acetaldehyde, Opt. Lett. **15**, 831–833 (1990)
20.228 J.C. Swindal, D.P. Dragonetti, R.T. Hahn, P.A. Furman, W.P. Acker: In-cylinder charge homogeneity during cold-start studied with fluorescent tracers simulating different fuel distillation temperatures, SAE Techn. Paper Ser. 950106 (1995)
20.229 D.A. Hansen, E.K.C. Lee: Radiative and nonradiative transitions in the first excited singlet state of simple linear aldehydes, J. Chem. Phys. **62**, 3272–3277 (1975)
20.230 D.A. Hansen, E.K. Lee: Radiative and nonradiative transistions in the first excited singlet state of symmetrical methyl-substituted acetones, J. Chem. Phys. **62**, 183–189 (1975)
20.231 A. Gandini, K. Kutschke: Primary process in photolysis of hexafluoroacetone vapour, 2. Fluorescence and phosphorescence, Proc. R. Soc. London Ser. A **306**, 511 (1968)
20.232 A. Gandini, K.O. Kutschke: The effect of mercury on the triplet state of hexafluoroacetone, Ber. Bunsenges. Phys. Chem **72**, 296–301 (1968)
20.233 H. Okabe, W.A. Noyes: The relative intensities of fluorescence and phosphorescence in biacetyl vapor, J. Am. Chem. Soc. **79**, 810–806 (1957)
20.234 H.W. Sidebottom, C.C. Badcock, J.G. Calvert, B.R. Rabe, E.K. Damon: Lifetime studies of the biacetyl excited singlet and triplet states in the gas phase at 25°C, J. Am. Chem. Soc. **94**, 13–19 (1972)
20.235 J.B. Liu, Q. Pan, C.S. Liu, J.R. Shi: Principles of flow field diagnostics by laser-induced biacetyl phosphorescence, Exp. Fluids **6**, 505–513 (1988)
20.236 P. Pringsheim: *Fluorescence and Phosphorescence* (Interscience, New York 1949)
20.237 T. Itoh, A. Kakuho, H. Hishinuma, T. Urushihara, Y. Takagi, K. Horie, M. Asano, E. Ogata, T. Yamashita: *Development of a New Compound Fuel and Fluorescent Tracer Combination for Use with Laser Induced Fluorescence* (Nissan Motor Co./University of Tokyo, Tokyo 1995)
20.238 P.G. Felton, F.V. Bracco, M.E.A. Bardsley: On the quantitative application of exciplex fluorescence to engine sprays, SAE Techn. Paper Ser. 930870 (1993)
20.239 A.P. Fröba, F. Rabenstein, K.U. Münch, A. Leipertz: Mixture of triethylamine and benzene as a new seeding material for the quantitative two-dimensional laser-induced exciplex fluorescence imaging of vapor and liquid fuel inside SI engines, Combust. Flame **112**, 199–209 (1998)
20.240 J.B. Ghandhi, P.G. Felton, D.F. Gajdezko, F.V. Bracco: Investigation of the fuel distribution in a two-stroke engine with an air-assisted injector, SAE Techn. Paper Ser. 940394 (1994)
20.241 M. Richter, B. Axelsson, K. Nyholm, M. Aldén: Real-time calibration of planar laser-induced fluorescence air-fuel ratio measurements in combustion environments using in situ Raman scattering, Proc. Combust. Inst **27**, 51–57 (1998)
20.242 D. Frieden, V. Sick, J. Gronki, C. Schulz: Quantitative oxygen imaging in an engine, Appl. Phys. B **75**, 137–141 (2002)
20.243 J.C. Sacadura, L. Robin, F. Dionnet, D. Gervais, P. Gastaldi, A. Ahmed: Experimental investigation of an optical direct injection SI engine using FARLIF, SAE Techn. Paper Ser. 2000-01-1794 (2000)
20.244 W. Koban, J.D. Koch, R.K. Hanson, C. Schulz: Absorption and fluorescence of toluene vapor at elevated temperatures, Phys. Chem. Chem. Phys. **6**, 2940–2945 (2004)
20.245 W. Koban, J.D. Koch, V. Sick, N. Wermuth, R.K. Hanson, C. Schulz: Predicting LIF signal strength for toluene and 3-pentanone under engine-related temperature and pressure conditions, Proc. Combust. Inst. **30**, 1545–1553 (2005)
20.246 W. Koban, C. Schulz: Toluene as a tracer for fuel, temperature and oxygen concentrations, SAE Techn. Paper Ser. 2005-01-2091 (2005)
20.247 M. Schütte, H. Finke, G. Grünefeld, S. Krüger, P. Andresen, B. Stiebels, B. Block, H. Meyer, W. Hentschel: Spatially resolved air/fuel ratio and residual gas measurements by sponaneous Raman scattering in a firing direct injection fasoline engine, SAE Techn. Paper Ser. 2000-01-1795 (2000)
20.248 B. Mewes, G. Bauer, D. Brüggemann: Fuel vapor measurements by linear Raman spectroscopy using spectral discriminattion from droplet interferences, Appl. Opt. **38**, 1040–1045 (1999)
20.249 G. Grünefeld, V. Beushausen, P. Andresen, W. Hentschel: Spatially resolved Raman scattering for multi-species and temperature analysis in technically applied combustion systems: Spray flame and four-cylinder in-line engine, Appl. Phys. B. **58**, 333–342 (1994)
20.250 R. A. L. Tolboom, N. M. Sijtsema, N. J. Dam, J. J. t. Meulen, J. M. Mooij, J. D. M. Maassen: 2D stoichiometries from snapshot Raman measurements, in 40th AIAA Aerospace Sciences Meeting. AIAA paper 2002-0400
20.251 D.C. Kyritsis, P.G. Felton, F.V. Bracco: On the feasibility of quantitative, single-shot, spontaneous Raman imaging in an optically accessible engine cylinder, SAE Techn. Paper Ser. 1999-01-3537 (1999)
20.252 D. Geyer: 1D Raman/Rayleigh experiments in a turbulent opposed jet, PhD Thesis (TU Darmstadt, Darmstadt 2004)
20.253 C. Schulz, V. Sick, J. Wolfrum, V. Drewes, M. Zahn, R. Maly: Quantitative 2D single-shot imaging of

NO concentrations and temperatures in a transparent SI engine, Proc. Combust. Inst. **26**, 2597–2604 (1996)
20.254 J. Engström, J. Nygren, M. Aldén, C.F. Kaminski: Two-line atomic fluorescence as a temperature probe for highly sooting flames, Opt. Lett. **25**, 1469–1471 (2000)
20.255 A. Arnold, B. Lange, T. Bouché, Z. Heitzmann, G. Schiff, W. Ketterle, P. Monkhouse, J. Wolfrum: Absolute temperature fields in flames by 2D-LIF of OH using excimer lasers and CARS spectroscopy, Ber. Bunsenges. Phys. Chem. **96**, 1388–1392 (1992)
20.256 M.C. Thurber, F. Griseh, R.K. Hanson: Temperature imaging with single- and dual wavelength acetone planar laser-induced fluorescence, Opt. Lett. **22**, 251–253 (1997)
20.257 N.P. Tait, D.A. Greenhalgh: PLIF imaging of fuel fraction in practical devices and LII imaging of soot, Ber. Bunsenges. Phys. Chem. **97**, 1619–1625 (1993)
20.258 J. Kazenwadel, W. Koban, T. Kunzelmann, C. Schulz: Fluorescence imaging of natural gas/air mixing without tracers added, Chem. Phys. Lett. **345**, 259–264 (2001)
20.259 W. Koban, C. Schulz: FAR-LIF: Myth and Reality. In: *European Combustion Meeting* (The Combustion Institute, Louvain-la-Neuve 2005)
20.260 K. Kikuchi, C. Sato, M. Watabe, H. Ikeda, Y. Takahashi, T. Miyashi: New aspects on fluorescence quenching by molecular oxygen, J. Am. Chem. Soc. **115**, 5180–5184 (1993)
20.261 C. Schulz, J.B. Jeffries, D.F. Davidson, J.D. Koch, J. Wolfrum, R.K. Hanson: Impact of UV absorption by CO_2 and H_2O on NO LIF in high-pressure combustion applications, Proc. Combust. Inst. **29**, 2725–2742 (2002)
20.262 C.T. Bowman: Control of combustion-generated nitrogen oxide emissions: Technology driven by regulation, Proc. Combust. Inst. **24**, 859–878 (1994)
20.263 A.M. Wodtke, M. Huwel, H. Schlüter, G. Meijer, P. Andresen, H. Voges: High-sensitivity detection of NO in a flame using a tunable ArF laser, Opt. Lett. **13**, 910–912 (1988)
20.264 C. Schulz, B. Yip, V. Sick, J. Wolfrum: A laser-induced fluorescence scheme for imaging nitric oxide in engines, Chem. Phys. Lett. **242**, 259–264 (1995)
20.265 M.D. DiRosa, K.G. Klavuhn, R.K. Hanson: LIF spectroscopy of NO and O_2 in high-pressure flames, Comb. Sci. Tech. **118**, 257–283 (1996)
20.266 W.P. Partridge Jr., M.S. Klassen, D.D. Thomsen, N.M. Laurendeau: Experimental assessment of O_2 interferences on laser-induced fluorescence measurements of NO in high-pressure, lean premixed flames by use of narrow-band and broadband detection, Appl. Opt. **34**, 4890–4904 (1996)
20.267 P. Jamette, P. Desgroux, V. Ricordeau, B. Deschamps: Laser-induced fluorescence detection of NO in the combustion chamber of an optical GDI engine with A-X(0,1) excitation, SAE Techn. Paper Ser. 2001-01-1926 (2001)
20.268 W.G. Bessler, C. Schulz, T. Lee, J.B. Jeffries, R.K. Hanson: Laser-induced-fluorescence detection of nitric oxide in high-pressure flames with A-X(0,1) excitation. In: *Proc. Western States Section of the Combustion Institute Spring Meeting* (The Combustion Institute, Oakland 2001)
20.269 C. Schulz, J.D. Koch, D.F. Davidson, J.B. Jeffries, R.K. Hanson: Ultraviolet absorption spectra of shock-heated carbon dioxide and water between 900 and 3050 K, Chem. Phys. Lett. **355**, 82–88 (2002)
20.270 F. Hildenbrand, C. Schulz: Measurements and simulation of in-cylinder UV-absorption in spark ignition and Diesel engines, Appl. Phys. B **73**, 165–172 (2001)
20.271 A.O. Vyrodow, J. Heinze, M. Dillmann, U.E. Meier, W. Stricker: Laser-induced fluorescence thermometry and concentration measurements on NO A-X (0,0) transitions in the exhaust gas of high pressure CH_4/air flames, Appl. Phys. B. **61**, 409–414 (1995)
20.272 A. Bräumer, V. Sick, J. Wolfrum, V. Drewes, M. Zahn, R. Maly: Quantitative two-dimensional measurements of nitric oxide and temperature distributions in a transparent square piston SI engine, SAE Techn. Paper Ser. 952462 (1995)
20.273 J.B. Jeffries, C. Schulz, D.W. Mattison, M. Oehlschlaeger, W.G. Bessler, T. Lee, D.F. Davidson, R.K. Hanson: UV absorption of CO_2 for temperature diagnostics of hydrocarbon combustion applications, Proc. Combust. Inst. **30**, 1591–1599 (2005)
20.274 C. Schulz, V. Sick, J. Heinze, W. Stricker: Laser-induced fluorescence detection of nitric oxide in high-pressure flames using A-X(0,2) excitation, Appl. Opt. **36**, 3227–3232 (1997)
20.275 F. Hildenbrand, C. Schulz, M. Hartmann, F. Puchner, G. Wawrschin: In-cylinder NO-LIF imaging in a realistic GDI engine using KrF excimer laser excitation, SAE Techn. Paper Ser. 1999-01-3545 (1999)
20.276 M. Hofmann, H. Kronemayer, B.F. Kock, H. Jander, C. Schulz: Laser-induced incandescence and multi-line NO-LIF thermometry for soot diagnostics at high pressures. In: *European Combustion Meeting* (The Combustion Institute, Louvain-la-Neuve 2005)
20.277 W.G. Bessler, C. Schulz, T. Lee, D.I. Shin, M. Hofmann, J.B. Jeffries, J. Wolfrum, R.K. Hanson: Quantitative NO-LIF imaging in high-pressure flames, Appl. Phys. B **75**, 97–102 (2002)
20.278 T. Lee, W.G. Bessler, H. Kronemayer, C. Schulz, J.B. Jeffries, R.K. Hanson: Quantitative temperature measurements in high-pressure flames with multi-line nitric oxide (NO)-LIF thermometry. In: *4th Joint Meeting of the U.S. Sections of the Combustion Institute* (Drexel University, Philadelphia 2005)

20.279 W.G. Bessler, C. Schulz, T. Lee, J.B. Jeffries, R.K. Hanson: Strategies for laser-induced fluorescence detection of nitric oxide in high-pressure flames. I. A-X(0,0) excitation, Appl. Opt. **41**, 3547–3557 (2002)

20.280 W.G. Bessler, C. Schulz, T. Lee, J.B. Jeffries, R.K. Hanson: Strategies for laser-induced fluorescence detection of nitric oxide in high-pressure flames. II. A-X(0,1) excitation, Appl. Opt. **42**, 2031–2042 (2003)

20.281 W.G. Bessler, C. Schulz, V. Sick, J.W. Daily: A versatile modeling tool for nitric oxide LIF spectra. In: *3rd Joint Meeting of the US Sections of the Combustion Institute* (The Combustion Institute, Chicago 2003)

20.282 M. Tamura, J. Luque, J.E. Harrington, P.A. Berg, G.P. Smith, J.B. Jeffries, D.R. Crosley: Laser-induced fluorescence of seeded nitric oxide as a flame thermometer, Appl. Phys. B **66**, 503–510 (1998)

20.283 W. Bessler, F. Hildenbrand, C. Schulz: Vibrational temperature imaging using two-line laser-induced fluorescence of seeded NO. In: *Laser Applications to Chemical and environmental analysis*, OSA Technical Digest Series, Vol. 3 (Opt. Soc. Am., Washington 2000) pp. 149–151

20.284 R. Cattolica: OH rotational temperature from two-line laser-excited fluorescence, Appl. Opt. **20**, 1156–1166 (1981)

20.285 J.W. Daily, W.G. Bessler, C. Schulz, V. Sick: Role of non-stationary collisional dynamics in determining nitric oxide LIF spectra, AIAA 2004-0389 (2004)

20.286 T. Lee, W.G. Bessler, C. Schulz, M. Patel, J.B. Jeffries, R.K. Hanson: UV planar laser-induced fluorescence imaging of hot carbon dioxide in a high-pressure flame, Appl. Phys. B **79**, 427–430 (2004)

20.287 H. Kronemayer, W. Bessler, C. Schulz: Gas-phase temperature measurements in evaporating sprays and spray flames based on NO multiline LIF, Appl. Phys. B **81**, 1071–1074 (2005)

20.288 T. Lee, W.G. Bessler, H. Kronemayer, C. Schulz, J.B. Jeffries: Quantitative temperature measurements in high-pressure flames with multi-line nitric oxide (NO)-LIF thermometry, Appl. Opt. **31**, 6718–6728 (2005)

20.289 I. Düwel, H.-W. Ge, H. Kronemayer, R.W. Dibble: Experimental and numerical characterization of a turbulent spray flame, Proc. Combust. Inst. **31**, 2247–2255 (2007)

20.290 W.G. Bessler, C. Schulz, M. Hartmann, M. Schenk: Quantitative in-cylinder NO-LIF imaging in a direct-injected gasoline engine with exhaust gas recirculation, SAE Techn. Paper Ser. 2001-01-1978 (2001)

20.291 C. Schulz, J. Wolfrum, V. Sick: Comparative study of experimental and numerical NO profiles in SI combustion, Proc. Combust. Inst. **27**, 2077–2084 (1998)

20.292 F. Hildenbrand, C. Schulz, V. Sick, H. Jander, H.G. Wagner: Applicability of KrF excimer laser induced fluorescence in sooting high-pressure flames, in VDI Flammentag Dresden, VDI Berichte **1492**, 269–274 (1999)

20.293 F. Hildenbrand, C. Schulz, J. Wolfrum, F. Keller, E. Wagner: Laser diagnostic analysis of NO formation in a direct injection Diesel engine with pump-line nozzle and common-rail injection systems, Proc. Combust. Inst. **28**, 1137–1144 (2000)

20.294 F. Hildenbrand, C. Schulz, V. Sick, G. Josefsson, I. Magnusson, Ö. Andersson, M. Aldén: Laser spectroscopic invesitigation of flow fields and NO-formation in a realistic SI engine, SAE Techn. Paper Ser. 980148 (1998)

20.295 A. D'Alessio: Laser light scattering and fluorescence diagnostics of rich flames produced by gascons and liquid fuels. In: *Particulate carbon: Formation during combustion*, ed. by D.C. Siegla, G.W. Smith (Plenum, New York 1981) p. 207

20.296 R.W. Weeks, W.W. Duley: Aerosol-particle sizes from light emission during excitation by TEA CO_2 laser pulses, J. Appl. Phys **45**, 4661–4662 (1973)

20.297 A.C. Eckbreth: Effects of laser-modulated particle incandescence on Raman scattering diagnostics, J. Appl. Phys. **48**, 4473–4479 (1977)

20.298 L.A. Melton: Soot diagnostics based on laser heating, Appl. Opt. **23**, 2201–2208 (1984)

20.299 T. Ni, J.A. Pinson, S. Gupta, R.J. Santoro: Two-dimensional imaging of soot volume fraction by the use of laser-induced incandescence, Appl. Opt. **34**, 7083–7091 (1995)

20.300 D.J. Bryce, N. Ladommatos, H. Zhao: Quantitative investigation of soot distribution by laser-induced incandescence, Appl. Opt. **39**, 5012–5022 (2000)

20.301 C.R. Shaddix, K.C. Smyth: Laser-induced incandescence measurements of soot production in steady and flickering methane, propane, and ethylene diffusion flames, Combust. Flame **107**, 418–452 (1996)

20.302 P.O. Witze, S. Hochgreb, D. Kayes, H.A. Michelsen, C.R. Shaddix: Time-resolved laser-induced incandescence and laser elastic-scattering measurements in a propane diffusion flame, Appl. Opt. **40**, 2443–2452 (2001)

20.303 B. Quay, T.-W. Lee, T. Ni, R.J. Santoro: Spatially resolved measurements of soot volume fraction using laser-induced incandescence, Combust. Flame **97**, 384–392 (1994)

20.304 J. Appel, B. Jungfleisch, M. Marquardt, R. Suntz, H. Bockhorn: Assessment of soot volume fractions from laser-induced incandescence by comparison with extinction measurements in laminar, premixed, flat flames, Proc. Combust. Inst. **26**, 2387–2395 (1996)

20.305 B. Axelsson, R. Collin, P.-E. Bengtsson: Laser-induced incandescence for soot particle size and

volume fraction measurements using on-line extinction calibration, Appl. Phys. B **72**, 367–372 (2001)
20.306 H. Geitlinger, T. Streibel, R. Suntz, H. Bockhorn: Two-dimensional imaging of soot volume fractions; particle number densities; and particle radii in laminar and turbulent diffusion flames, Proc. Combust. Inst. **27**, 1613–1621 (1998)
20.307 T.R. Meyer, S. Roy, V.M. Belovich, E. Corporan, J.R. Gord: Simultaneous planar laser-induced incandescence, OH planar laser-induced fluorescence, and droplet Mie scattering in swirl-stabilized spray flames, Appl. Opt. **44**, 445–454 (2005)
20.308 H. Bockhorn, H. Geitlinger, B. Jungfleisch, T. Lehre, A. Schön, T. Streibel, R. Suntz: Progress in characterization of soot formation by optical methods, Phys. Chem. Chem. Phys. **4**, 3780–3793 (2002)
20.309 S. Will, S. Schraml, A. Leipertz: Comprehensive two-dimensional soot diagnostics based on laser-induced incandescence, Proc. Combust. Inst. **26**, 2277–2284 (1996)
20.310 S. Will, S. Schraml, K. Bader, A. Leipertz: Performance characteristics of soot primary particle size measurements by time-resolved laser-induced incandescence, Appl. Opt. **37**, 5647–5658 (1998)
20.311 B. Axelsson, R. Collin, P.-E. Bengtsson: Laser-induced incandescence for soot particle size measurements in premixed flat flames, Appl. Opt. **39**, 3683–3690 (2000)
20.312 T. Lehre, B. Jungfleisch, R. Suntz, H. Bockhorn: Size distributions of nanoscaled particles and gas temperatures from time-resolved laser-induced-incandescence measurements, Appl. Opt. **42**, 2021–2030 (2003)
20.313 D. Woiki, A. Giesen, P. Roth: Time-resolved laser-induced incandescence for soot particle sizing during acetylene pyrolysis behind shock waves, Proc. Combust. Inst. **28**, 2531–2537 (2000)
20.314 R.L. Vander Wal, T.M. Ticich, A.B. Stephens: Can soot primary particle size be determined using laser-induced incandescence?, Combust. Flame **116**, 291–296 (1999)
20.315 B.F. Kock, T. Eckhardt, P. Roth: In-cylinder sizing of Diesel particles by time-resolved laser-induced incandescence (TR-LII), Proc. Combust. Inst. **29**, 2775–2781 (2002)
20.316 D.R. Snelling, G.J. Smallwood, R.A. Sawchuk, W.S. Neill, D. Gareau, D.J. Clavel, W.L. Chippior, F. Liu, Ö.L. Gülder: In-situ real-time characterization of particulate emissions from a Diesel engine exhaust by laser-induced incandescence, SAE Techn. Paper Ser. 2000-01-1994 (2000)
20.317 S. Schraml, S. Will, A. Leipertz: Performance characteristics of TIRE-LII soot diagnostics in exhaust gases of Diesel engines, SAE Techn. Paper Ser. 2000-01-2002 (2000)
20.318 R.L. Vander Wal, T.M. Ticich, J.R. West Jr.: Laser-induced incandescence applied to metal nanostructures, Appl. Opt. **38**, 5867–5879 (1999)
20.319 B.F. Kock, C. Kayan, J. Knipping, H.R. Orthner, P. Roth: Comparison of LII and TEM sizing during synthesis of iron particle chains, Proc. Combust. Inst. **30**, 1689–1697 (2005)
20.320 T. Lehre, R. Suntz, H. Bockhorn: Time-resolved two-color LII: size distributions of nano-particles from gas-to-particle synthesis, Proc. Combust. Inst. **30**, 2585–2593 (2005)
20.321 R.L. Vander Wal: Laser-induced incandescence: Detection issues, Appl. Opt. **35**, 6548–6559 (1996)
20.322 B. Mewes, J.M. Seitzman: Soot volume fraction and particle size measurements with laser-induced incandescence, Appl. Opt. **36**, 709–717 (1997)
20.323 M. Hofmann, W.G. Bessler, C. Schulz, H. Jander: Laser-induced incandescence (LII) for soot diagnostics at high pressure, Appl. Opt. **42**, 2052–2062 (2003)
20.324 P.-E. Bengtsson, M. Aldén: Soot-visualization strategies using laser techniques, Appl. Phys. B **60**, 51–59 (1995)
20.325 C. Schoemaecker Moreau, E. Therssen, X. Mercier, J.F. Pauwels, P. Desgroux: Two-color laser-induced incandescence and cavity ring-down spectroscopy for sensitive and quantitative imaging of soot and PAHs in flames, Appl. Phys. B **78**, 485–492 (2004)
20.326 K.C. Smyth, C.R. Shaddix: The elusive history of m = 1.57 – 0.56i for the refractive index of soot, Combust. Flame **107**, 314–320 (1996)
20.327 D.R. Snelling, G.J. Smallwood, F. Liu, Ö.L. Gülder, W.D. Bachalo: A calibration-independent LII technique for soot measurement by detecting abolute light intensity, Appl. Opt. **44**, 6773–6785 (2005)
20.328 C. Schulz, B.F. Kock, M. Hofmann, H.A. Michelsen, S. Will, B. Bongie, R. Suntz, G. Smallwood: Laser-induced incandescence: Recent trends and current questions, Appl. Phys. B **83**, 333–354 (2006)
20.329 D. R. Snelling, F. Liu, G. J. Smallwood, L. Ö. Gülder: Evaluation of the nanoscale heat and mass transfer model of LII: Prediction of the excitation intensity. In: 34th National Heat Transfer Conference (Pittsburgh 2000)
20.330 B.F. Kock, B. Tribalet, C. Schulz, P. Roth: Two-color time-resolved LII applied to soot particle sizing in the cylinder of a Diesel engine, Combust. Flame **147**, 79–92 (2006)
20.331 D.L. Hofeldt: Real-time soot concentration measurement technique for engine exhaust streams, SAE Techn. Paper Ser. 930079 (1993)
20.332 H. Bladh, P.-E. Bengtsson: Characteristics of laser-induced incandescence from soot in studies of a time-dependent heat and mass-transfer model, Appl. Phys. B **78**, 241–248 (2004)
20.333 H.A. Michelsen: Understanding and predicting the temporal response of laser-induced incandescence

from carbonaceous particles, J. Chem. Phys. **118**, 7012–7045 (2003)
20.334 D.R. Snelling, F. Liu, G.J. Smallwood, L. Ö. Gülder: Determination of the soot absorption function and thermal accomodation coefficient using low-fluence LII in a laminar coflow ethylene diffusion flame, Combust. Flame **136**, 180–190 (2004)
20.335 H.A. Michelsen, F. Lin, B.F. Kock, H. Bladh, A. Boiarcinc, M. Charwoth, T. Dreier, R. Hadef, M. Hofmann, J. Reimann, S. Will, P.-E. Bengtsson, H. Bockhorn, F. Foncher, K.-P. Geigle, C. Mounaïm-Rousselle, C. Schulz, R. Stirn, B. Tribalet, S. Suntz: Modeling laser-induced incandescence of soot: A summary and comparison of LII models, Appl. Phys. B **87**, 503–521 (2007)
20.336 M. Hofmann, B. Kock, C. Schulz: A web-based interface for modeling laser-induced incandescence (LIISim). In: Proceedings of the European Combustion Meeting, Chania, Greece, 2007 The Combustion Institute
20.337 R.W. Dibble, R.E. Hollenbach: Laser Rayleigh thermometry in turbulent flames, Proc. Combust. Inst. **18**, 1489–1499 (1981)
20.338 C. Espey, J.E. Dec, T.A. Litzinger, D.A. Santavicca: Planar laser Rayleigh scattering for quantitative vapor-fuel imaging in a Diesel jet, Combust. Flame **109**, 65–86 (1997)
20.339 Ö. Andersson, R. Collin, M. Aldén, R. Egnell: Quantitative imaging of equivalence ratios in DME sprays using a chemically preheated combustion vessel, SAE Techn. Paper Ser. 2000-01-2785 (2000)
20.340 C. Schulz, J. Gronki, S. Andersson: Multi-species laser-based imaging measurements in a Diesel spray, SAE Techn. Paper Ser. 2004-01-1917 (2004)
20.341 S. Vogel, C. Hasse, J. Gronki, S. Andersson, N. Peters, J. Wolfrum, C. Schulz: Numerical simulation and laser-based imaging of mixture formation, ignition and soot formation in a Diesel spray, Proc. Combust. Inst. **30**, 2029–2036 (2005)
20.342 A.I. Vogel: Physical properties and chemical constitution of aliphatic hydrocarbons, J. Chem. Soc. **9**, 133–142 (1946)
20.343 R.C. Weast: *Handbook of Chemistry and Physics*, 54th edn. (CRC, Cleveland 1973)
20.344 Landolt-Börnstein: *Eigenschaften der Materie in ihren Aggregatzuständen. Tabellen* (Springer, Berlin, Heidelberg 1962)
20.345 J.R. Partington: *An Advanced Treatise on Physical Chemistry*, Vol. 9 (Longmans, Green, London 1953)
20.346 W.C. Gardiner, Y. Hidaka, T. Tanzawa: Refractivity of combustion gases, Combust. Flame **40**, 213–219 (1981)
20.347 D. Hoffman, K.-U. Münch, A. Leipertz: Two-dimensional temperature determination in sooting flames by filtered Rayleigh scattering, Opt. Lett. **21**, 525–527 (1996)
20.348 F. Beyrau, A. Bruer, T. Seeger, A. Leipertz: Gas-phase temperature measurement in the vaporizing spray of a gasoline direct-injection injector by use of pure rotational coherent anti-Stokes Raman scattering, Opt. Lett. **29**, 247–249 (2004)
20.349 D. Klick, K.A. Marko, L. Rimai: Broadband single-pulse CARS spectra in a fired internal combustion engine, Appl. Opt. **20**, 1178–1185 (1981)
20.350 K. Kohse-Höinghaus, R.S. Barlow, M. Aldén, J. Wolfrum: Combustion at the focus: Laser diagnostics and control, in Proc. Combust. Inst. **30**, 89–123 (2005)
20.351 P.T. Moseley, J.O.W. Norris, D.E. Williams: *Techniques and Mechanisms in Gas Sensing* (Adam Hilger, New York 1991)
20.352 V. Ebert, J. Wolfrum: Absorption Spectroscopy. In: *Optical Measurements – Techniques and Applications*, 2nd edn., ed. by F. Mayinger, O. Feldmann (Springer, Berlin, Heidelberg 2001) pp. 227–266
20.353 G. Herzberg: *The Spectra and Structures of Simple Free Radicals: An Introduction to Molecular Spectroscopy* (Dover, New York 1988)
20.354 G. Herzberg: *Spectra of Diatomic Molecules*, Vol. I, 2nd edn. (Krieger, Malobar, FL 1989)
20.355 G. Herzberg: *Infrared and Raman Spectra of Polyatomic Molecules*, Vol. II (Krieger, Malobar, FL 1991)
20.356 G. Herzberg: *Electronic Spectra of Polyatomic Molecules*, Vol. III (Krieger, Malobar, FL 1991)
20.357 J. Wolfrum, T. Dreier, V. Ebert, C. Schulz: Laser-based combustion diagnostics. In: *Encyclopedia of Analytical Chemistry*, ed. by R.A. Meyers (Wiley, Chichester 2000) pp. 2118–2148
20.358 V. Ebert, R. Hemberger, W. Meienburg, J. Wolfrum: In-situ gas analysis with infrared lasers, Ber. Bunsenges. **97**, 1527–1534 (1993)
20.359 R. Villarreal, P. Varghese: Frequency-resolved absorption tomography with tunable diode lasers, Appl. Opt. **44**, 6786–6795 (2005)
20.360 V. Ebert, C. Schulz, H.R. Volpp, J. Wolfrum, P. Monkhouse: Laser diagnostics of combustion processes: from chemical dynamics to technical devices, Israel J. Chem. **39**, 1–24 (1999)
20.361 V. Ebert, J. Fitzer, I. Gerstenberg, K.U. Pleban, H. Pitz, J. Wolfrum, M. Jochem, J. Martin: Simultaneous laser-based in situ detection of oxygen and water in a waste incinerator for active combustion control purposes, Proc. Combust. Inst. **27**, 1301–1308 (1998)
20.362 V. Ebert, H. Teichert, P. Strauch, T. Kolb, H. Seifert, J. Wolfrum: High sensitivity in-situ CO-detection in a 3 MW_{th} rotary kiln for special waste incineration using new 2.3 µm distributed feedback diode lasers, Proc. Combust. Inst. **30**, 1611–1618 (2005)
20.363 H. Teichert, T. Fernholz, V. Ebert: Simultaneous in situ measurement of CO, H_2O, and gas temperatures in a full-sized coal-fired power plant by near-infrared diode lasers, Appl. Opt. **42**, 2043–2051 (2003)
20.364 V. Ebert, T. Fernholz, C. Giesemann, H. Pitz, H. Teichert, J. Wolfrum, H. Jaritz: Simultaneous

diode-laser-based in situ detection of multiple species and temperature in a gas-fired power plant, Proc. Combust. Inst. **28**, 423–430 (2000)
20.365 D.R. Herriott: Folded optical delay lines, Appl. Opt. **4**, 883–889 (1965)
20.366 D.R. Herriott, H. Kogelnik, R. Kompfner: Off-axis paths in spherical mirror interferometers, Appl. Opt. **3**, 523–526 (1964)
20.367 J.U. White: Long optical path of large aperture, J. Opt. Soc. Am. **32**, 285–288 (1942)
20.368 J. White: Very long optical path in air, J. Opt. Soc. Am. **66**, 411–416 (1976)
20.369 V. Ebert, H. Teichert, C. Giesemann, H. Saathoff, U. Schurath: Fibre-coupled in-situ laser absorption spectrometer for the selective detection of water vapor traces down to the ppb-level, Tech. Mess. **72**, 23–30 (2005)
20.370 W. Gurlit, R. Zimmermann, C. Giesemann, T. Fernholz, V. Ebert, J. Wolfrum, U. Platt, J.P. Burrows: Lightweight diode laser spectrometer CHILD (compact high-altitude in-situ laser diode) for balloon-borne measurements of water vapor and methane, Appl. Opt. **44**, 91–102 (2005)
20.371 H.E. Schlosser, J. Wolfrum, V. Ebert, B.A. Williams, R.S. Sheinson, J.W. Fleming: In situ determination of molecular oxygen concentrations in full-scale fire-suppression tests using tunable diode laser absorption spectroscopy, Proc. Combust. Inst. **29**, 353–360 (2002)
20.372 L.F. Mollenauer, J.C. White: *Tunable Lasers* (Springer, Berlin, Heidelberg 1987)
20.373 F.K. Kneubühl, M.W. Sigrist: *Laser* (Teubner, Stuttgart 1991)
20.374 L. Ajili, G. Scalari, D. Hofstetter, M. Beck, J. Faist, H. Beere, G. Davies, E. Linfield, D. Ritchie: Continuous-wave operation of far-infrared quantum cascade lasers, Electron. Lett. **38**, 1675–1676 (2002)
20.375 L. Ajili, J. Faist, H. Beere, D. Ritchie, G. Davies, E. Linfield: Loss-coupled distributed feedback far-infrared quantum cascade lasers, Electron. Lett. **41**, 419–420 (2005)
20.376 R. Köhler, A. Tredicucci, F. Beltram, H.E. Beere, E.H. Linfield, A.G. Davies, D.A. Ritchie, R.C. Iotti, F. Rossi: Terahertz semiconductor-heterostructure laser, Nature **417**, 156–159 (2002)
20.377 T. Tsuboi, N. Arimitsu, D. Ping, J.M. Hartmann: Light absorption by hydrocarbon molecules at 3.392 μm of He-Ne laser, Jpn. J. Appl. Phys. **24**, 8–13 (1985)
20.378 W.G. Mallard, W.C. Gardiner: Absorption of the 3.39 μm He-Ne laser line by methane from 300 to 2400 K, Quant. Spectrosc. Radiat. Transfer **20**, 135–149 (1978)
20.379 R.K. Mongia, E. Tomita, F.K. Hsu, L. Talbot, R.W. Dibble: Use of an optical probe for time-resolved in situ measurement of local air-to-fuel ratio and extent of fuel mixing with applicators to low NO_x emissions in premixed gas turbines, Proc. Combust. Inst. **26**, 2749–2755 (1996)
20.380 S.A. Trushin: Photoacoustic air pollution monitoring with an isotopic CO_2 laser, Ber. Bunsenges. Phys. Chem. Chem. Phys. **96**, 319–322 (1992)
20.381 P.K. Cheo, C. Zhiping, C. Li, Z. Yi: Applications of a tunable CO_2 sideband laser for high-resolution spectroscopic measurements of atmospheric gases, Appl. Opt. **32**, 836–841 (1993)
20.382 D.E. Cooper, T.F. Gallagher: Frequency modulation spectroscopy with a CO_2 laser: results and implications for ultrasensitive point monitoring of the atmosphere, Appl. Opt. **24**, 710–716 (1985)
20.383 W. Meienburg, H. Neckel, J. Wolfrum: In-situ measurement of ammonia concentration in industrial combustion systems, Proc. Combust. Inst. **23**, 231–236 (1990)
20.384 A. Arnold, H. Becker, R. Hemberger, W. Hentschel, W. Ketterle, M. Köllner, W. Meienburg, P. Monkhouse, H. Neckel, M. Schäfer, K.P. Schindler, V. Sick, R. Suntz, J. Wolfrum: Laser in-situ monitoring of combustion processes, Appl. Opt. **29**, 4860–4872 (1990)
20.385 R. Hemberger, S. Muris, K.U. Pleban, J. Wolfrum, I.S. Zaslonko, P. Kilpinen, A.E.J. Akanetuk: An experimental and modeling study of the selective noncatalytic reduction of NO by ammonia in the presence of hydrocarbons, Combust. Flame **99**, 660–668 (1994)
20.386 P. Günter: *Nonlinear Optical Effects and Materials*, Springer Ser. Opt. Sci, Vol. 72 (Springer, Berlin, Heidelberg 2000)
20.387 J.A. Silver: Frequency modulation spectroscopy for trace species detection: Theory and comparison among experimental methods, Appl. Opt. **31**, 707–717 (1992)
20.388 P. Vogel, V. Ebert: Near shot noise detection of oxygen in the A-band with vertical-cavity surface-emitting lasers, Appl. Phys. B **72**, 127–135 (2001)
20.389 M. Tacke: Lead salt lasers. In: *Long Wavelength Infrared Emitters Based on Quantum Wells and Superlattices*, ed. by M. Helm (Gordon+Breach, Amsterdam 2000) pp. 347–396
20.390 R. Grisar, G. Schmidke, M. Tacke, G. Restelli: *Monitoring of Gaseous Pollutants by Tunable Diode Lasers* (Kluwer, Dordrecht 1989)
20.391 R.T. Ku, J.O. Sample, E.D. Hinkley: Long-path monitoring of atmospheric carbon monoxide with a tunable diode laser system, Appl. Opt. **14**, 854–861 (1975)
20.392 S.M. Schoenung, R.K. Hanson: CO and temperature measurements in a flat flame by laser absorption spectroscopy and probe techniques, Combust. Sci. Technol. **24**, 227–237 (1981)
20.393 P.L. Varghese, R.K. Hanson: Collision width measurements of CO in combustion gases using a tunable diode laser, J. Quant. Spectrosc. Radiat. Transfer **26**, 339–347 (1981)

20.394 R.K. Hanson: Absorption spectroscopy in sooting flames using a tunable diode laser, Appl. Opt. **19**, 482–484 (1980)

20.395 M. Tacke, J.R. Meyer, A.R. Adams: Lead-salt lasers, Philos. T. Roy. Soc. A **359**, 547–566 (2001)

20.396 P. Werle: Spectroscopic trace gas analysis using semiconductor diode lasers, Spectrochim. Acta A **52**, 805–822 (1996)

20.397 J.H. Miller, S. Elreedy, B. Ahvazi, F. Woldu, P. Hassanzadeh: Tunable diode-laser measurement of carbon monoxide concentration and temperature in a laminar methane-air diffusion flame, Appl. Opt. **32**, 6082–6089 (1993)

20.398 U. Gustafsson, G. Somesfalean, J. Alnis, S. Svanberg: Frequency-modulation spectroscopy with blue diode lasers, Appl. Opt. **39**, 3774–3780 (2000)

20.399 C. Lin, M. Grau, O.D. and, M.-C. Amann: Low threshold room-temperature continuous-wave operation of 2.24–3.04 µm GaInAsSb/AlGaAsSb quantum-well laser, Appl. Phys. Lett. **84**, 5088–5090 (2004)

20.400 V. Ebert, C. Giesemann, J. Koeth, H. Teichert: New room-temperature 2.3 µm DFB-diode lasers: First spectroscopic characterization and CO-detection. In: *Laser Applications to Chemical and Environmental Analysis OSA TEchnical Digest Series* (Opt. Soc. Am., Washington 2004), Paper TuF-98

20.401 J. Faist, F. Capasso, D.L. Sivco, C. Sirtori, A.L. Hutchinson, A.Y. Cho: Quantum cascade laser, Science **264**, 553–555 (1994)

20.402 E. Schlosser, J. Wolfrum, L. Hildebrandt, H. Seifert, B. Oser, V. Ebert: Diode laser based in situ detection of alkali atoms: development of a new method for determination of residence-time distribution in combustion plants, Appl. Phys. B **75**, 237–247 (2002)

20.403 D. Wandt, M. Laschek, K. Przyklenk, A. Tünnermann, H. Welling: External cavity laser diode with 40 nm continuous tuning range around 825 nm, Opt. Commun. **130**, 81–84 (1996)

20.404 V. Ebert, H. Teichert, C. Giesemann, T. Fernholz, E. Schlosser, P. Strauch, H. Seifert, T. Kolb, J. Wolfrum: Rapid multi-parameter in-situ spectrometer for sensitive detection of CO, O_2, H_2O and temperature in industrial rotary kilns. In: *17. External TECFLAM Seminar Joint Research Project Combustion Control and Simulation*, ed. by W. Meier (AG TECFLAM, Stuttgart 2003) pp. 122–149

20.405 A.R. Awtry, J.W. Fleming, V. Ebert: Simultaneous diode laser-based in-situ measurement of liquid water content and oxygen mole fraction in dense water mist environments, Opt. Lett. **31**, 900–902 (2006)

20.406 T. Fernholz, H. Teichert, V. Ebert: Digital, phase-sensitive detection for in situ diode-laser spectroscopy under rapidly changing transmission conditions, Appl. Phys. B **75**, 229–236 (2002)

20.407 V. Ebert, J. Fitzer, I. Gerstenberg, K.-U. Pleban, H. Pitz, J. Wolfrum, M. Jochem, J. Martin: Simultaneous laser-based in-situ-detection of oxygen and water in a waste incinerator for active combustion control purposes, Proc. Combust. Inst. **27**, 1301–1308 (1998)

20.408 E. Schlosser, T. Fernholz, H. Teichert, V. Ebert: In situ detection of potassium atoms in high-temperature coal-combustion systems using near-infrared-diode lasers, Spectrochim. Acta A **58**, 2347–2359 (2002)

20.409 M. Grabrysch, C. Corsi, F.S. Pavone, M. Inguscio: Simultaneous detection of CO and CO_2 using a semiconductor DFB diode laser at 1.578 µm, Appl. Phys. B **65**, 75–79 (1997)

20.410 D.B. Oh, M.E. Paige, D.S. Bomse: Frequency modulation multiplexing for simultaneous detection of multiple gases by use of wavelength modulation spectroscopy with diode lasers, Appl. Opt. **37**, 2499–2501 (1998)

20.411 L.G. Blevins, B.W. Peterson: Obtaining and interpreting near-infrared wavelength modulation absorption signals from hot fire gases: Practical issues. In: *Combustion Institute Technical Meeting Eastern States Section* (Raleigh, NC 1999) pp. 85–88

20.412 L. G. Blevins, W. M. Pitts: Carbon monoxide measurement using a near-infrared tunable diode laser. In: *Annual Conference on Fire Research: Book of Abstracts* (1998) pp. 21–22

20.413 K. Muta, M. Tanoura, H. Honda: In-situ measurement of CO by tunable diode laser absorption spectroscopy in a large scale waste test furnace. In: *Proc. International Laser Sensing Symposium* (Fukui 1999)

20.414 V. Ebert, K. U. Pleban, J. Wolfrum: In-situ oxygen-monitoring using near-infrared diode lasers and wavelength modulation spectroscopy. In: *Laser Applications to Chemical and Environmental Analysis*, OSA Technical Digest Series (Opt. Soc. Am., Washington, 1998) p. 206–209

20.415 J.J. Nikkari, J.M. Di Iorio, M.J. Thomson: In situ combustion measurements of CO, H_2O and temperature with a 1.58 µm diode laser an two-tone frequency modulation, Appl. Opt. **41**, 446–452 (2002)

20.416 M.G. Allen, B.L. Upschulte, D.M. Sonnenfroh, W.J. Kessler, P.A. Mulhall: Overview of diode laser measurement in large-scale test facilities, Proc. Aerodynamic Measurement Technology and Ground Testing Conference **21**, 2452–2454 (2000)

20.417 D.M. Sonnenfroh, M.G. Allen: Observation of CO and CO_2 Absorption near 1.57 µm with an external-cavity diode laser, Appl. Opt. **36**, 3298–3300 (1997)

20.418 C.E. Wieman, L. Hollberg: Using diode lasers for atomic physics, Rev. Sci. Instrum. **62**, 1–20 (1991)

20.419 J.C. Camparo: The diode laser in atomic physics, Contemp. Phys. **26**, 443–477 (1985)

20.420 L.C. Philippe, R.K. Hanson: Laser diode wavelength-modulation spectroscopy for simultaneous measurement of temperature, pressure, and velocity in shock-heated oxygen flows, Appl. Opt. **32**, 6090–6103 (1993)

20.421 S.T. Sanders, D.W. Mattison, L. Ma, J.B. Jeffries, R.K. Hanson: Wavelength-agile diode laser sensing strategies for monitoring gas properties in optically harsh flows: Application in cesium-seeded pulse detonation engine, Opt. Express **10**, 505–514 (2002)

20.422 M.F. Miller, W.J. Kessler, M.G. Allen: Diode laser-based air mass flux sensor for subsonic aero-propulsion inlets, Appl. Opt. **35**, 4905–4912 (1996)

20.423 Z.C. Owens, D.W. Mattison, E.A. Barbour, C.I. Morris, R.K. Hanson: Flowfield characterization and simulation validation of multiple-geometry PDEs using cesium-based velocimetry, Proc. Combust. Inst. **30**, 2791–2798 (2005)

20.424 E.R. Furlong, D.S. Baer, R.K. Hanson: Combustion control using a multiplexed diode-laser sensor system, Proc. Combust. Inst. **26**, 2851–2858 (1996)

20.425 R.M. Mihalcea, D.S. Baer, R.K. Hanson: Diode laser sensor for measurements of CO, CO_2, and CH_4 in combustion flows, Appl. Opt. **36**, 8745–8752 (1997)

20.426 R. M. Mihalcea, D. S. Baer, R. K. Hanson: Diode-laser absorption sensor system for combustion monitoring and control applications. In: *AIAA Paper* 97-3356 (1997)

20.427 D.S. Baer, R.K. Hanson, M.E. Newfield, N.K.J.M. Gopaul: Multiplexed diode-laser sensor system for simultaneous H_2O, O_2, and temperature measurements, Opt. Lett. **19**, 1900–1902 (1994)

20.428 M.G. Allen: Diode laser absorption sensors for gas-dynamic and combustion flows, Meas. Sci. Technol. **9**, 545–562 (1998)

20.429 D. Wandt, M. Laschek, A. Tünnermann, H. Welling: Continuously tunable external-cavity diode laser with a double-grating arrangement, Opt. Lett. **22**, 390–392 (1997)

20.430 A.P. Larson, L. Sandström, S. Höjer, H. Ahlberg, B. Broberg: Evaluation of distributed Bragg reflector lasers for high-sensitivity near-infrared gas analysis, Opt. Eng. **36**, 117–123 (1997)

20.431 X. Zhou, X. Liu, J. B. Jeffries, R. K. Hanson: Diode Laser Sensors for Combustion Control. In: *AIAA Paper* 2003–1010 (2003)

20.432 E.R. Furlong, D.S. Baer, R.K. Hanson: Real-time adaptive combustion control using diode-laser absorption sensors, Proc. Combust. Inst. **27**, 103–111 (1998)

20.433 E.R. Furlong, R.M. Mihalcea, M.E. Webber, D.S. Baer, T.P. Parr, R.K. Hanson: Diode-laser sensor system for closed-loop control of a 50-kW incinerator, AIAA Paper 97-2833 (1997)

20.434 L. Ma, S.T. Sanders, J.B. Jeffries, R.K. Hanson: Monitoring and control of a pulse detonation engine using a diode-laser fuel concentration and temperature sensor, Proc. Combust. Inst. **29**, 161–168 (2002)

20.435 F. Schuler, F. Rampp, J. Martin, J. Wolfrum: TACCOS – a thermography-assisted combustion control system for waste incinerators, Combust. Flame **99**, 431–439 (1994)

20.436 V. Ebert, J. Fitzer, I. Gerstenberg, H. Pitz, K.U. Pleban, J. Wolfrum, M. Jochem, J. Martin: Online monitoring of water vapour with a fiber coupled NIR-diode laser spectrometer, VDI Berichte **1366**, 145–154 (1998)

20.437 J. T. C. Liu, J. B. Jeffries, R. K. Hanson: Diode laser absorption diagnostics for measurements in practical combustion flow fields. In: *AIAA Paper* 2003–4581 (2003)

20.438 F. Greger, K.T. Hartinger, P.B. Monkhouse, J. Wolfrum, H. Baumann, B. Bonn: In situ alkali concentration measurements in a pressurized fluidized bed coal combustor by excimer laser induced fragmentaiton fluorescence, Proc. Combust. Inst. **26**, 3301–3307 (1996)

20.439 K.T. Hartinger, S. Nord, P.B. Monkhouse: Quenching of fluorescence from Na(3^2P) and K(4^2P) Atoms following photodissociation of NaCl and KCl at 193 nm, Appl. Phys. B **64**, 363–367 (1997)

20.440 R.C. Oldenburg, S.L. Baughcum: Photofragment fluorescence as an analytical technique: application to gas-phase alkali chlorides, Anal. Chem. **58**, 1430–1436 (1986)